united nations
educational, scientific
and cultural
organization

international atomic
energy agency

the
abdus salam
international centre for theoretical physics

School on "Exploring the Atmosphere by Remote Sensing Techniques"
18 October - 5 November 1999

1151-10

"Atmospheric Spectroscopy & Radiative Transfer"

K. Chance
Harvard College Observatory
Center for Astrophysics
Cambridge (MA)
USA

Please note: These are preliminary notes intended for internal distribution only.

Given this blackbody definition, our first simple picture of the Sun is of a blackbody radiator at about 5900 degrees K (some authors use 5750, 5780 - corresponding to a "solar constant" of [illegible] ....) The Earth, on the average is approximately a blackbody radiator at about 250 K.

The sun has an average angular size in the sky of [illegible] degree.

On the average, the solar radiation impinging on the Earth must be equal to the radiation from the Earth, or the Earth would be heating up (or cooling down). The balance between solar radiation in and Earth radiation out is shown by these

Two figures of solar radiation versus Earth radiation

The detailed spectrum of the Sun is actually much more complicated due to absorption and emission by various species in the various parts of the Sun's atmosphere. Here is an example of a solar source function in one of the standard radiative transfer models:

LOWTRAN7 solar source function

This figure shows in more detail (at higher spectral resolution) the solar source function in the visible and parts of the UV and IR:

KPNO solar spectrum.

Additional solar facts:

(a) To a very high level of approximation, the Sun's radiation received at the Earth is completely unpolarized.

(b) The distance from the Earth to the Sun varies by several percent over the year, due to the ellipticity of the Earth's orbit:

Figure of solar distance versus date.

The average distance (1 astronomical unit, AU) is 1.495978707e8 km.

(c) There can be substantial spatial variability of the Sun's spectrum (due to, e.g., sunspots/faculae, limb darkening)

(d) The Sun's output is constant to within better than 1% in the IR, visible, and the UV at wavelengths longer than about 250 nm:

Two Figures for solar variability

A set of relevant solar facts and a solar spectrum is available on our ftp site: solar.dat

(2) INTRODUCTION TO RADIATIVE TRANSFER

First, from a spectroscopist's point of view: I have a gas cell and a source of radiation:

$I_0(\sigma) \rightarrow [\tau(\sigma), T] \rightarrow I(\sigma)$ σ in cm^{-1},

Figure of cell with I0 (sig), blackbody term; I = I0 * e- + B (1 - e-)

Lectures on Atmospheric Spectroscopy and Radiative Transfer

The overall purpose of the material I will present is to attempt to demonstrate how molecular spectroscopy is applied to the measurement of quantities in the atmosphere. My motivation is the hope that at least one of the students here will become a scientist in this field and will make use of the background and, I hope, the sense of rigor that I am trying to present here.

~~I am providing a set of problems that are optional, to be solved later, at your leisure. I hope that they will help you to internalize the concepts presented here and to provide you with a more detailed understanding of them.~~

I have set up an ftp site for some lecture materials:
~~ftp cfa~~ ftp.harvard.edu
login anonymous
cd outgoing/kchance/ictp (kchance@cfa.harvard.edu)

Day 1.

INTRODUCTION

I am presenting information in slightly different order than I would if my lectures are standalone. In particular, I am presenting overviews of solar properties and of basic radiative transfer today, so that they are in place for some of the following lectures by my colleagues. Normally I would have presented the sections in this syllabus in the order 3, 4, 5, 1, 2. This is in order to provide some justification for why we are studying this topic (Atmospheric Spectroscopy and Radiative Transfer) and to provide an overview of the atmosphere showing where areas of concern and active investigation are.

BLACKBODY ASIDE

I do need to introduce one concept now - that of blackbody radiation. We will look at it in more detail later in the week.

The blackbody radiance is the power emitted per unit area by a non-reflecting, non- transmitting surface that can be characterized by a single temperature, T.

R = $R_\sigma d\sigma = \frac{2\pi h c^2 \sigma^3}{e^{c_2\sigma/T} - 1} d\sigma$ $\sigma(cm^{-1}) = \frac{\nu}{c}$

$c_2 = \frac{hc}{k}$

in erg s-1 cm-2; c2 = 1.438769 cm-deg K.
If the angular dependence is included (we will discuss that later),

B = $B_\sigma d\sigma = \frac{2hc^2\sigma^3 d\sigma}{e^{c_2\sigma/T} - 1}$

in erg s-1 cm-2 sr-1. We'll come back to blackbodies later in more detail to describe why they are an important concept and to relate it to the concepts of temperature, equilibrium, and Boltzmann statistics. We will also show the blackbody behavior in terms of photons emitted, how it is expressed when the abscissa is in wavelength units, and

(1) SOLAR PROPERTIES

$$I(\sigma) = I_0(\sigma) e^{-\tau(\sigma)} + R(\sigma, T)(1 - e^{-\tau(\sigma)})$$

1 - e- is the emissivity (epsilon), [redacted] is the optical thickness = absorption cross section alpha (cm2) * concentration rho (cm-3) * cell - or atmosphere - length (cm) = dimensionless. The cross section (or "mass absorption coefficient) is the measure of how strongly a substance absorbs at a given wavelength of light, on a per-molecule basis. We well investigate it in great detail in the next few days. "Optical thickness" generally refers to the total difference in this quantity while "optical depth" refers to the quantity evaluated at some specified point within. Note that I often misuse these terms, so be careful!

The positive contribution due to blackbody emission is a "source term" - there are other source terms, such as scattering (which we will address later, but you can see how scatterers embedded in our gas cell - perhaps dust particles or something else - could scatter light OUT of our beam, thus contributing to extinction, or could scatter light from the sides INTO our beam, becoming a source of radiation).

For atmospheric conditions (temperatures of 200-300, the sun as the radiation source) usually the blackbody emission source is unimportant above about 4500 cm-1, but dominates below about 3000 cm-1. The exact crossover point depends on the details of the measurement geometry. (The problem set includes an exercise to investigate this for several cases.) Thus, emission spectroscopy of the atmosphere is normally done at wavelengths longer than about 3000 cm-1. For shorter wavelengths, when emission is negligible, we have the (Beer, Lambert, Bouget) law of exponential absorption - saturation implies less energy absorption per molecule, although the relative absorption stays the same.

If the cell is of infinitesimal length, the equation becomes:

$$I = I_0(1 - \tau) + R \cdot \tau \quad ; \quad dI = -I_0 \tau + R\tau$$

from which we can re-arrange to give a radiative transfer equation in either distance or optical depth:

RTEs $$-\frac{dI}{d\tau} = I_0 - R = -\frac{dI}{\alpha \cdot \rho \cdot dS}$$

and, generalizing to an arbitrary source function:

general RTEs $$-\frac{dI}{d\tau} = I_0 - S$$

One final example on this topic. Often, in atmospheric studies, we address radiative transfer through atmospheres that are modeled as a series of shells. For the case of two shells (or two gas cells), if the cells are at the same temperature:

$I_0 \longrightarrow \boxed{\tau_1, T} \xrightarrow{I_1} \boxed{\tau_2, T} \longrightarrow I_2$

$$I_1 = I_0 e^{-\tau_1} + R(T)(1 - e^{-\tau_1})$$

$$I_2 = [I_0 e^{-\tau_1} + R(T)(1 - e^{-\tau_1})] e^{-\tau_2} + R(T)(1 - e^{-\tau_2})$$

$$= I_0 e^{-(\tau_1 + \tau_2)} + R(T)(1 - e^{-(\tau_1 + \tau_2)})$$ optical depths add

While if they are at different temperatures:

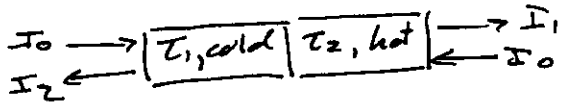

$I_1 \neq I_2$

There is a buffering toward the nearest layer or cell:

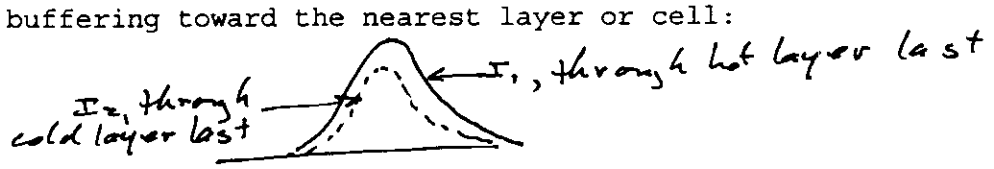

Now you have most of the information needed to explain limb brightening/darkening.

1. For applicable radiative transfer, the student should review the development of blackbody radiation, and Einstein A and B coefficients, spectral line profiles and line saturation. I recommend the first four chapters of "Quantitative Molecular Spectroscopy and Gas Emissivities", S.S. Penner for this purpose.

2. For the underlying spectroscopy, I recommend a brief review of the material in chapters 5-10 of "Spectra of Atoms and Molecules", P.F. Bernath (or an equivalent general spectroscopy book covering rotational, vibrational, Raman, and electronic spectroscopy). Chapter 1 of this book could serve as a substitute for much of the material in the more inclusive (but harder to locate) book by Penner.

3. For basic atmospheric structure and radiative properties I suggest sections 3.1 and 3.2, and chapter 4 of "Aeronomy of the Middle Atmosphere", second edition, G. Brasseur and S. Solomon. Chaper 5 gives a nice (optional) overview of the chemical composition.

The "musts" are summarized as follows:

(1) The most important prerequisite is a review of basic spectroscopy for those who do not have such background. The Bernath book is very good, but any text which covers introductory spectroscopy and explains the principles of rotational, vibrations, Raman, and electronic spectroscopy will suffice. Students who have studied the topic need not review it further; in any case, you do not need to distribute specific material.

(2) The minimum for the radiative transfer is Penner pp 1-16, 17-22, 23-33, and 38-46.

(3) The minimum for structure and radiative properties is Brasseur and Solomon pp 87-108 and 119-123 (from my second edition; this corresponds to Chapters 4.1, 4.2, 4.3, and the first 5 pages of 4.43).

HOWEVER - A bright and motivated student who has not had the opportunity to review any material should still be able to gain substantial benefit from just the lectures (if I do my job correctly!)

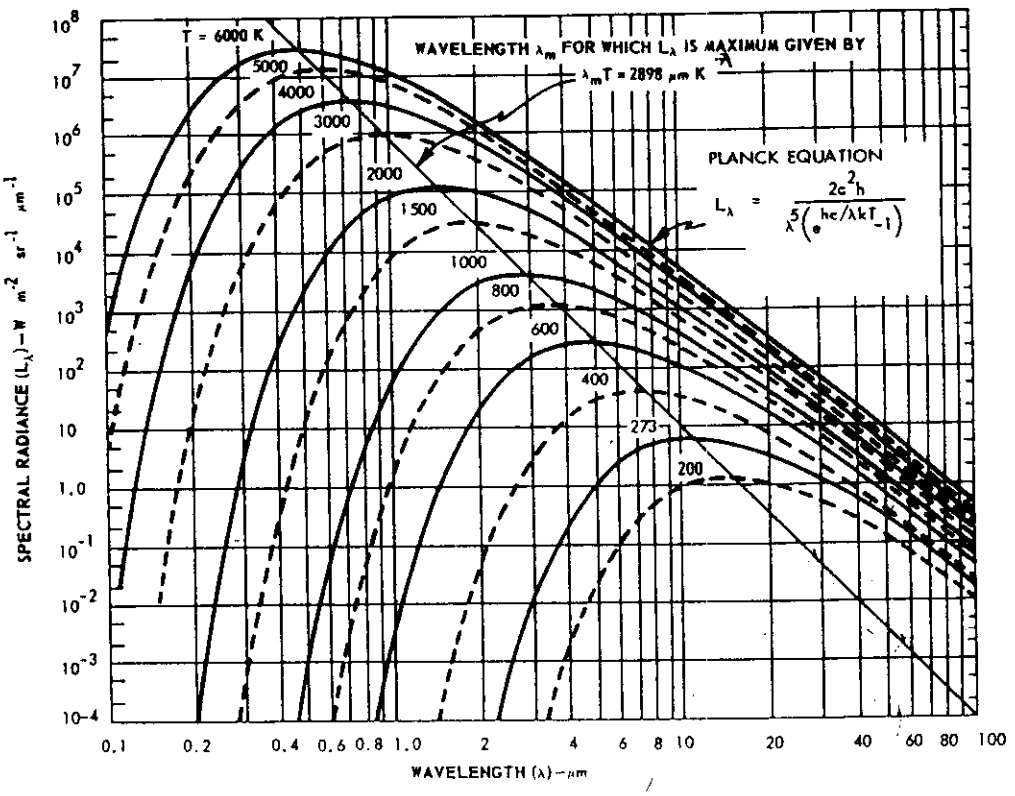

Fig. 4-1 Spectral radiance L_λ of a blackbody at the absolute temperature T shown on each curve. The diagonal line intersecting the curves at their maxima shows Wien's displacement law. Subdivisions of the ordinate scale are at 2 and 5. (Adapted from Reference 8 with permission).

$*\sigma_m(cm^{-1}) =$
$3.451\,T(^\circ K)$

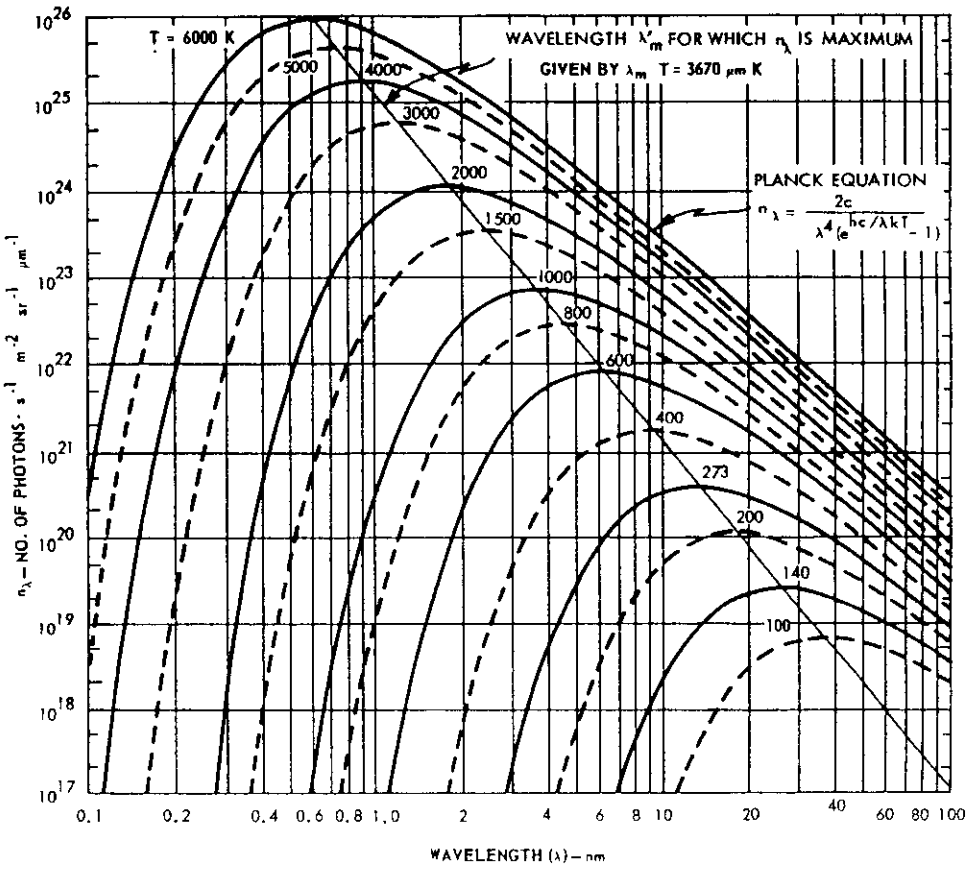

Fig. 4-2 Number of photons per second emitted per square meter per steradian per micrometer by a blackbody at various absolute temperatures. The diagonal line intersecting the curves at their maxima shows Wien's displacement law. (Adapted from Reference 8 with permission).

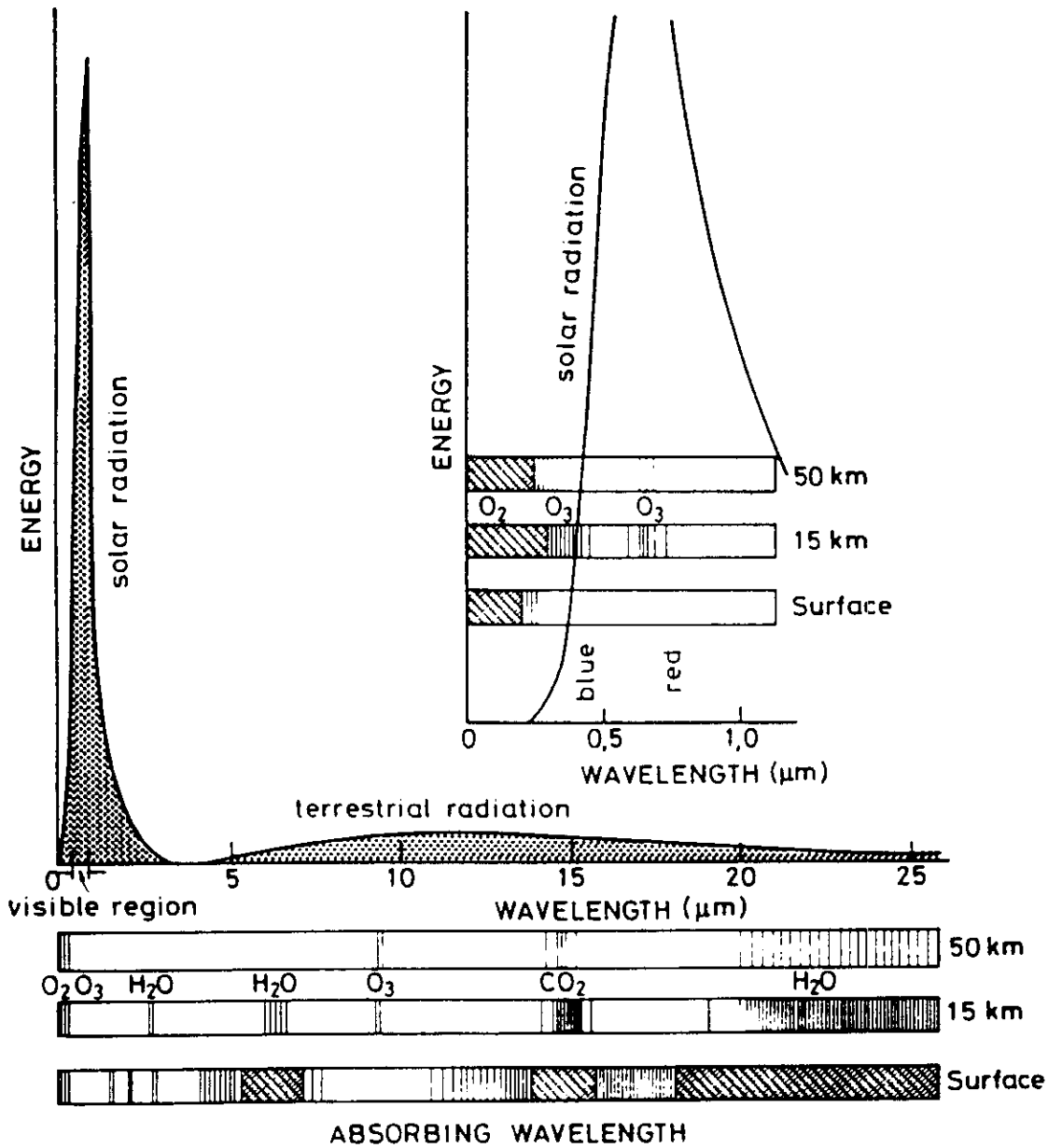

Fig. 4.2. Spectral distribution of solar and terrestrial radiation. Atmospheric absorption at different wavelengths. After Iribarne and Cho (1980). (Copyright by Reidel Publishing Company).

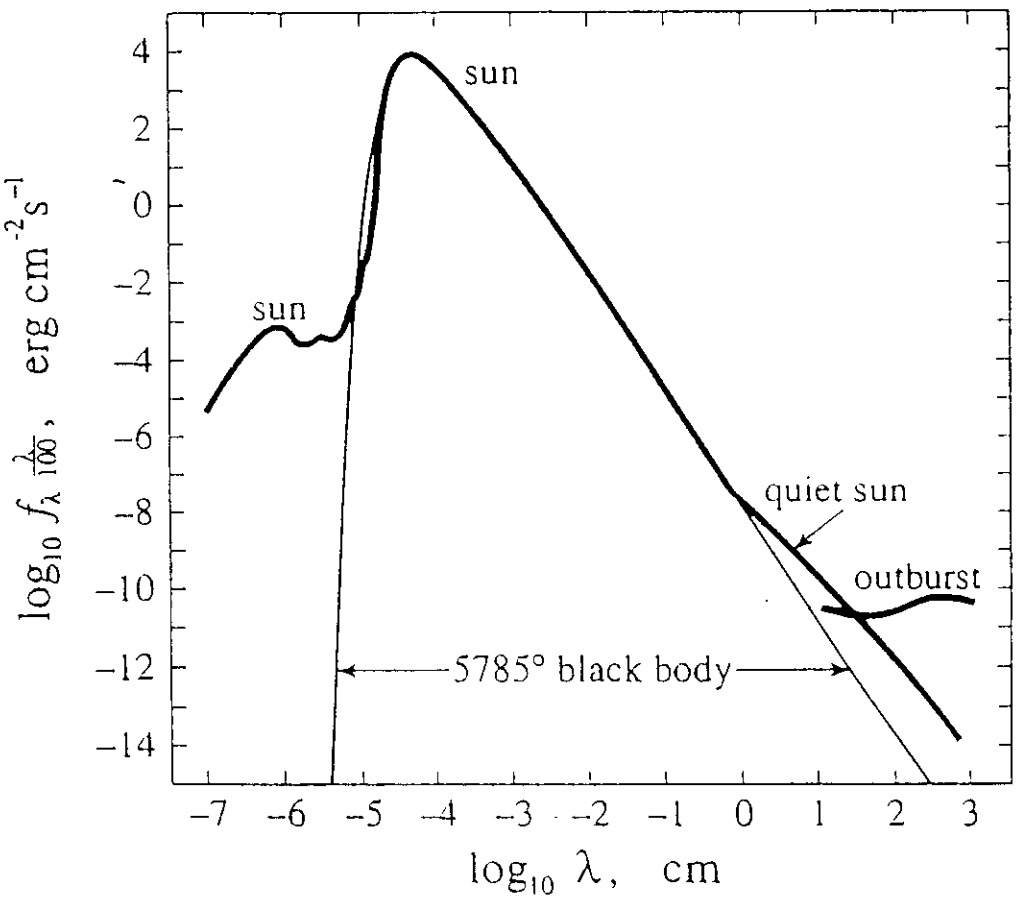

Figure D.1 The solar spectral irradiance from 1 nm to 10 m. All spectral features have been smoothed out. "Outburst" indicates a radio disturbance.

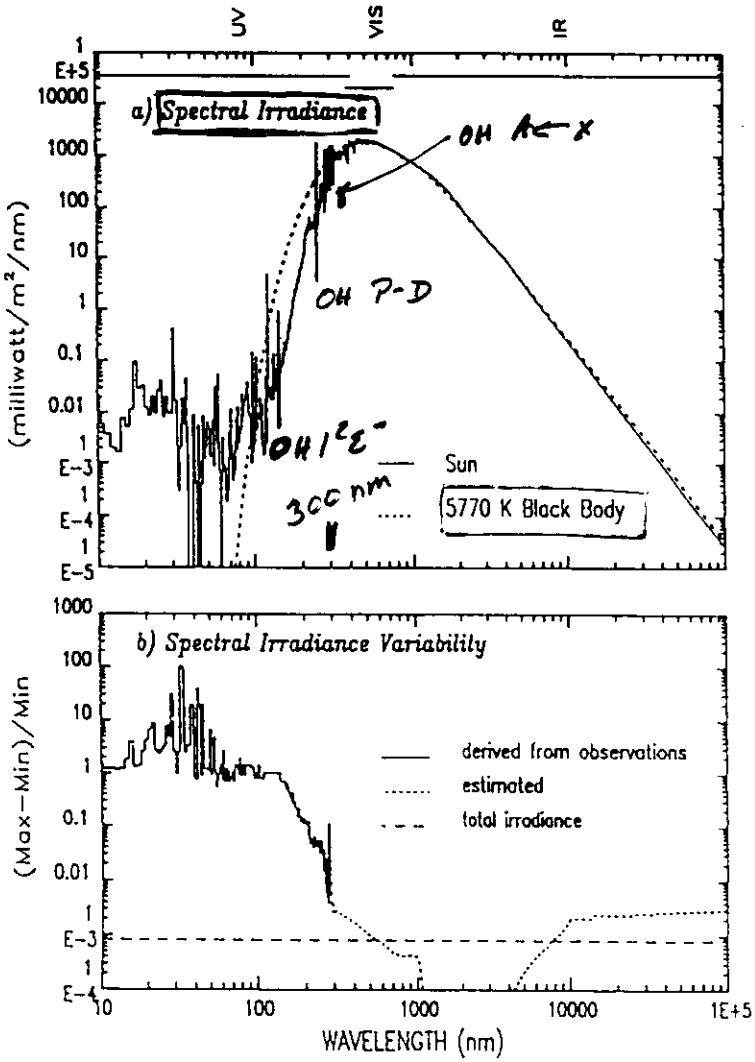

Figure 2. (*a*) The Sun's spectral irradiance typical of solar minimum conditions, compared with the spectrum of a blackbody radiator at 5770°K. The broad spectral bands identified along the top of this figure are the ultraviolet (UV), visible (VIS), and infrared (IR). Not shown, at wavelengths longward of the IR, is the microwave, or radio, portion of the solar spectrum. (*b*) The approximate amplitude of the Sun's spectral irradiance variation from the maximum to the minimum of the 11-year activity cycle is also shown. The variations at $\lambda < 300$ nm (solid line) were derived from satellite observations during solar cycle 21. The variations at longer wavelengths (dotted line) were determined from knowledge of the solar cycle variation in the fraction of the Sun's disc covered with active regions and of their contrasts (shown in Figure 11 and discussed further in section 3.2). The dashed line indicates the variation during solar cycle 21 of the total (spectrally integrated) irradiance. Note that solar cycle variations at wavelengths from 1100 to 3500 nm are predicted to be out of phase with solar activity, with a maximum negative amplitude of −0.03% at 1400 nm.

/ARIATIONS IN THE SUN'S RADIATIVE OUTPUT

Judith Lean
E.O. Hulburt Center for Space Research
Naval Research Laboratory
Washington, D. C.

Reviews of Geophysics, 29, 4 / *November 1991*
pages 505-535
Paper number 91RG01895

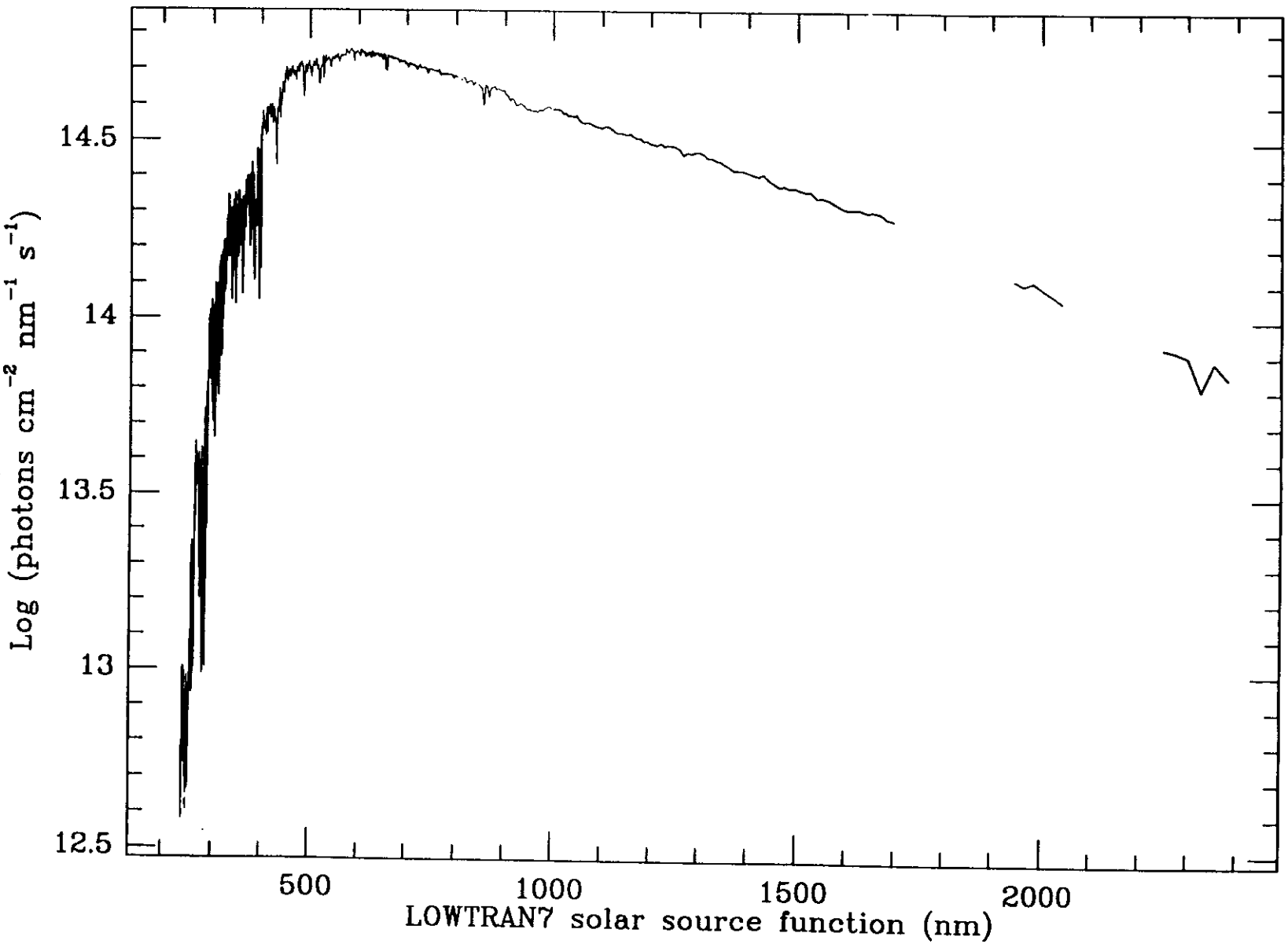
14.5
14
13.5
13
12.5
Log (photons cm^{-2} nm^{-1} s^{-1})
500
1000
1500
2000
LOWTRAN7 solar source function (nm)

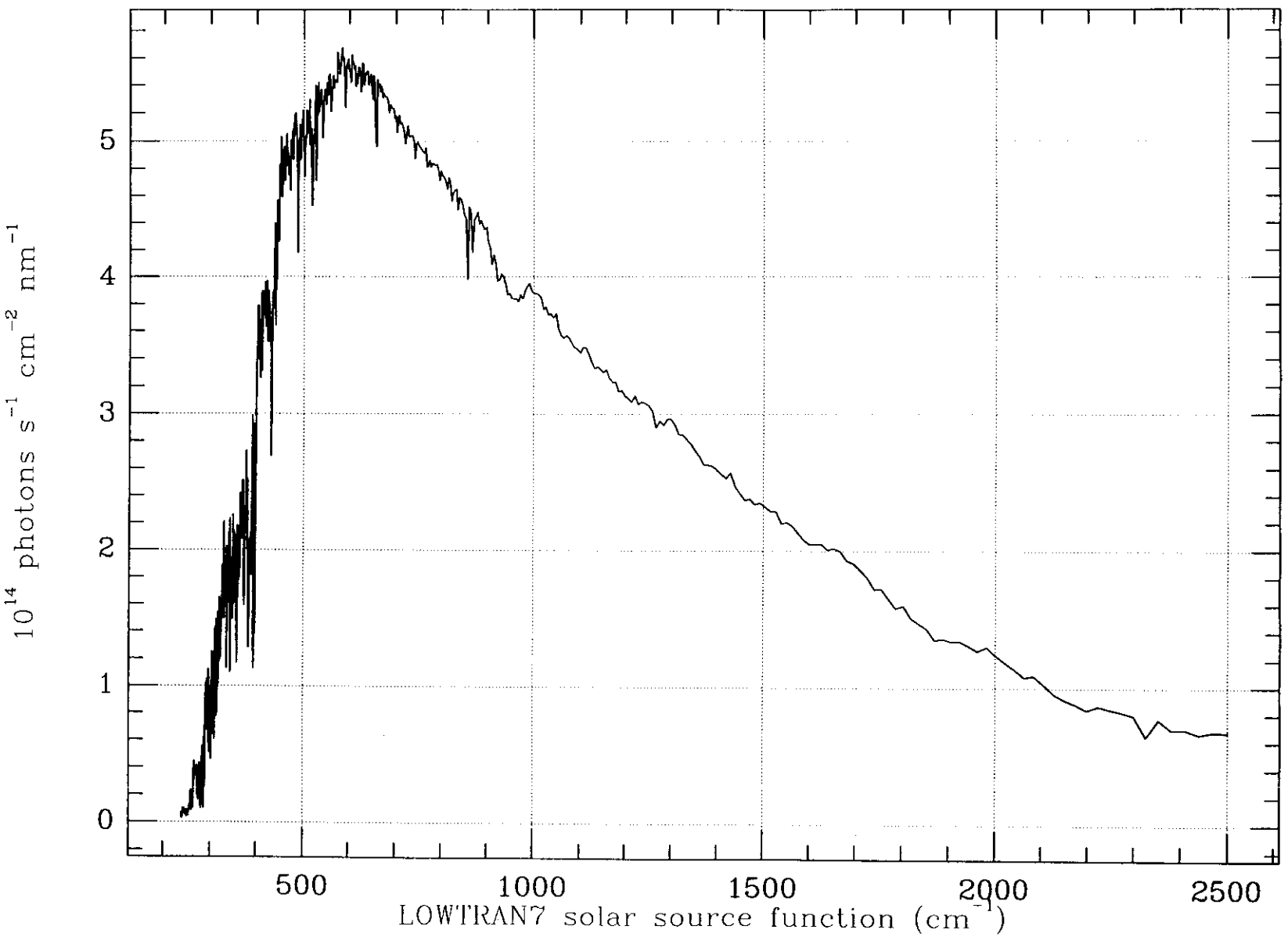
10^{14} photons s^{-1} cm^{-2} nm^{-1}
0
1
2
3
4
5
500
1000
1500
2000
2500
LOWTRAN7 solar source function (cm^{-1})

KITT PEAK SOLAR FLUX ATLAS (KURUCZ, FURENLID, BRAULT, AND TESTERMAN 1984)

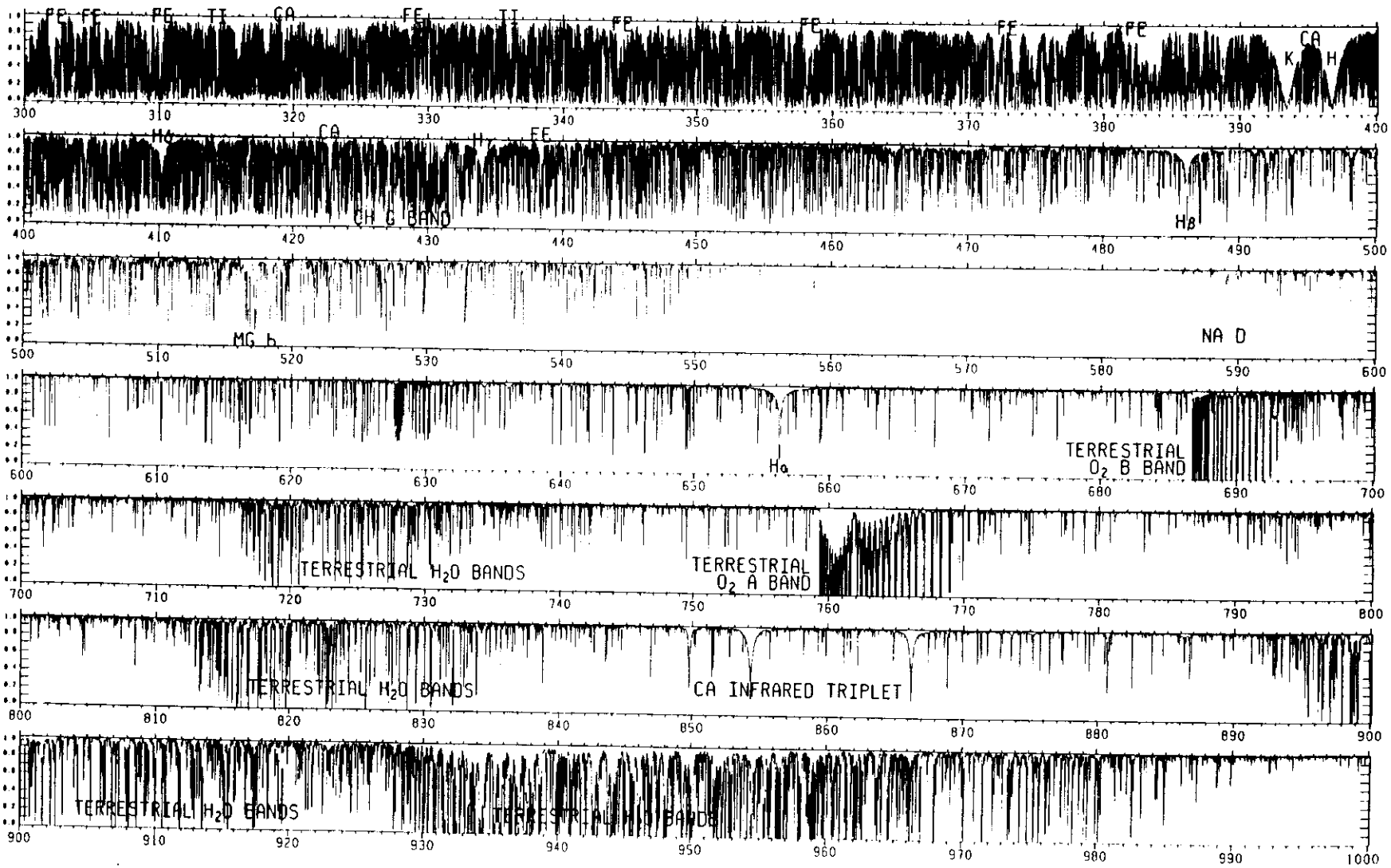

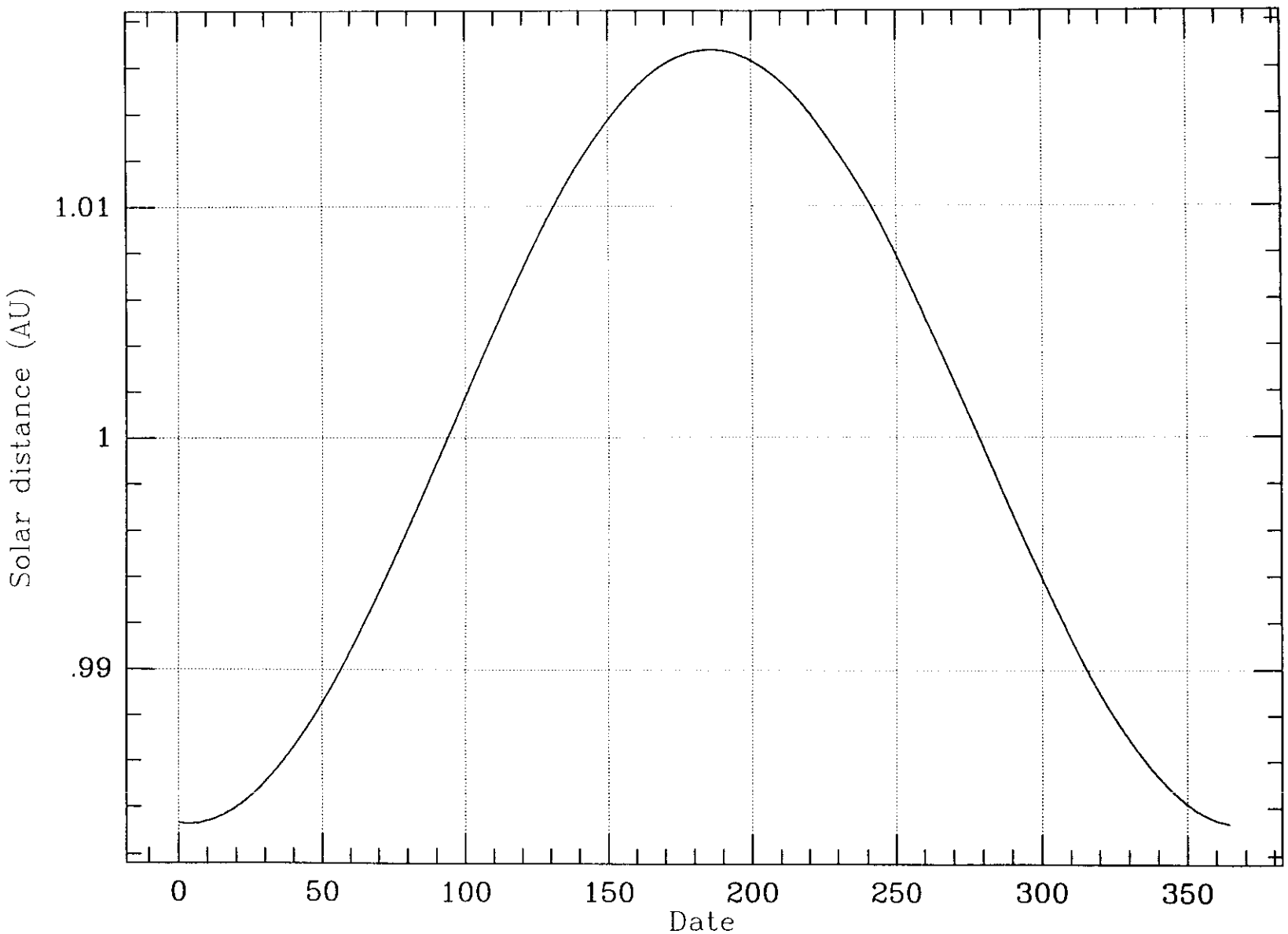
1.01
1
.99
Solar distance (AU)
0
50
100
150
200
250
300
350
Date

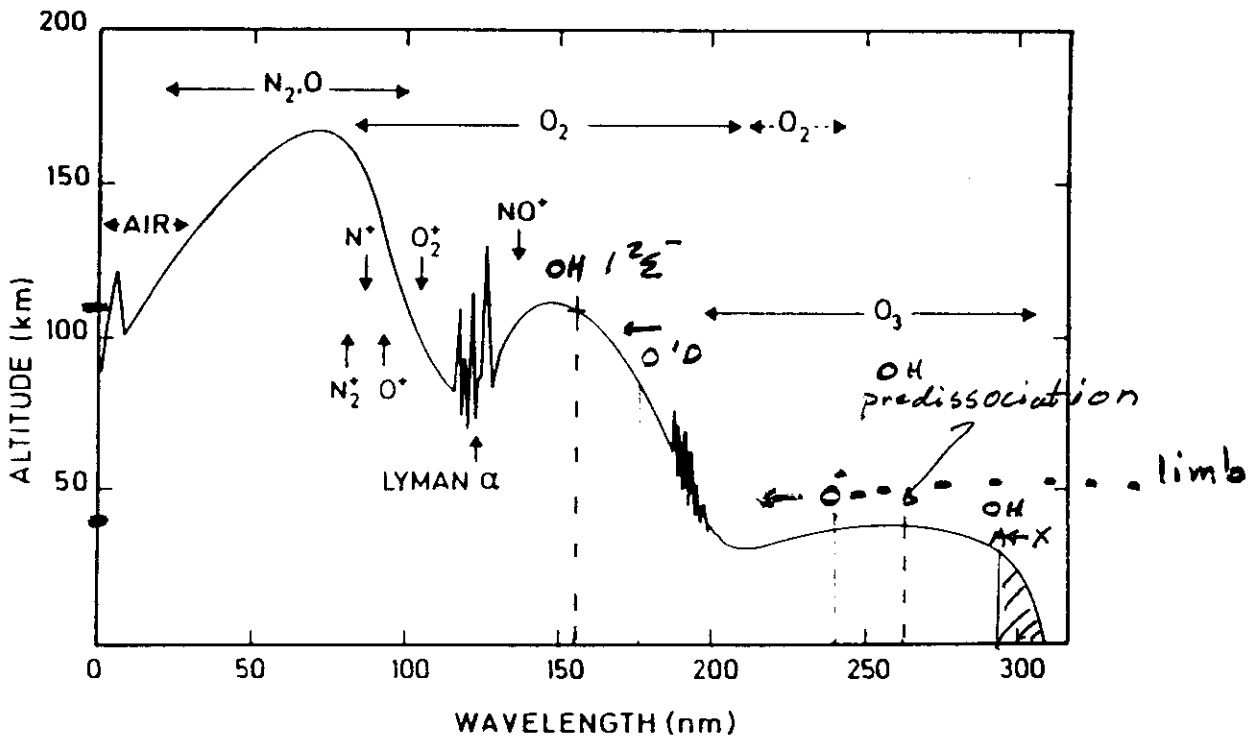

Fig. 4.3. Depth of penetration of solar radiation as a function of wavelength. Altitudes correspond to an attenuation of 1/e. The principle absorbers and ionization limits are indicated.

Atmospheric Spectroscopy and Radiative Transfer, Day 2

(3) SELECTED PROGRAMS

Selected atmospheric measurement programs: Examples from GOME and from FIRS (to motivate the need for quantitative atmospheric spectroscopy and to open discussion of techniques for measurement, spectral synthesis, and retrievals, and what information on composition and physical conditions may be learned from spectroscopic measurements).

(4) OVERVIEW OF THE ATMOSPHERE

Show the temperature and pressure structure of the atmosphere, with slides selected to indicate where the tropopause varies with location (mention seasonal variation, but do not go into any detail.

Show where various atmospheric processes occur, with help of German slide (tropospheric pollution/global urbanization; ozone depletion (where is the ozone; where is the ozone hole?); greenhouse warming.

Briefly mention clouds - location from German slide; also illustrate with GOME measurements of clear and cloudy pixels.

Note that the BRDF for actual clouds can vary at about the 20% level from a Lambertian surface (which will be defined in the next section).

Mention standard atmospheres - I have put an extract from the US standard atmosphere (z, P, T) on the ftp site; note that the scale heights for density and pressure are about 7 km in the troposphere, stratosphere, and mesosphere, as you can confirm yourselves from the data in the file.

Lapse rates (dry adiabatic lapse rate); photochemical heating; global warming potentials.

(5) BOLTZMANN STATISTICS AND RELATED ISSUES

I now need to describe a set of linked concepts that will allow us to describe atmospheres and their spectroscopic and radiative behavior accurately, so long as regions of the atmosphere behave locally as if they are very near to equilibrium - this is the assumption of local thermodynamic equilibrium (LTE). This assumption holds very well for most of the parts of the atmosphere that we will be concerned with: The troposphere and the stratosphere, with deviations beginning to show themselves in the upper stratosphere and the thermosphere. The force for "equilibrating" the atmospheric gas is collisions: As we shall see, when there are many non-reactive collisions among gas molecules for each reactive collision or photolysis event, the air will behave locally as if it is in equilibrium.

This section of the presentation require would a number of hours in a proper thermodynamics course to present rigorously; because of our limited time, I will present material in summary. The interested student should consult an appropriate texts (e.g., Davidson; Penner) for fuller detail.

We start by assuming that our gas - perhaps this parcel in the lecture room, is described by LTE. We also assume that the gas is characterized by a set of internal energy states:

Show example of energy states, including rotational, vibrational, and electronic (mention nuclear, but don't show):

* diagram of molecular energy states. (approximately UV/visible;
* infrared, submillimeter-wave/microwave).

The assumption of LTE is equivalent to stating that the relative populations in the different states are described by a Boltzmann distribution. The basic relationship here is that the ratio of fractional populations in two different states is given by:

f1/f2 = exp - (E1 - E2) / kT $f_1/f_2 = e^{-(E_1 - E_2)/kT}$

This results in a distribution among the possible energy states where:

f_i ~ exp (-E_i / kT) - an arbitrary zero of energy is implied.

The absolute fractional populations are then given by normalizing the above:

f_i = exp ( ) / S_j ( ) $f_i = e^{-E_i/kT} / \sum_j e^{-E_j/kT}$

The S_j ( ) is the "partition function", q. This is equivalent to stating that the gas can be described as having a temperature T, since temperature is an equilibrium concept.

We need to add the concept of degeneracy. This is simply that there may be more than one state with a given energy, usually due to the symmetry of the molecule in question: E_n = E_m. An example of this is in the rotational states of diatomic molecules. The rotational state J has a degeneracy of 2J+1, which would be obvious from an examination of the rotational wavefunction:

* draw states 0, ..., N for a diatomic.

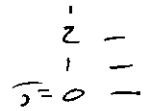

In this case, the Boltzmann distribution may be described by

* f_J = 2J+1 * exp (-E_J / kT) / q_J = g_J * exp ( ) / q_J,
where q_J = S ( ) $f_J = (2J+1) e^{-E_J/kT} / \sum_k (2k+1) e^{-} = g_J e^{-E_J/kT} / q_J$

This degeneracy may be broken in practice when an electric or magnetic field is present (depending of the details of the molecular electronic distribution). In the Earth's atmosphere the electric field is generally negligible (except for lightning events and upper atmospheric phenomena); The Earth's magnetic field (about 1/2 Gauss - weak) is generally negligible except in some special cases where it affects the spectrum measured by microwave techniques.

The underlying reason why the distribution in energy states assumed this Boltzmann distribution is that, considering collisions that re-distribute energy among the available energy states, the Boltzmann distribution is the one that is most probable; it corresponds to a very strong peak in the possible distribution of populations among energy states. A proper statistical analysis shows that distributions that vary significantly from the Boltzmann distribution are extremely likely to occur. When we are invoking this kind of "thermalizing" re-distribution by collisions, we are equivalently saying that the time scale for thermalizing events - collisions - is much shorter than

that for processes that move the system away from equilibrium - chemical reactions and photolysis events.

We showed rotational levels earlier - they are generally spaced by amounts from less than 1 cm-1 to several tens of cm-1. The range usually encountered for vibrational energy levels is from several 100 to several 1000 cm-1.

These are described by a Boltzmann distribution in population:

* f_v = g_v exp (-e_v / kT) / q_v; q_v = ...

Vibrational states may be degenerate or not, depending on the spatial symmetry of the molecule - something we don't have time to go into.

Finally, note that translation states are (usually to a very high degree of approximation) described as a continuum distribution in energies - the molecule can take on any value of translational energy any of the three spatial dimensions. In LTE, the distribution in each spatial coordinate is given by a Maxwell-Boltzmann distribution (Gaussian in velocity):

* f_v dv = SQRT (m / 2*pi*kT) * exp (-m*v*v / (2kT)) dv

$$f_v\,dv = \sqrt{\frac{m}{2\pi kT}}\; e^{-\left[mv^2/2kT\right]}dv$$

If you integrate over this distribution, you will note that there is 1/2 kT of energy in translational motion for each of the three spatial dimensions.

The quantity kT may be considered as a typical energy range for processes affecting equilibrium and state distributions. If the spacings of energy levels (among rotations, vibrations, or translations) is <<kT then that particular DEGREE OF FREEDOM" will be fully "turned on". A degree of freedom may be considered to be an orthogonal dimension for describing the energy content among the ensemble of molecules. Exchange of energy among the degrees of freedom occurs primarily through collisions. Under most atmospheric conditions, the various degrees of freedom may be considered to be only weakly coupled together.

* example of diatomic molecule - there are 3 degrees of freedom in a
* molecule for each atom, giving rise to 3 translational, 3
* rotational, and 3*N - 6 vibrational. Note exception for linear/rigid
* molecule.

Each degree of freedom in an ensemble of like molecules may contain up to (but no more than) 1/2 kT of energy. If the states are separated by amounts <<kT, the states are fully accessible to population by collisions, and that degree of freedom will contain 1/2 kT of energy.

Electronic states are important for atmospheric spectroscopy and photochemistry but the are usually high in energy in comparison to the kT of atmospheric conditions; atmospheric molecules are characterized by ground electronic states except for momentary excitations which serve as energy sources to the atmosphere. Such excitations momentarily push the system away from equilibrium, but the "bath" of molecules coupled by collisions drives them back. For the range of temperatures we encounter in the atmosphere, we need to usually be concerned with energy contained in molecules in the rotational,

vibrational, and translational degrees of freedom.

When we (later) consider intensities of absorption and emission lines, we will need to consider Boltzmann distributions for all types of energy states. Note from the form of the partition function given earlier that, if the various degrees of freedom are orthogonal (usually a very good approximation in the atmosphere), the overall partition function is the product of those for the different degrees of freedom:

q_total = q_trans * q_rot * q_vib * q_electronic * q_nuclear

So that a generalized fractional population would be given by

g_total * exp (-E_total / kT) / q_total

We will need this relationship when we discuss line intensities in detail.

Einstein A and B coefficients:

These are presented here for reference, but not derived. See Bernath for an excellent discussion. The Einstein A coefficient describes the lifetime of an excited state with respect to spontaneous emission:

A (s-1) = $\frac{64\pi^4}{3h\lambda^3}|\mu|^2$

where |mu|**2 is the square of the (usually dipole) transition moment connecting the two states.

The Einstein B coefficient determines the transition rate for absorption or induced emission given a blackbody radiation density:

rho = .../.

skip

B = .../.

Finally, to finish up on blackbodies, we define a Lambertian surface as one where the emitted (or scattered) radiation does not depend on the angle of view for the surface (book example); this implies that emission (or scattering) is proportional to cosine (normal angle).

Then, blackbody steradiancy leave as an exercise

B = (integral)

or

B = (equation)

The Stefan-Boltzmann constant describes the total power emitted by a blackbody (prove by integration): 5.67032W m-2 K-4

and Wien's law describes the wavenumber where the maximum power is

emitted:

sigma_max (cm-1) = do as an exercise!

The maximum number of photons are emitted at

n_max = do as an exercise!

Characteristics of the GOME Detector Channels

Channel	Range (nm)	Resolution (nm)	Baseline Detector	Material
Ia	237-307	0.22	0.61 of 1 × 1024 Reticon SR	Si
Ib	307-315	0.22	0.07 of 1 × 1024 Reticon SR	Si
IIa	311-312	0.24	0.01 of 1 × 1024 Reticon SR	Si
IIb	312-405	0.24	0.81 of 1 × 1024 Reticon SR	Si
III	394-611	0.40	1 × 1024 Reticon SR	Si
IV	578-794	0.40	1 × 1024 Reticon SR	Si

- the Polarisation Measurement Device (PMD)
- the Digital Data Handling Unit (DDHU)
- the optical bench structure
- the thermal control hardware.

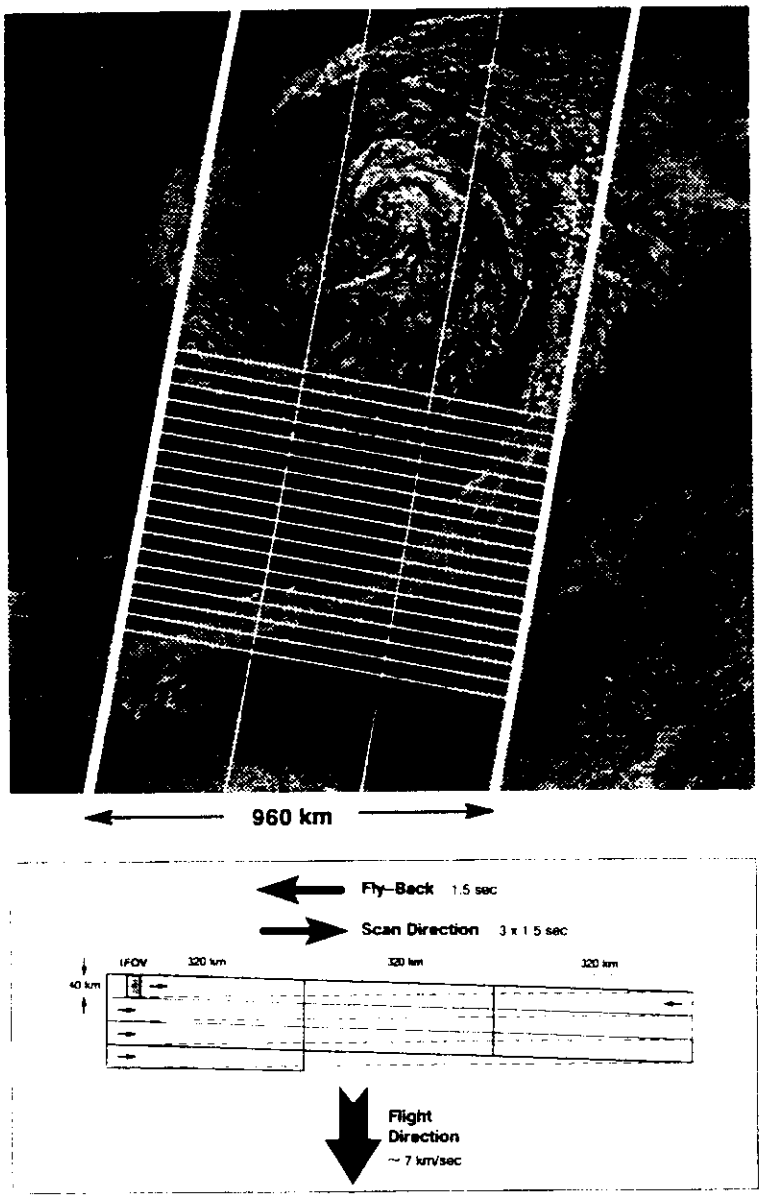

Figure 6. GOME scan pattern (graphic courtesy of DLR, Oberpfaffenhofen)

Table 1. Key optics performance parameters

Band	Wavelength range (nm)	Grating (l/mm)	Pixel resolution (nm)	Spectral resolution (nm)
1A	240—268	3600	0.11	0.22
1B	268—295			
2A	290—312	2400	0.12	0.24
2B	312—405			
3	400—605	1200	0.2	0.4
4	590—790	1200	0.2	0.4

Spectrometer optics

In the spectrometer optics, shown schematically in Figure 7, the light reflected off the scanning mirror is focussed by an anamorphic telescope such that the shape of the focus matches the entrance slit of the spectrometer (dimensions 10 mm x 100 µm. After the slit, the light is collimated by an off-axis parabolic mirror. It then strikes the quartz pre-disperser prism, causing a moderately wavelength dispersed beam. Another prism acts as channel separator: the upper edge of this prism reaches into the wavelength-dispersed beam, letting the longer wavelengths pass, reflecting the wavelength range 290–405 nm into Channel 2 by means of a dielectric reflecting coating, and guiding the wavelength range 240–295 nm internal to the prism into Channel 1. The unaffected wavelength range of 405–790 nm is then split up by a dichroic beam splitter into Channels 3 (400–605 nm) and 4 (590–790 nm).

Each individual channel consists of an off-axis parabola, a grating, and an objective with f-numbers of 2 (Channels 1 and 2) and 3 (Channels 3 and 4), finally focussing the light onto the detectors contained in their respective Focal-Plane Assemblies.

The most critical optical elements in the optical chain are the diffraction gratings, which have to provide both a high efficiency in the first diffraction order and a very low level of stray light and ghosting. Because of the criticality of the gratings for the final performance of the instrument, two parallel development programmes are under way, at the firms of Jobin-Yvon in France and Carl Zeiss in Germany. Some of the key performance requirements for the optics are summarised in Table 1.

Focal-Plane Assemblies

The FPAs are made from titanium and have a sealed quartz window at the side where they are flanged to the respective objective tubes. The rear side of the FPA, the so-called 'pin-plate', is a titanium plate provided with electrically isolated, vacuum-tight feed-throughs for the electrical connections to the detector. This is a Reticon RL 1024 SR random-access diode array detector with 1024 pixels, each pixel measuring 25 µm in the dispersion direction and 2.5 mm in the along-slit direction. Each diode is randomly accessible by an address bus and can be read out individually.

In the GOME instrument, the detectors of Channels 1 and 2 are split into several

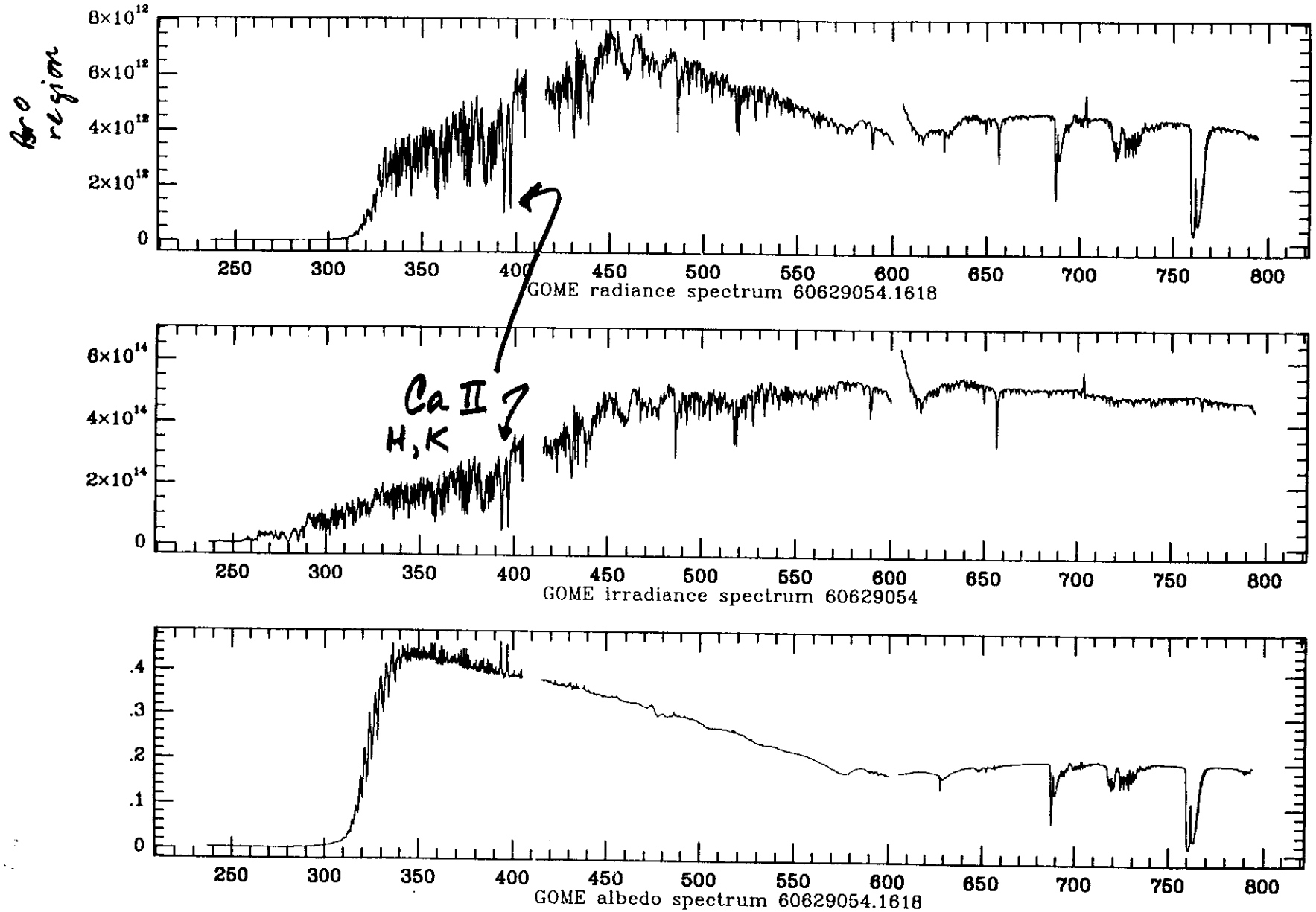
Bro region
8×10¹²
6×10¹²
4×10¹²
2×10¹²
0
250 300 350 400 450 500 550 600 650 700 750 800
GOME radiance spectrum 60629054.1618
6×10¹⁴
4×10¹⁴
2×10¹⁴
0
Ca II
H,K
250 300 350 400 450 500 550 600 650 700 750 800
GOME irradiance spectrum 60629054
.4
.3
.2
.1
0
250 300 350 400 450 500 550 600 650 700 750 800
GOME albedo spectrum 60629054.1618

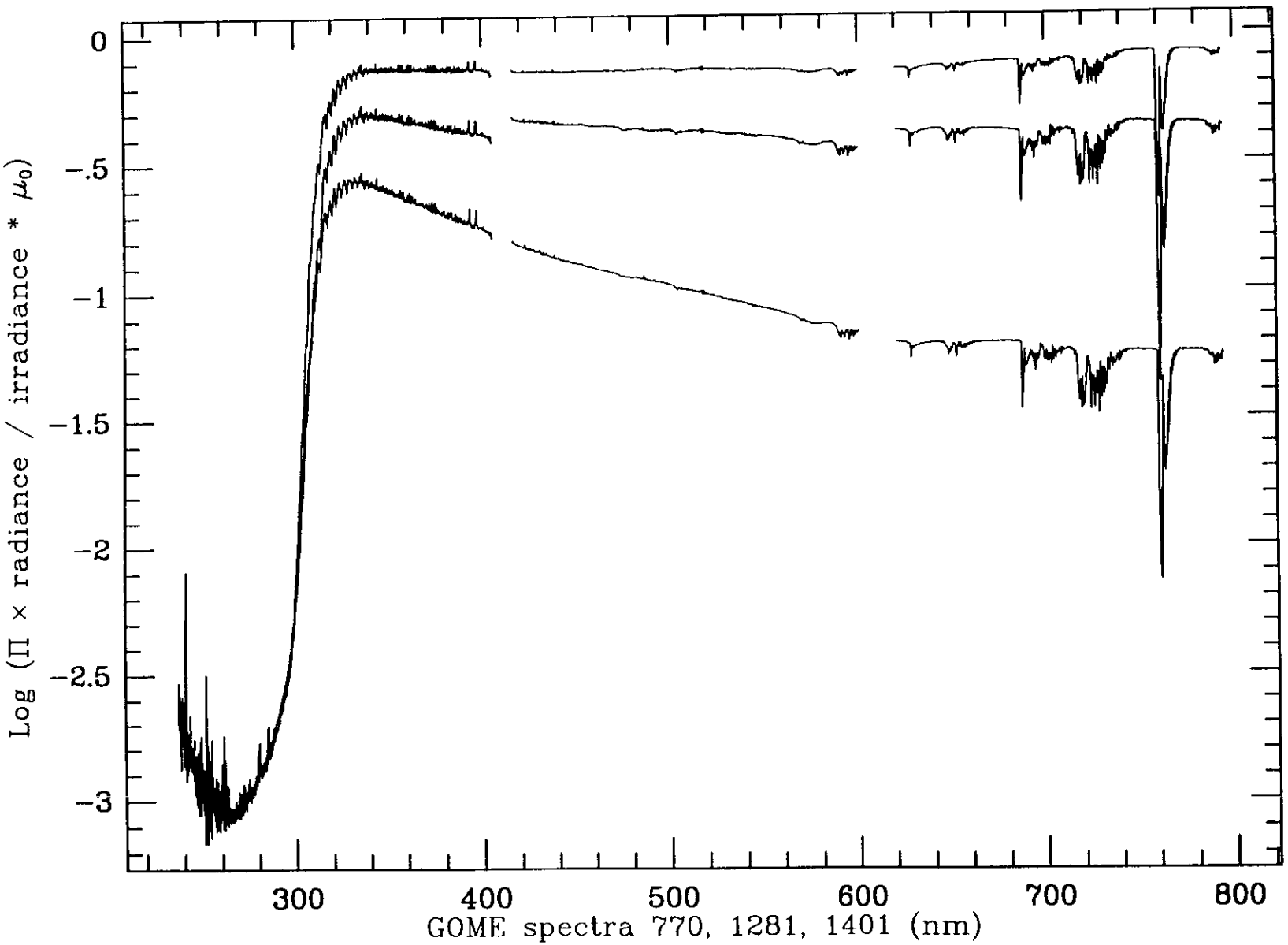
0
-.5
-1
-1.5
-2
-2.5
-3
Log (Π × radiance / irradiance * μ_0)
300
400
500
600
700
800
GOME spectra 770, 1281, 1401 (nm)

Quantities Retrieved from GOME Observations

Species	Retrievable Quantity*	Wavelength (nm)	Notes/Applications
BrO	Column (S)	310-345	
SO_2	Column (T)†	290-310	Industrial pollution, volcanos
OClO	Column (S)‡	320-420	Polar regions in spring
ClO	Column (S)‡	300-310	Polar regions in spring
NO_2	Column (S, T)	300-600	Lightning, combustion
H_2CO	Column (T)†	310-360	Biomass burning, tropical vegetation
O_3	Profile (S, T)	255-350, 480-680	Tropospheric ozone
O_2	Column (S, T)	690, 760	Cloud tops/ boundary layer
O_2-O_2	Column (T)	475, 530, 560, 630	Cloud tops/ boundary layer
H_2O	Column (S, T)	700-790	
NO	Column (S, M)	255-280	Above 40 km in emission

* S = stratosphere; T = troposphere; M = mesosphere
†Observable in regions with relatively high concentrations.
‡Observable in perturbed "O_3 hole" regions.

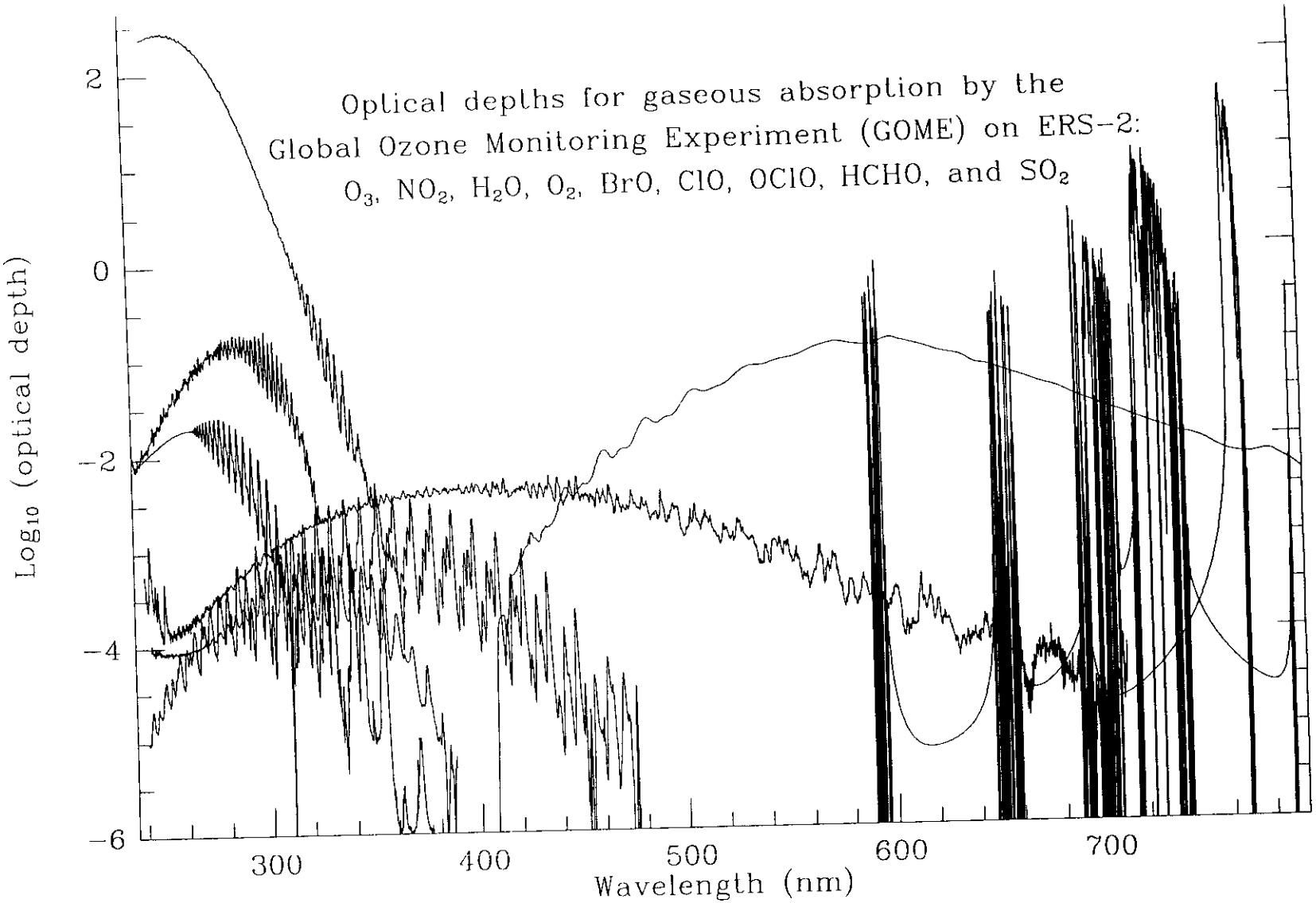
Optical depths for gaseous absorption by the
Global Ozone Monitoring Experiment (GOME) on ERS-2:
O_3, NO_2, H_2O, O_2, BrO, ClO, OClO, HCHO, and SO_2
Log_{10} (optical depth)
2
0
−2
−4
−6
300
400
500
600
700
Wavelength (nm)

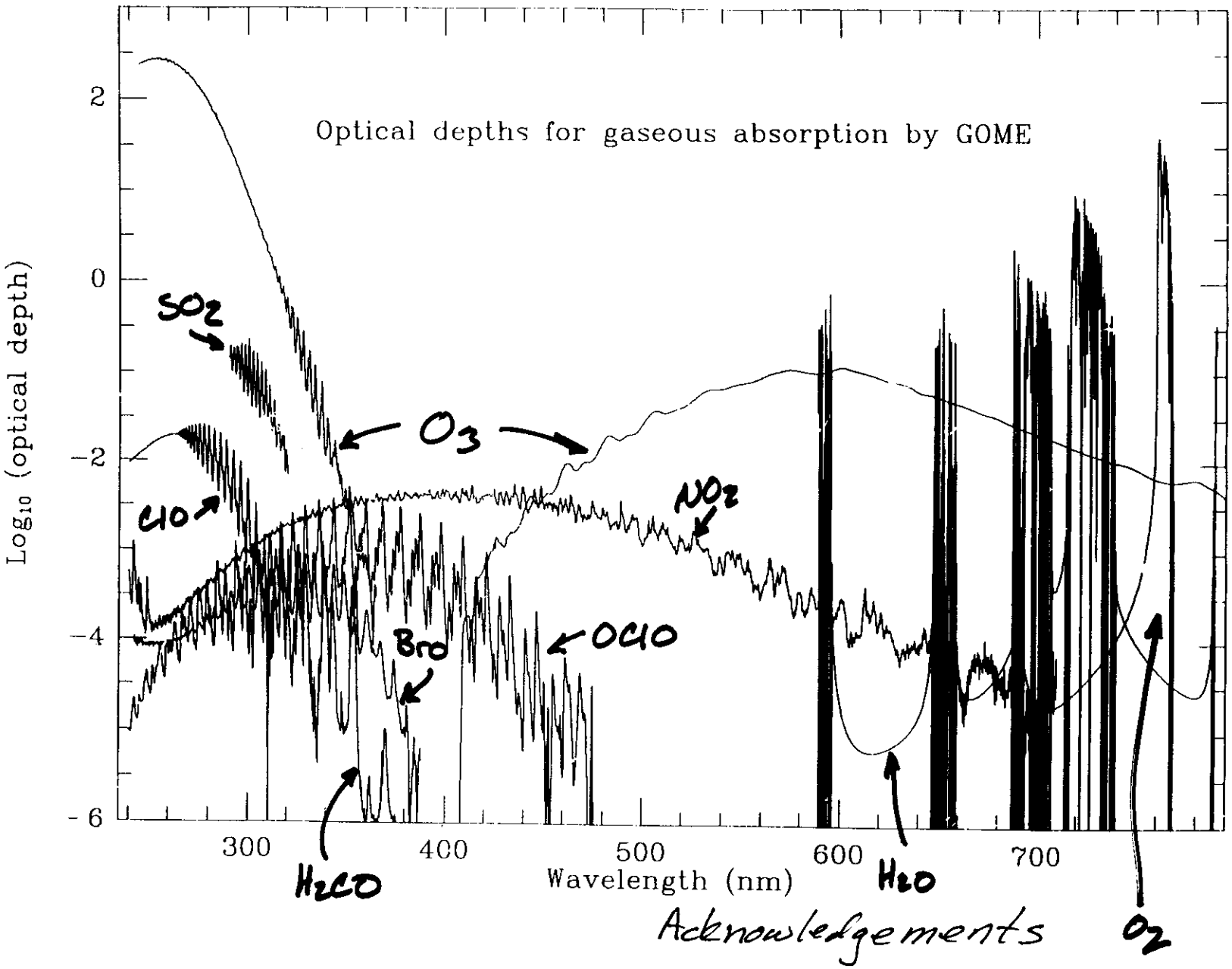

Acknowledgements

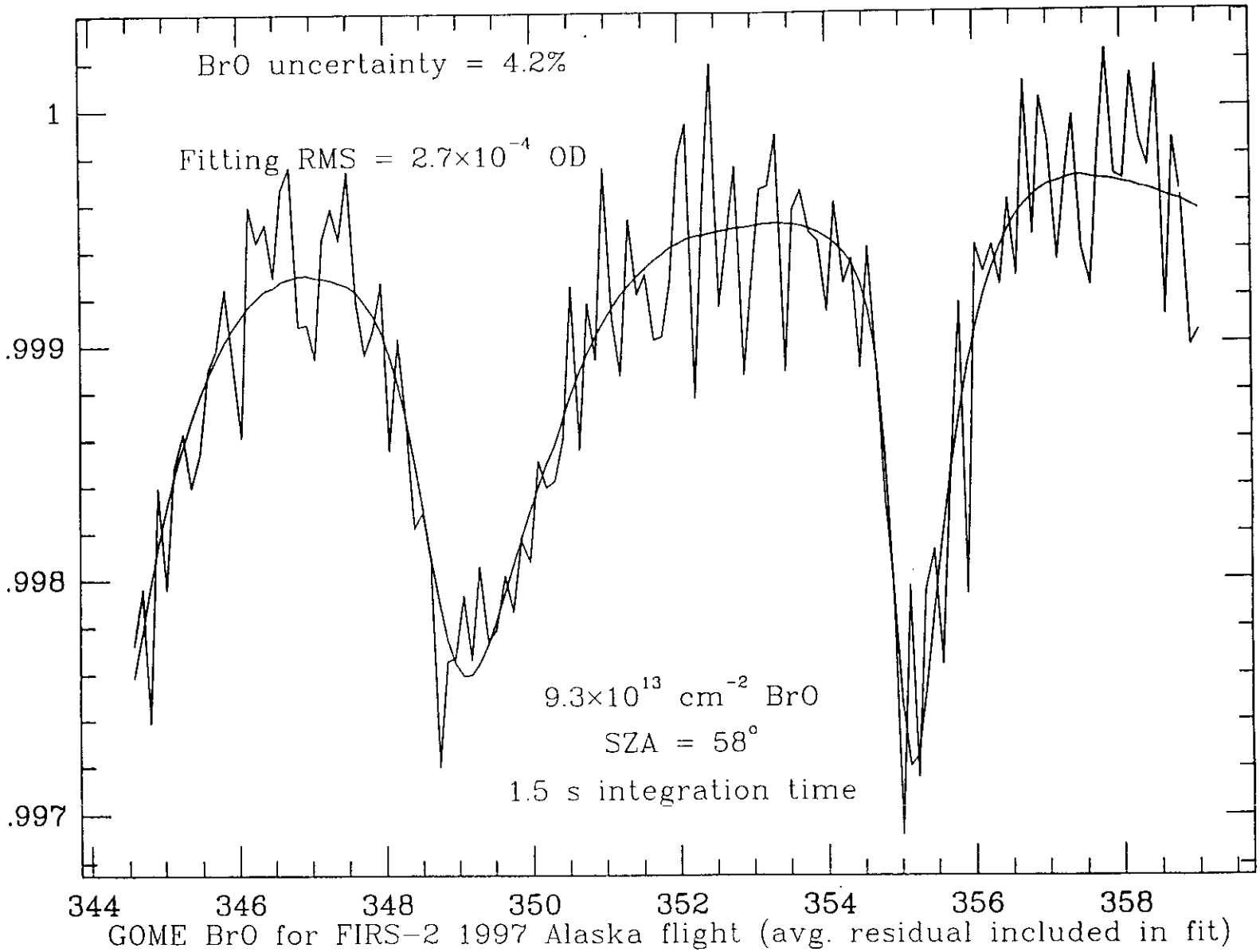

GOME BrO for FIRS-2 1997 Alaska flight (avg. residual included in fit)

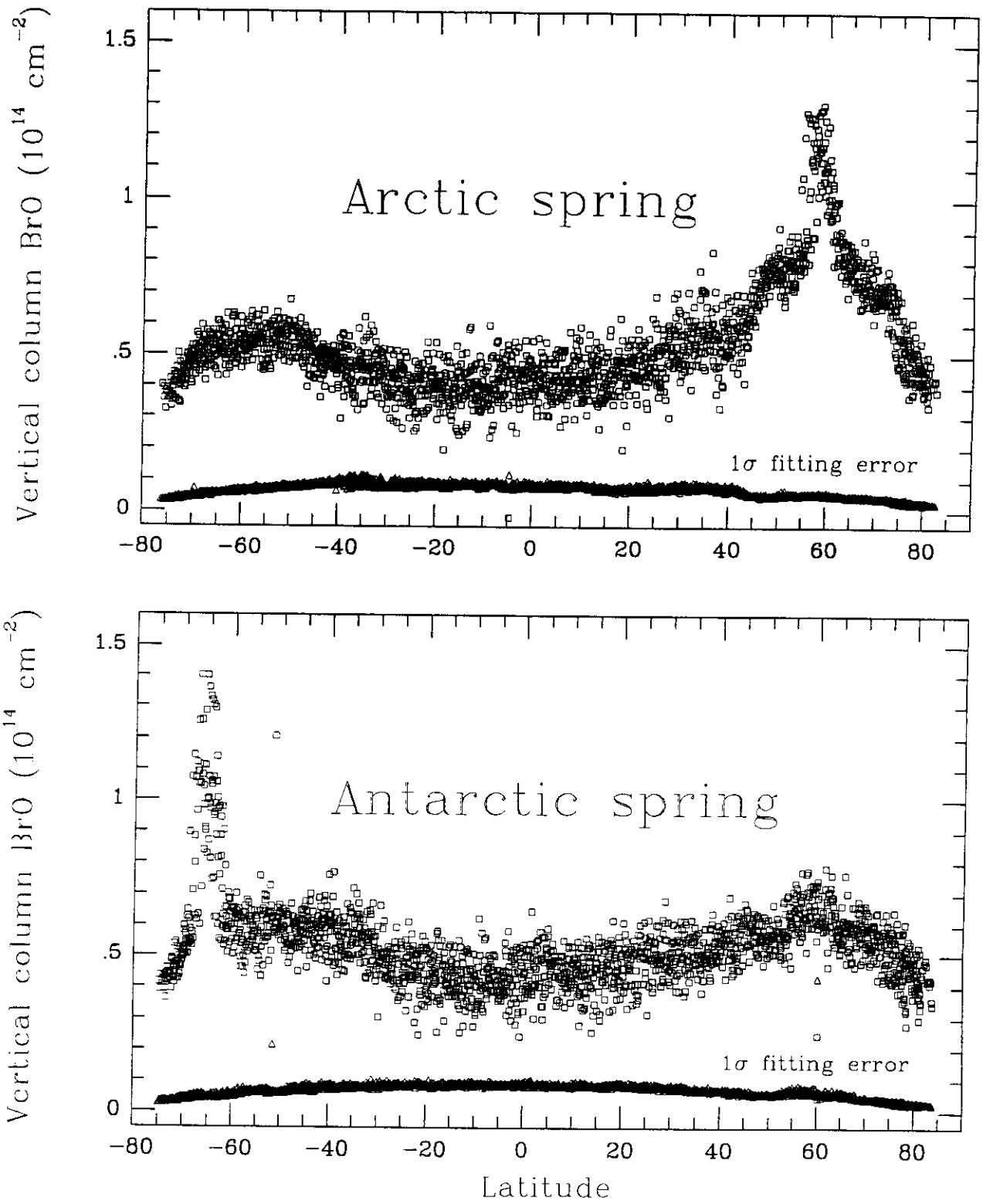
Arctic spring
1σ fitting error
Vertical column BrO (10^{14} cm^{-2})
1.5
1
.5
0
−80
−60
−40
−20
0
20
40
60
80
Antarctic spring
1σ fitting error
Vertical column BrO (10^{14} cm^{-2})
Latitude

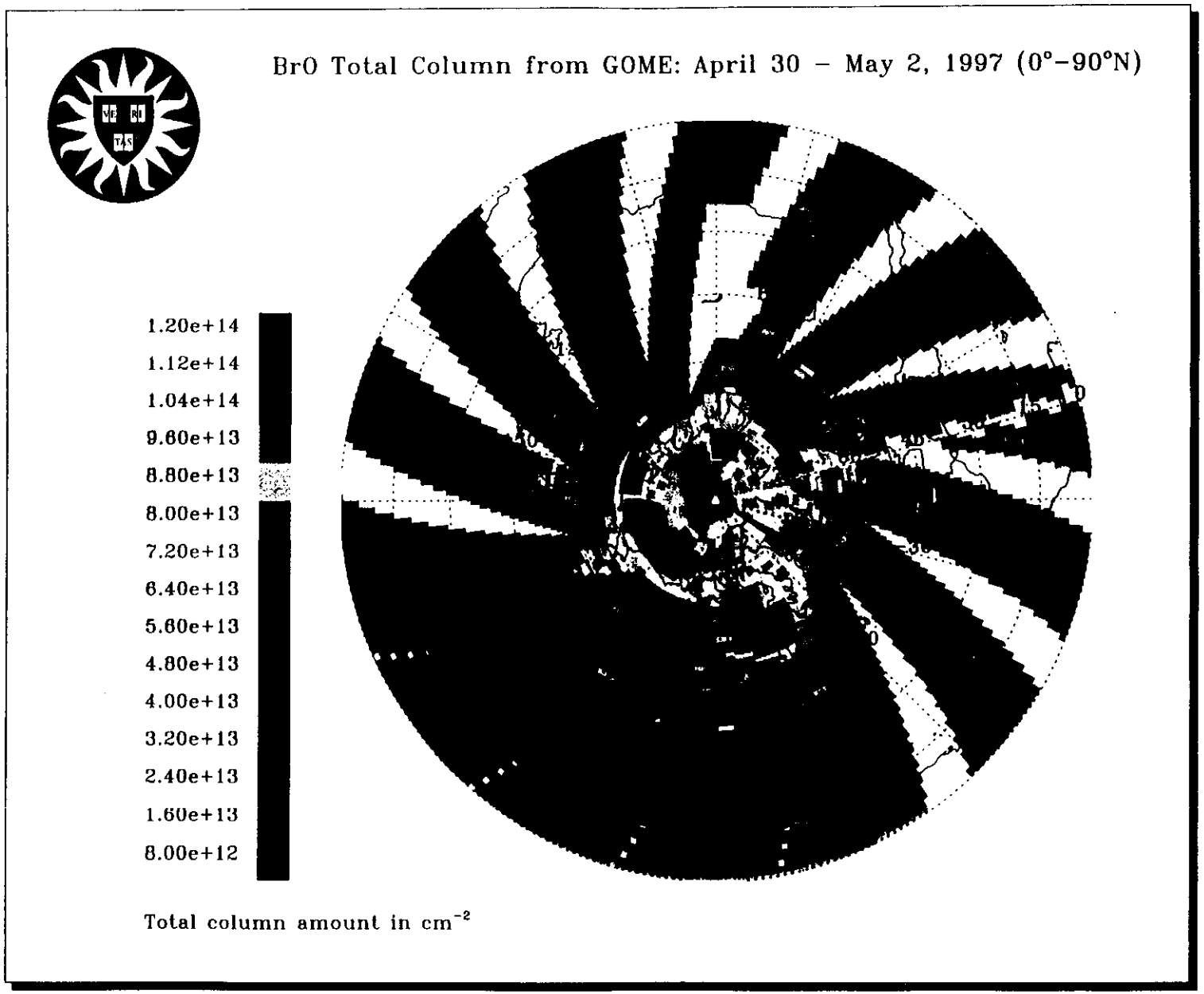
BrO Total Column from GOME: April 30 – May 2, 1997 (0°–90°N)
1.20e+14
1.12e+14
1.04e+14
9.60e+13
8.80e+13
8.00e+13
7.20e+13
6.40e+13
5.60e+13
4.80e+13
4.00e+13
3.20e+13
2.40e+13
1.60e+13
8.00e+12
Total column amount in cm^{-2}

SO_2 Concentration from GOME (Orbit 61204081)

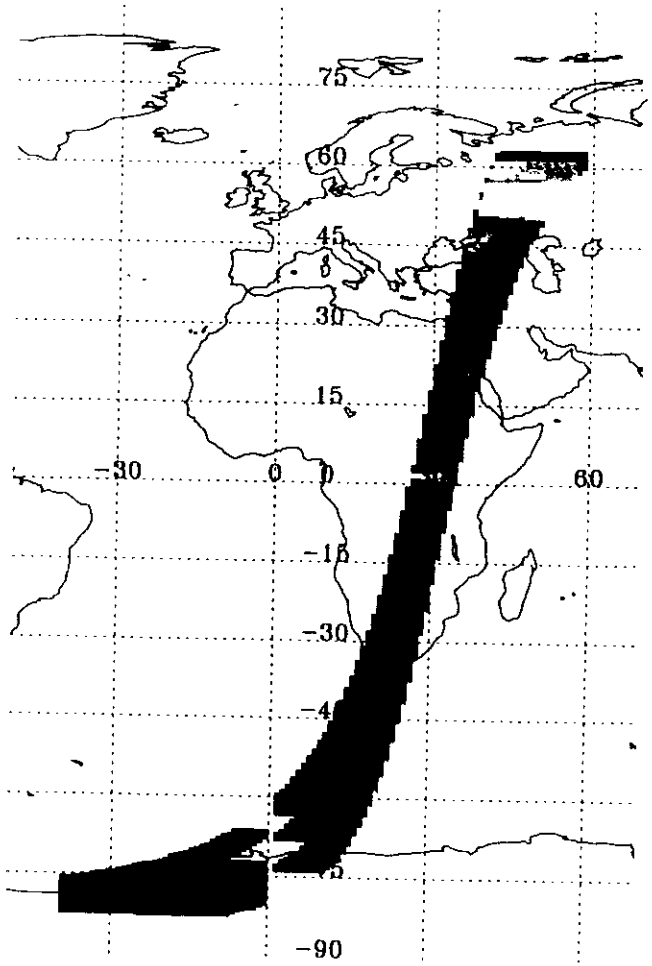

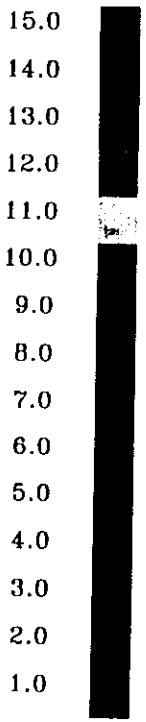

Concentration in DU

Thomas Wagner, Carsten Leue, Ulrich Platt,
University of Heidelberg, Germany

GOME SCD OClO, 19.01.1997

Shape of the polar vortex
(35 PV units at 475K,
ECMWF analysis)

SCD OClO [molec/cm²]

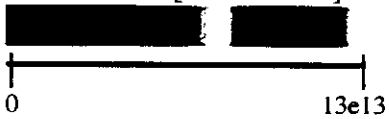

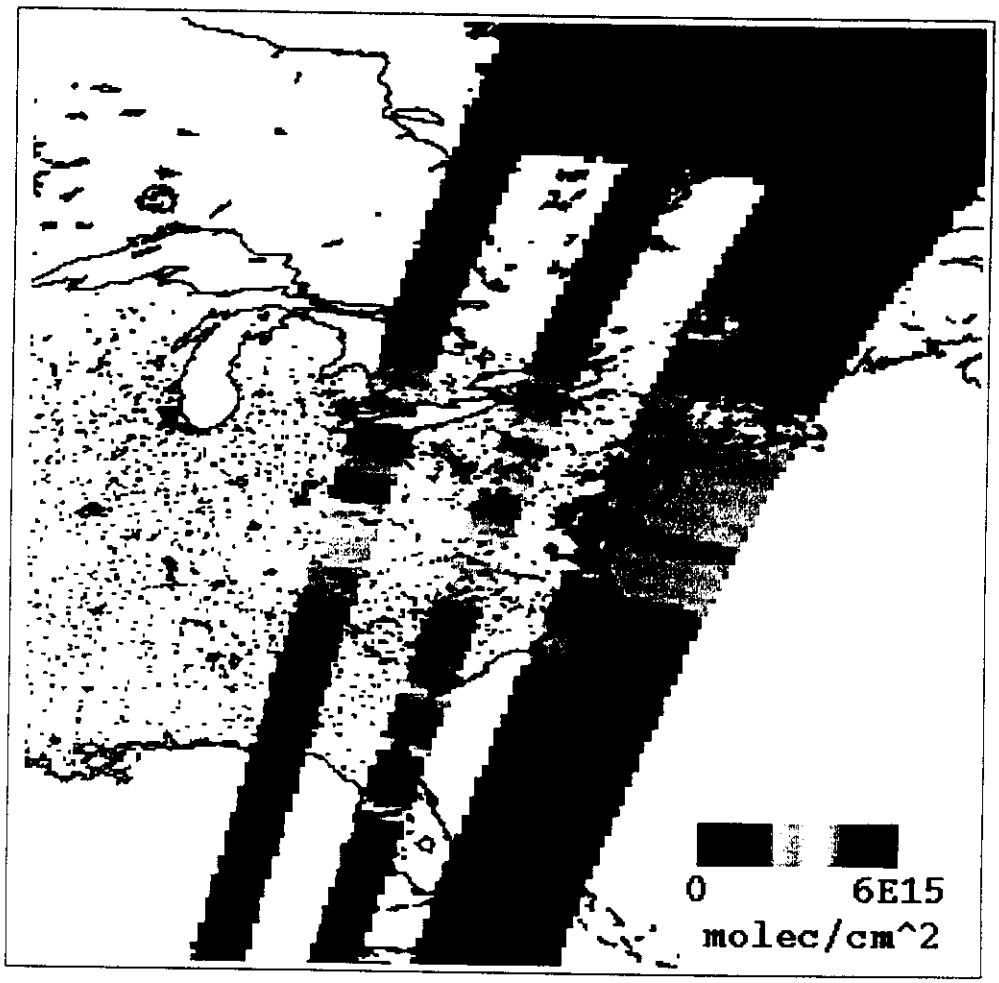

Figure 3: Vertical column content of NO_2 over North America as seen by the GOME instrument on 6 January, 1996. The maximum concentration is around 6×10^{15} mol cm^{-2}

VE RI
TAS
Thomas P. Kurosu, Kelly Chance, and Robert J.D. Spurr
(Harvard–Smithsonian Center for Astrophysics)
The Global Ozone Monitoring Experiment (GOME) onboard the ERS-2 satellite is an across-track multiwavelength spectrometer which measures solar light reflected from the Earth's atmosphere and surface in the UV and visible. CRAG — the Cloud Retrieval Algorithm for GOME — combines spectral threshold tests on GOME's broad-band PMD radiances (~150 nm spectral resolution) with the spectral fitting of parameters derived from GOME's moderately high resolution spectra (0.4
first step
dynamical updating
global threshold sets
PURA
PMD reflectances
GOME fit-
time
PMD subpixel cloud fraction
true-color com-
posite
thresholds are crucial
minimization
O2 A band
basic parameters
three
CRAG results
Ring effect
off-line
native method
reduce
distortion
Fraunhofer spectrum
correlation plot
Clouds
depolarization
spheric radiation
degree of po-
larization p
Lambertian
highly reflecting surfaces
contour plots
Greenland
ice

36-40 km

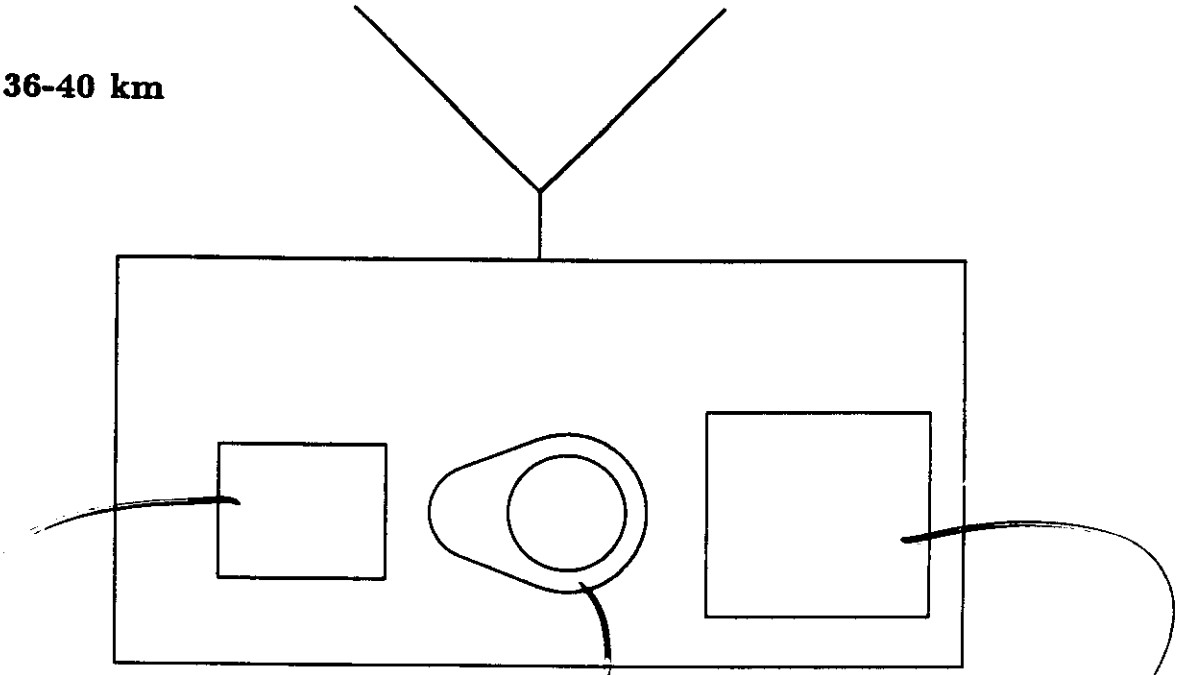

Smithsonian Astrophysical Observatory FIRS-2 Instrument

SAP
0.02° absolute pointing

Telescope
22 cm aperture
IFOV = 0.2° × 1°
$A\Omega = 7 \times 10^{-3}$ cm^2 sr

Double-beam FTS
0.004 cm^{-1} resolution
NEEW $\sim 1 \times 10^{-5}$ cm^{-1}

FIR: 80-210 cm^{-1}
IR: 350-700 cm^{-1}

FIR
O (thermosphere), O_2, O_3
OH, HO_2, H_2O, H_2O_2
HF, HCl, HBr, HOCl, (ClO - from MLS/SLS)
NO_2, CO

IR
HNO_3, $ClNO_3$, N_2O, (N_2O_5 - tentative)
H_2O, HCN
CO_2 (pressure, temperature)

Emission $\Longrightarrow$ Full diurnal coverage
Nine balloon flights, 1987-1994
140 hours of spectra from NASA DC-8, 0-90° N

SAO Investigators

W.A. Traub
K.V. Chance
D.G. Johnson
K.W. Jucks

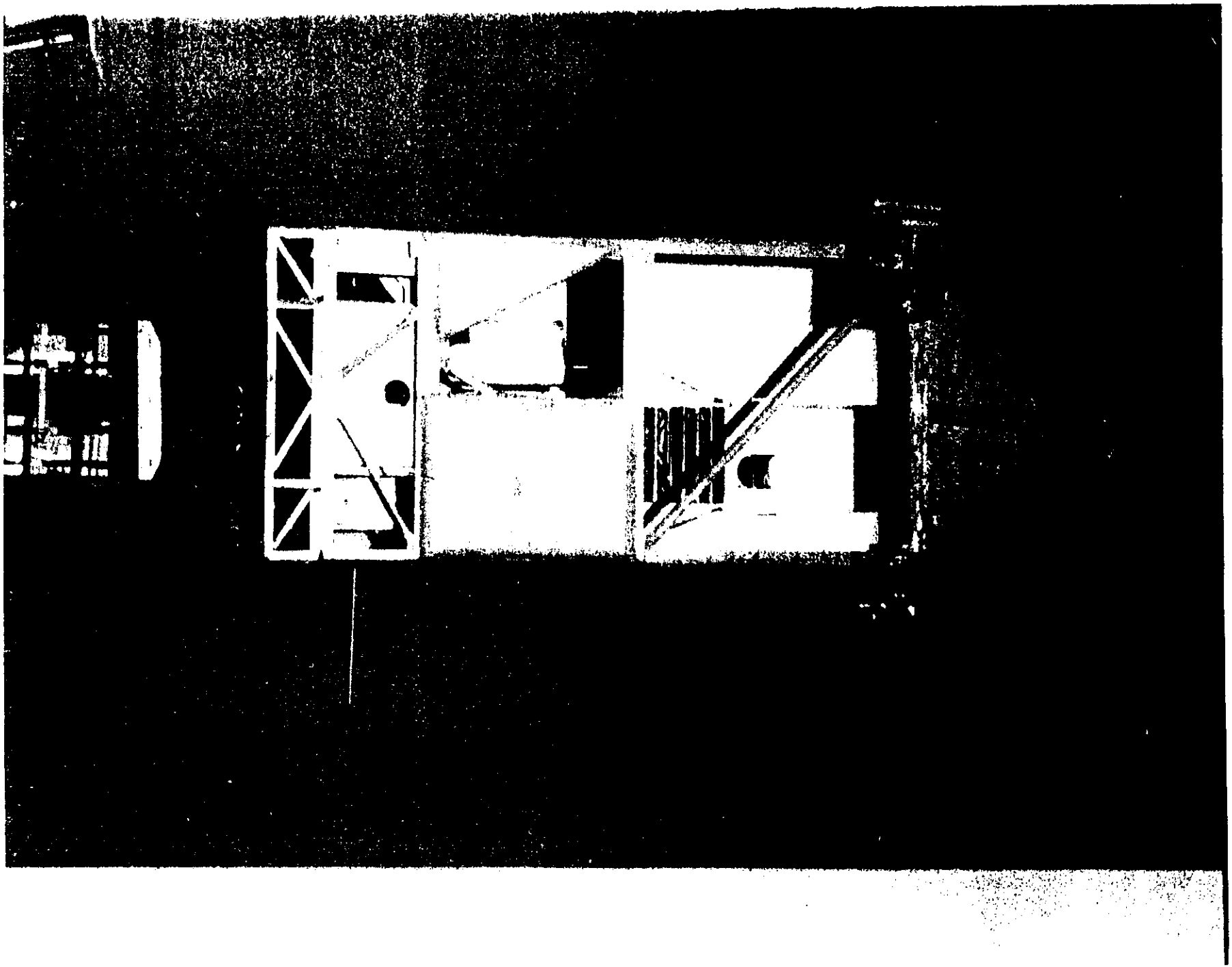

FIRS-2 Measurement Applications

- Atmospheric modeling: FIRS-2 determines details of stratospheric photochemistry, improving predictive capability of models.
- Global warming studies: FIRS-2 determines details of the atmospheric radiative properties of greenhouse gases, especially CO_2.
- Industrial processes: FIRS-2 measures effects of chlorofluorocarbons and halons on the ozone layer.
- Agricultural processes: FIRS-2 measures gaseous by-products of agriculture; nitrous oxide, bromine species resulting from methyl bromide use.

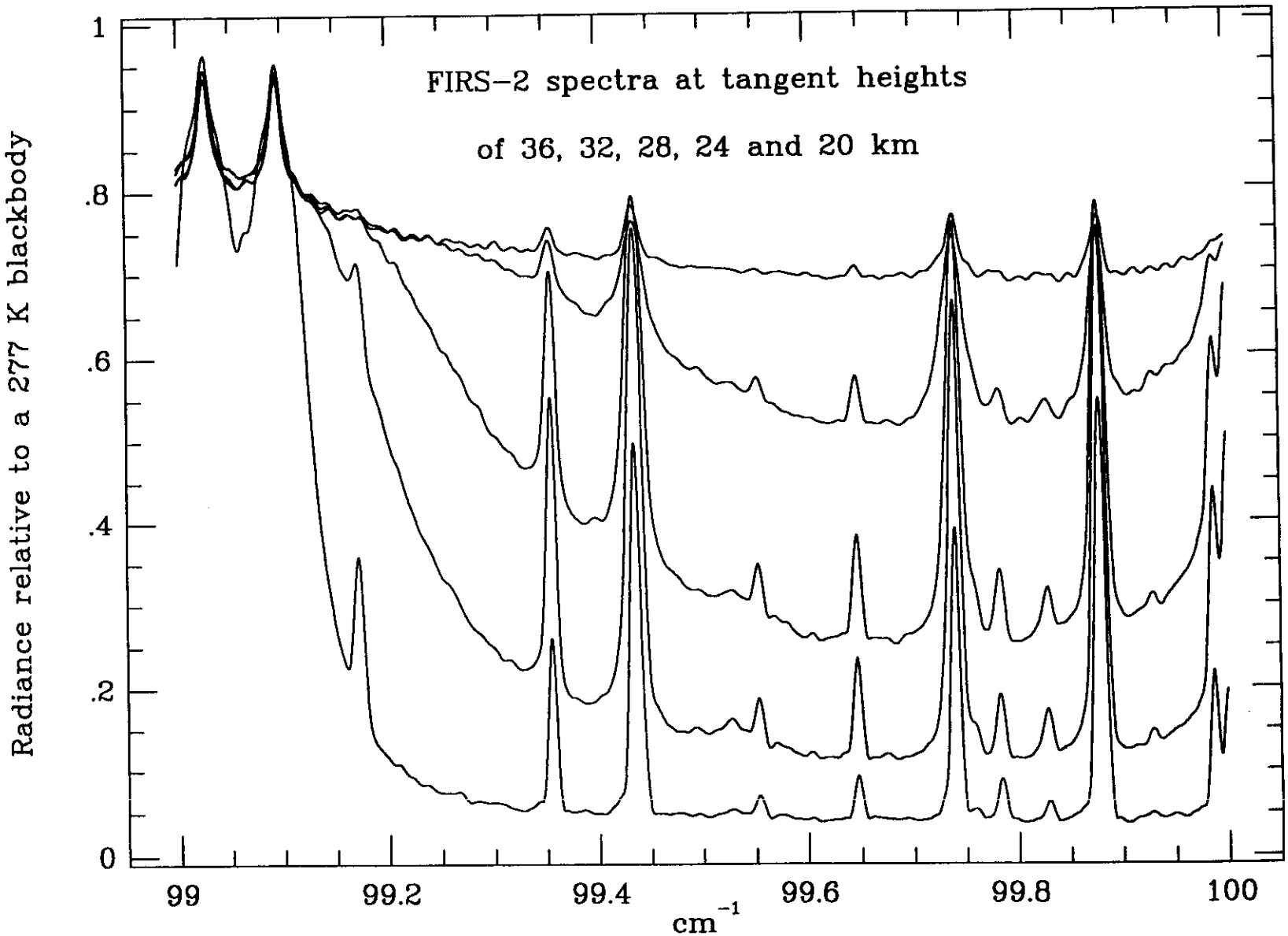
FIRS–2 spectra at tangent heights
of 36, 32, 28, 24 and 20 km
Radiance relative to a 277 K blackbody
1
.8
.6
.4
.2
0
99
99.2
99.4
99.6
99.8
100
cm^{-1}

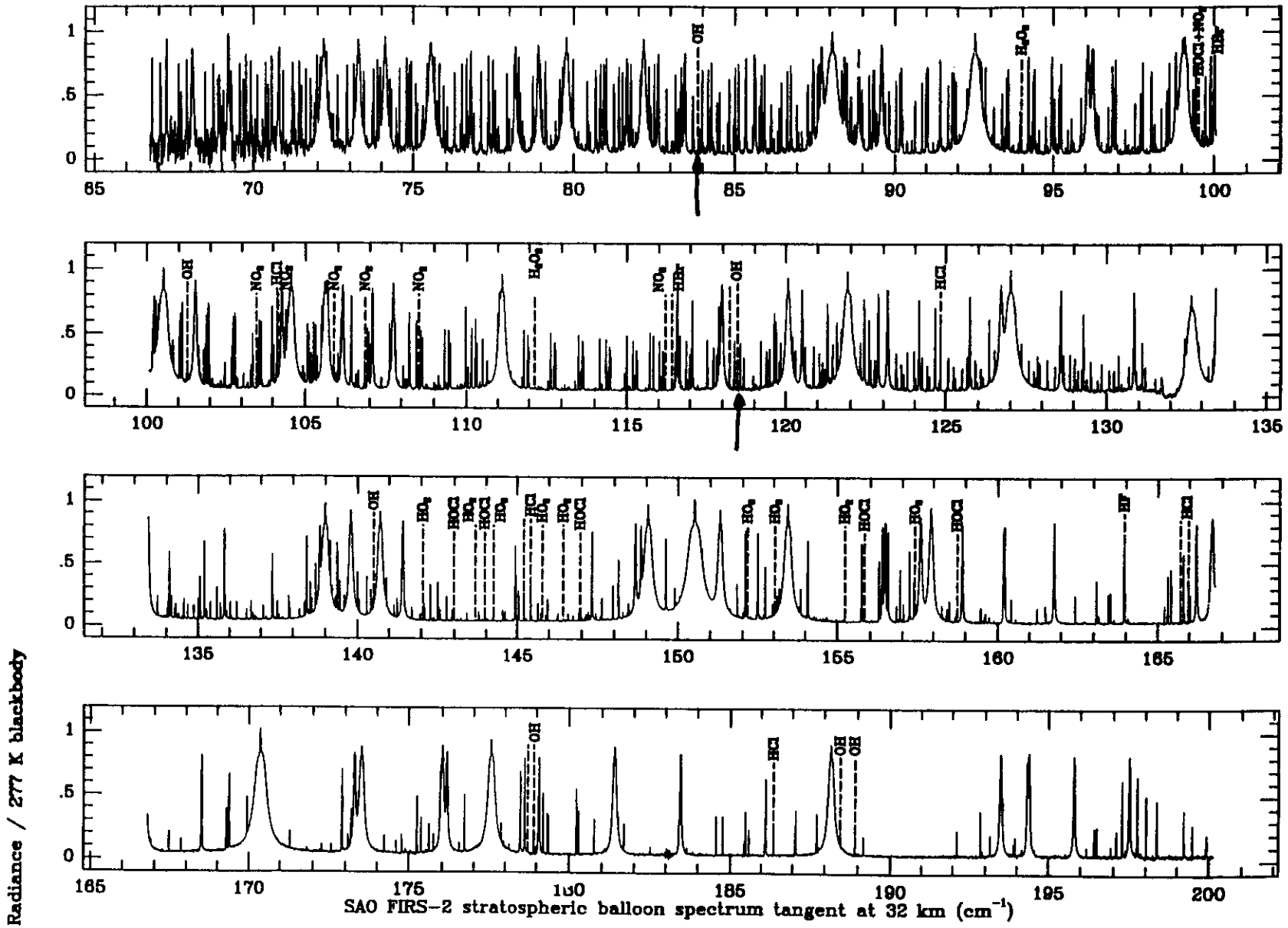
Radiance / 277 K blackbody
SAO FIRS-2 stratospheric balloon spectrum tangent at 32 km (cm^{-1})

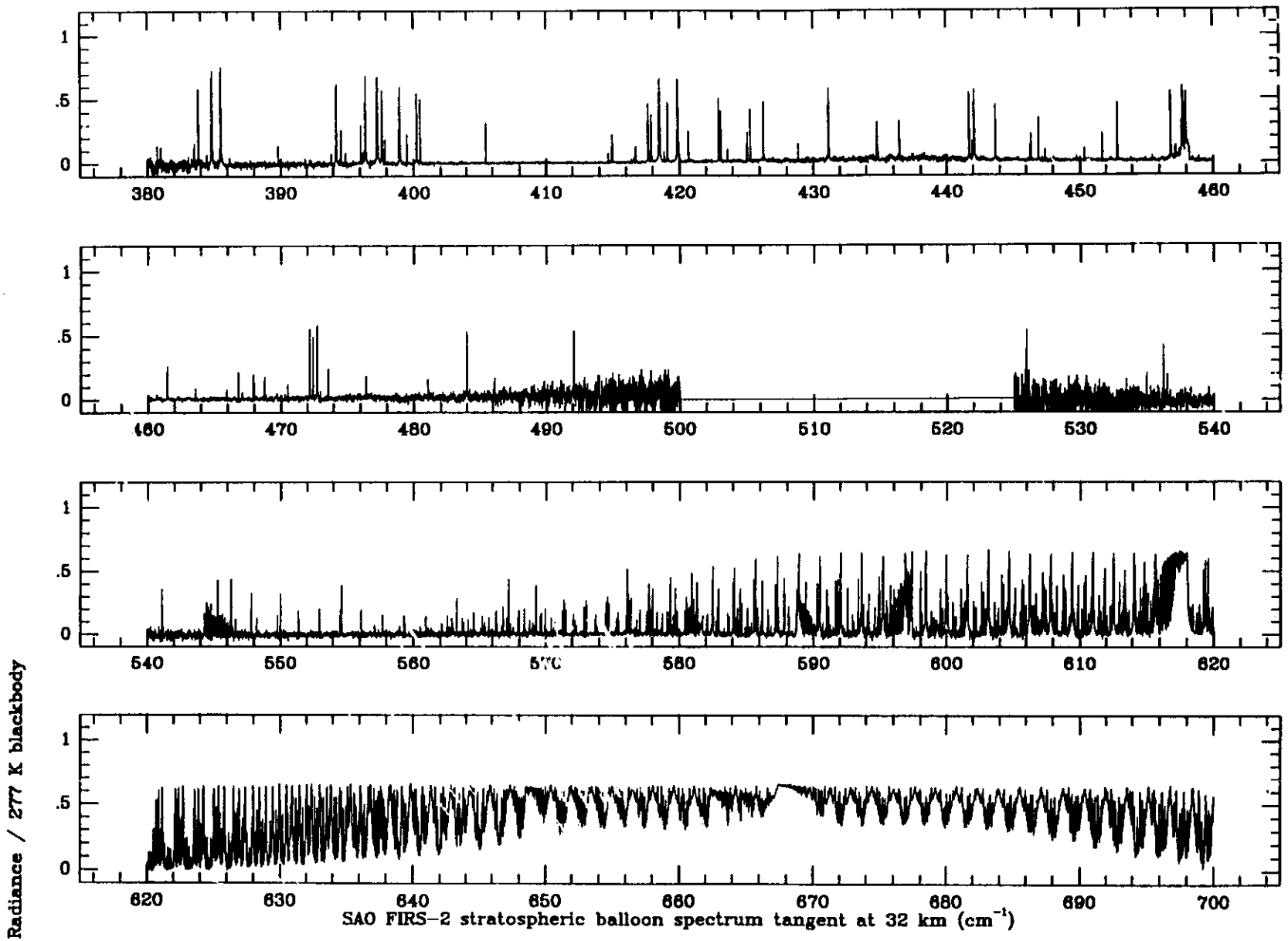
1
.5
0
380
390
400
410
420
430
440
450
460
480
470
490
500
510
520
530
540
550
560
570
580
590
600
610
620
630
640
650
660
670
680
690
700
Radiance / 277 K blackbody
SAO FIRS-2 stratospheric balloon spectrum tangent at 32 km (cm^{-1})

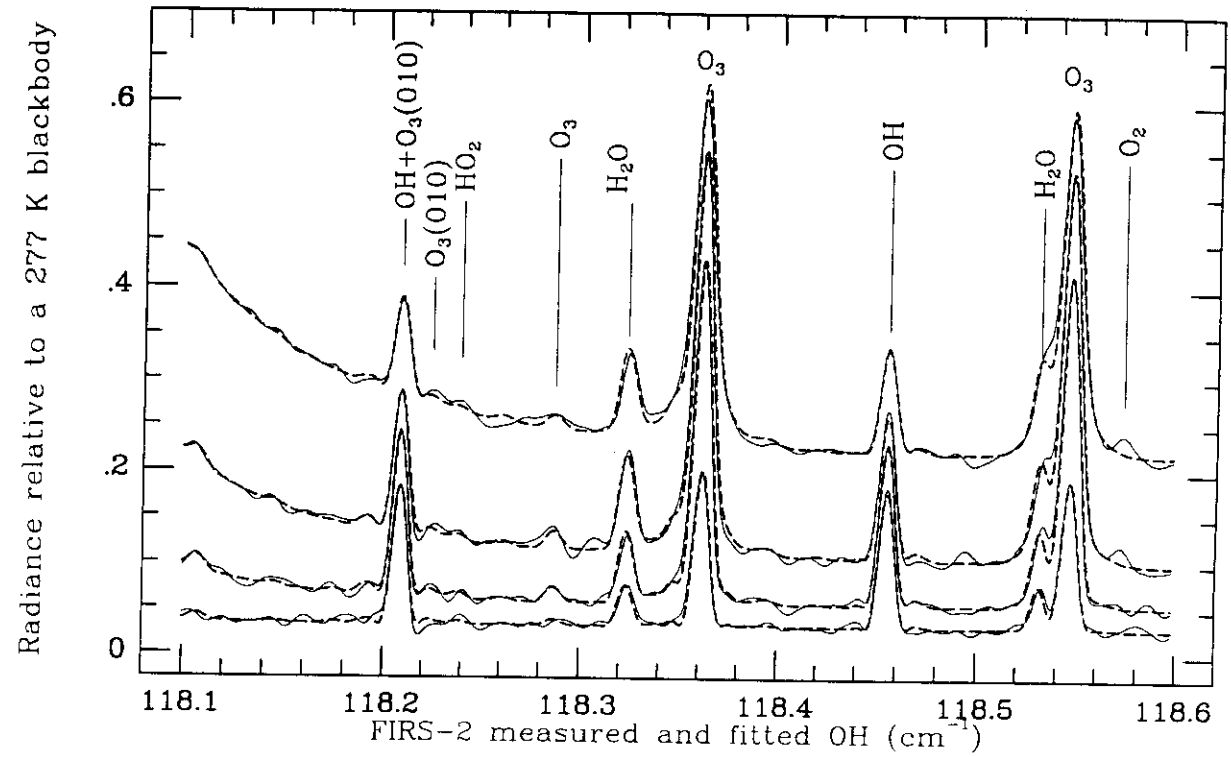
Radiance relative to a 277 K blackbody
.6
.4
.2
0
OH+O3(010)
O3(010)
HO2
O3
H2O
O3
OH
H2O
O3
O2
118.1
118.2
118.3
118.4
118.5
118.6
FIRS-2 measured and fitted OH (cm-1)

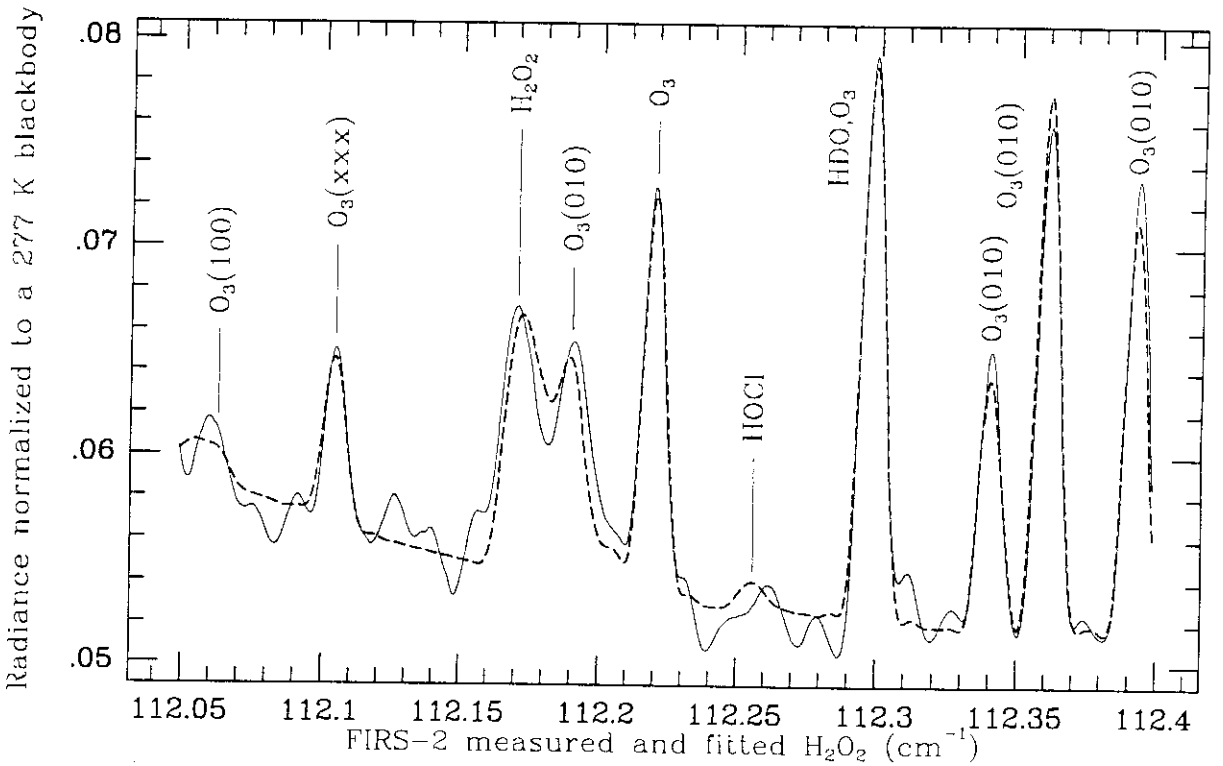
Radiance normalized to a 277 K blackbody
.08
.07
.06
.05
O3(100)
O3(xxx)
H2O2
O3(010)
O3
HOCl
HDO,O3
O3(010)
O3(010)
O3(010)
112.05
112.1
112.15
112.2
112.25
112.3
112.35
112.4
FIRS-2 measured and fitted H2O2 (cm-1)

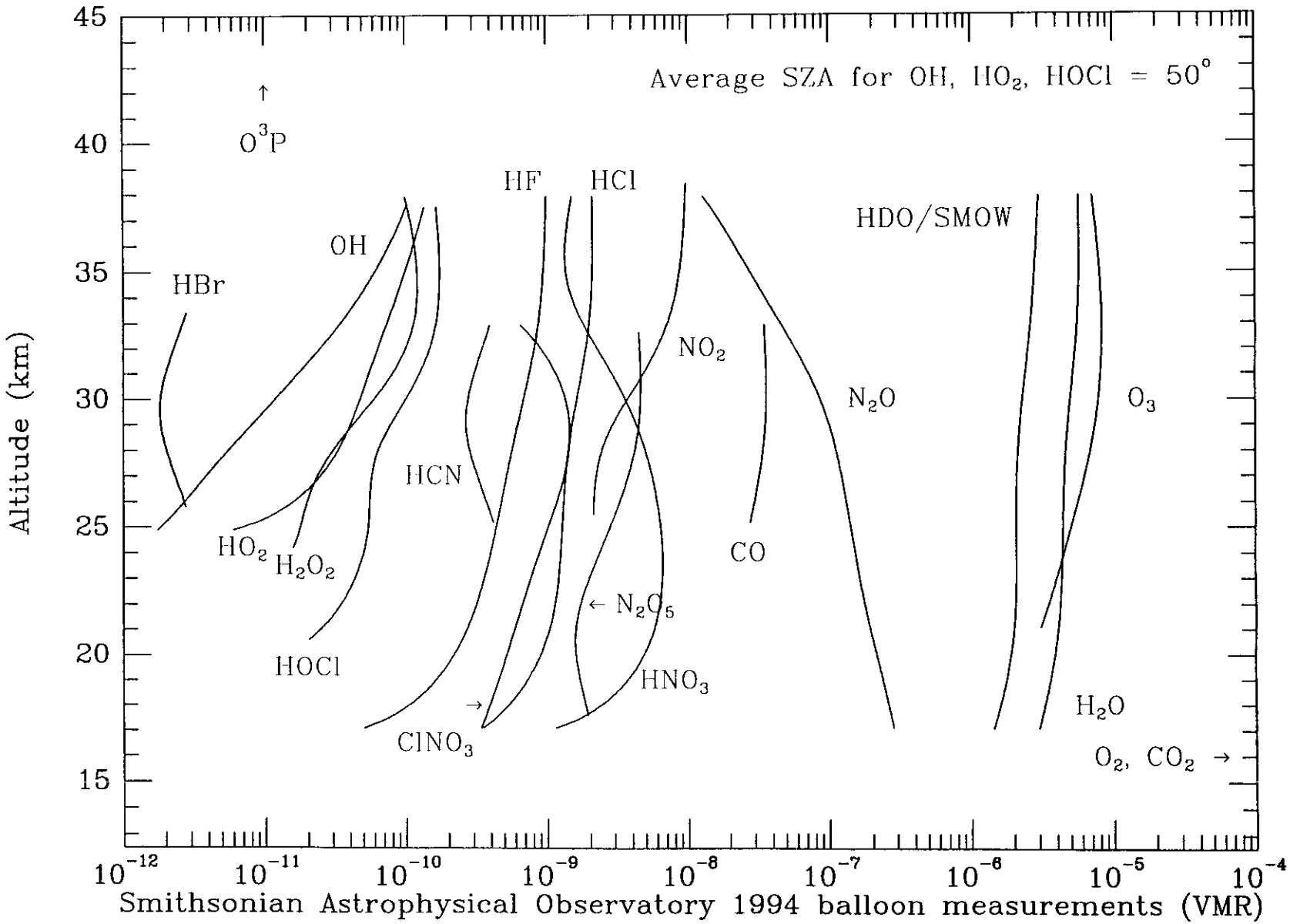
Average SZA for OH, HO_2, HOCl = 50°
O^3P
HF
HCl
HDO/SMOW
OH
HBr
NO_2
N_2O
O_3
HCN
HO_2
H_2O_2
CO
N_2O_5
HOCl
HNO_3
$ClNO_3$
H_2O
O_2, CO_2
Altitude (km)
45
40
35
30
25
20
15
10^{-12}
10^{-11}
10^{-10}
10^{-9}
10^{-8}
10^{-7}
10^{-6}
10^{-5}
10^{-4}
Smithsonian Astrophysical Observatory 1994 balloon measurements (VMR)

Conclusions from FIRS-2 measurements

- We have made the first simultaneous measurement of HO_x, Cl_x, and NO_x species throughout the middle atmosphere. The relative contributions to ozone destruction from the HO_x, NO_x, and Cl_x catalytic cycles are determined from 20-40 km.
- Comprehensive budgets of NO_y, and Cl_y are measured.
- Chlorine budget studies suggest that a small channel exists for production of HCl from ClO + OH and/or ClO + HO_2, diminishing the effectiveness of the Cl_x catalytic cycle in the upper stratosphere.
- O_3 formation and loss rates in the upper stratosphere are now shown to be in balance; under-prediction of stratospheric O_3 above 35 km was a long-standing problem.
- OH near 40 km has been under-predicted.
- HBr measurements provide constraint on bromine budget, Br_x chemistry (in particular, it provides limits to the effectiveness of BrO + HO_2).
- Closely-coupled chemical relationships in the upper stratosphere have been tested, e.g.

$$[HOCl] = k_1[HO_2][ClO]/(j_{HOCl} + k_2[OH])$$

$$[H_2O_2] = k_3[HO_2]^2/(j_{H_2O_2} + k_4[OH])$$

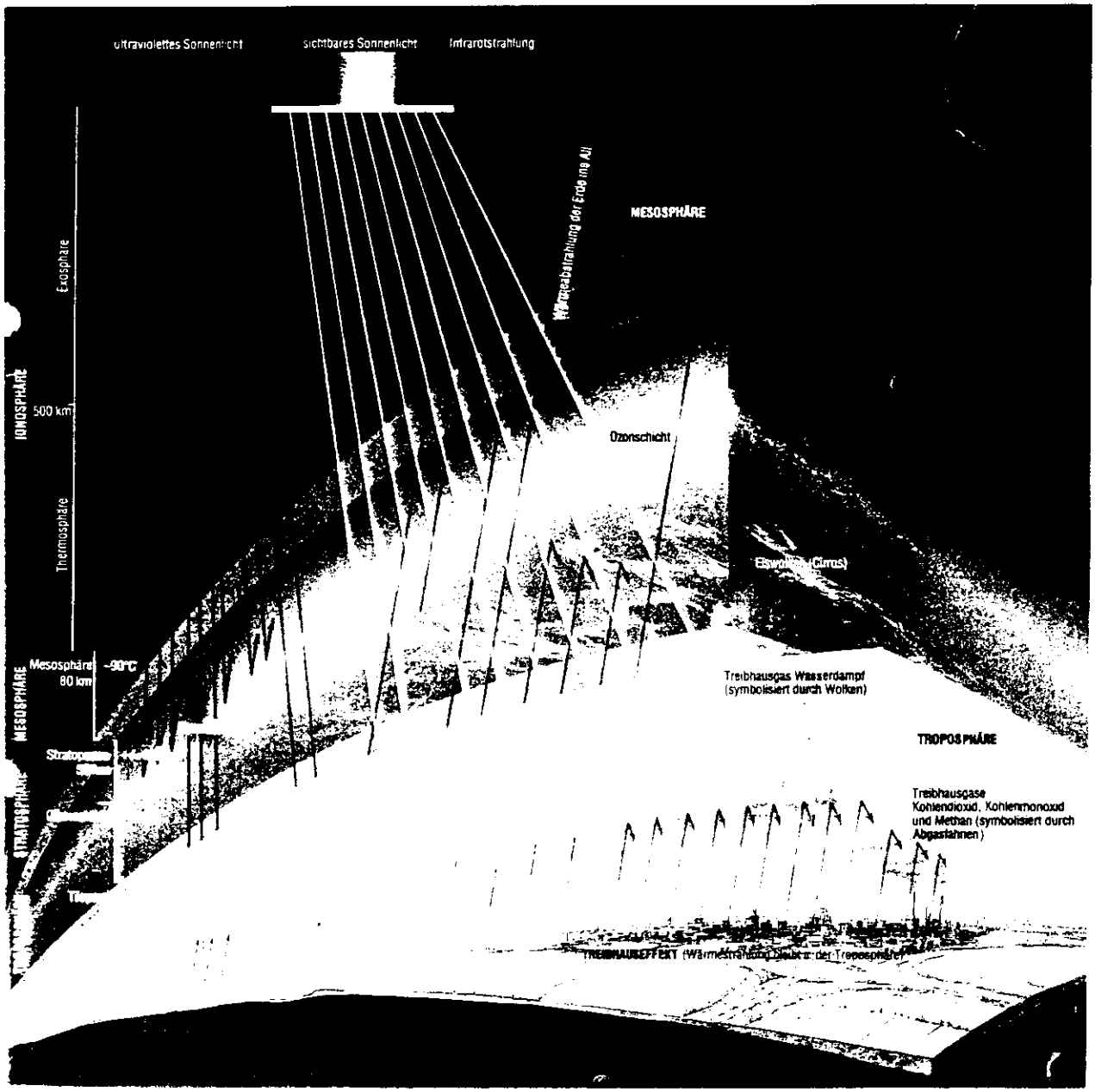
ultraviolettes Sonnenlicht
sichtbares Sonnenlicht
Infrarotstrahlung
Wärmeabstrahlung der Erde ins All
MESOSPHÄRE
Exosphäre
IONOSPHÄRE
500 km
Thermosphäre
Ozonschicht
Eiskristall-Cirrus
Treibhausgas Wasserdampf
(symbolisiert durch Wolken)
TROPOSPHÄRE
Mesosphäre
80 km
~90°C
MESOSPHÄRE
Stratosphäre
STRATOSPHÄRE
Treibhausgase
Kohlendioxid, Kohlenmonoxid
und Methan (symbolisiert durch
Abgasfahnen)
TREIBHAUSEFFEKT (Wärmestrahlung Obere der Troposphäre)

3.2 Vertical structure and some observed dynamical characteristics

The earth's atmosphere is commonly described as a series of layers defined by their thermal characteristics (Fig. 3.1). Specifically, each layer is a region where the change in temperature with respect to altitude has a constant sign. The layers are called "spheres" and the boundary between

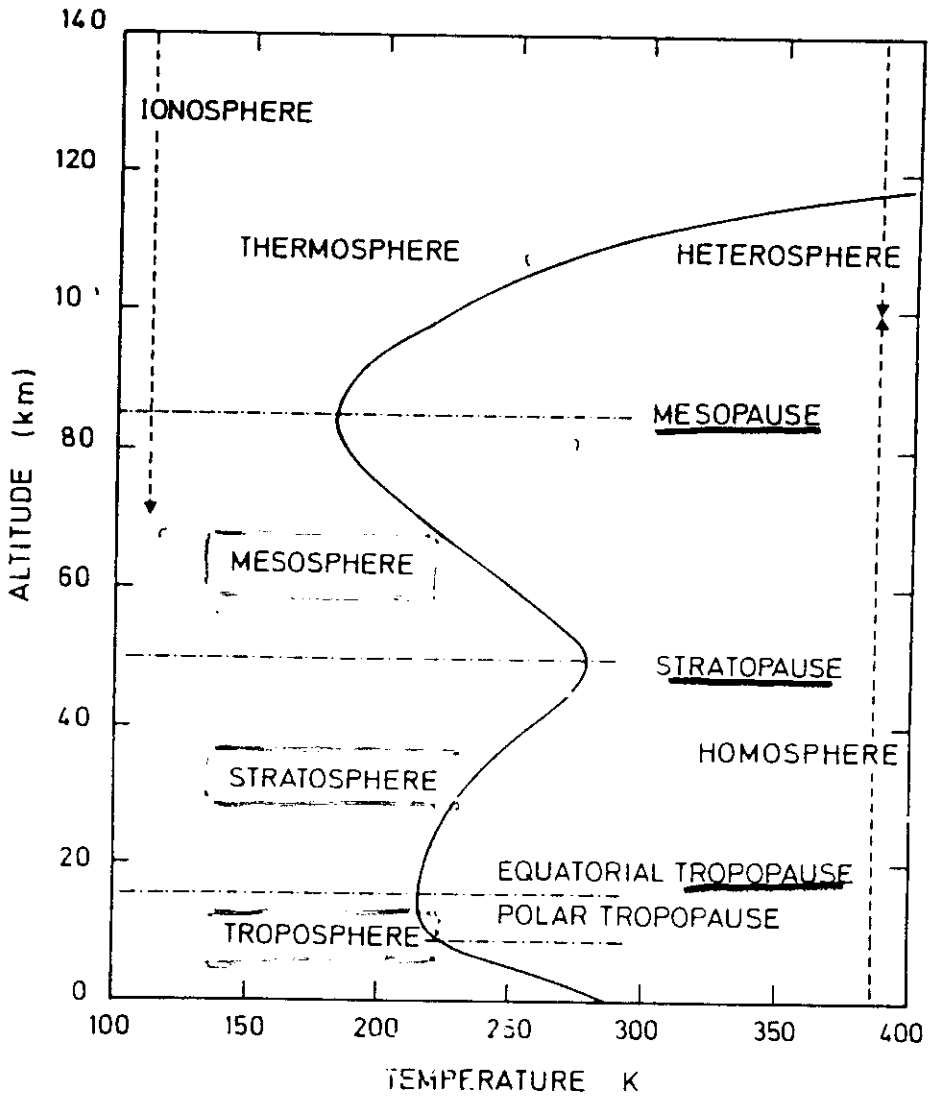

Fig. 3.1. Thermal structure of atmospheric layers.

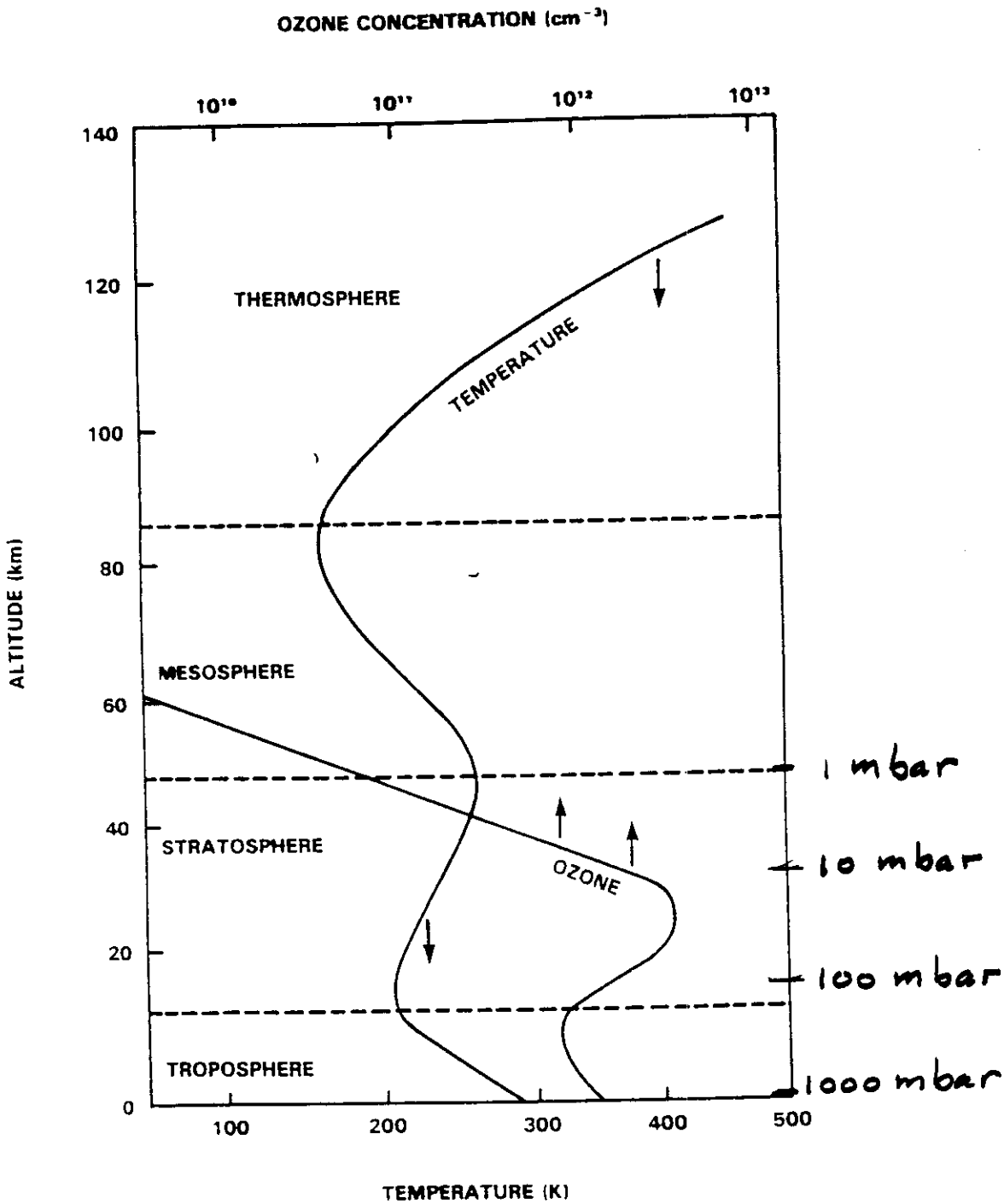

Figure 1. Temperature profile and ozone distribution in the atmosphere.

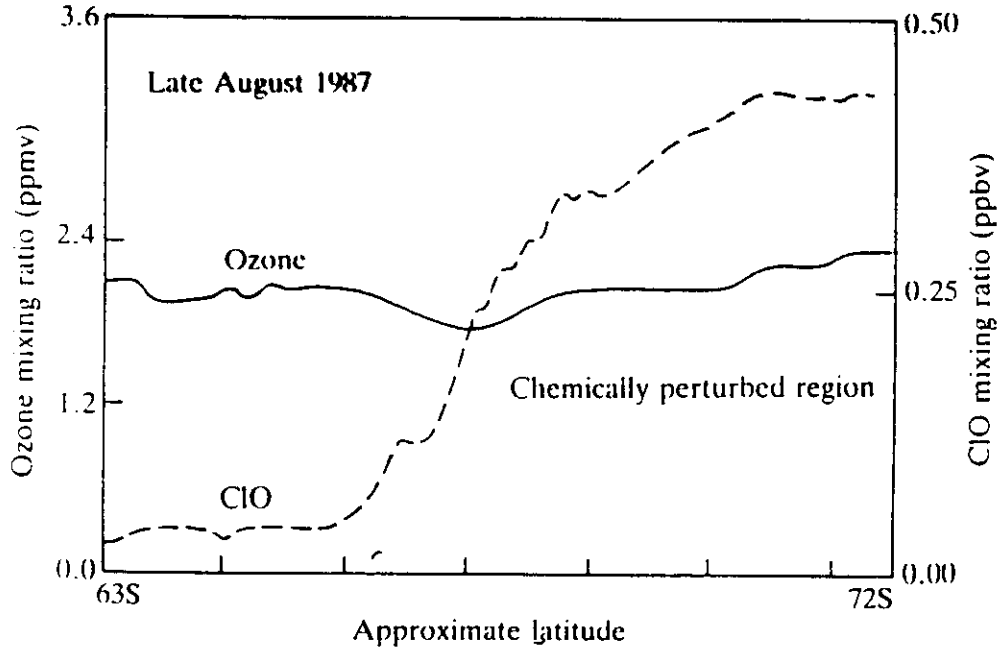

Fig. 4.31. Latitude dependence of ozone and chlorine monoxide (ClO) on entering the chemically perturbed region: late August 1987.

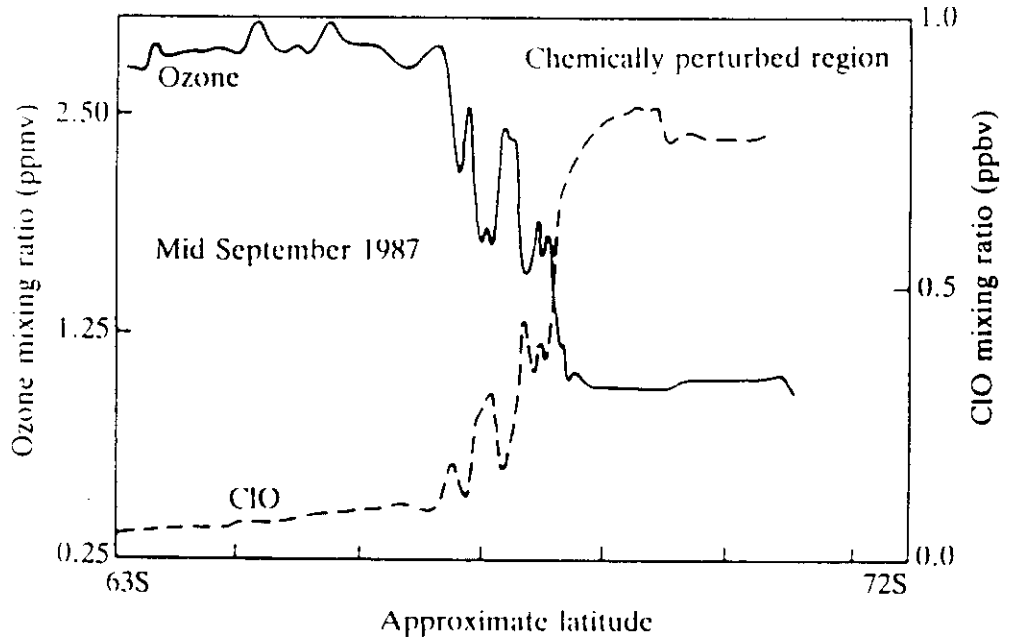

Fig. 4.32. Latitude dependences as for Figure 4.31, but now in mid-September.

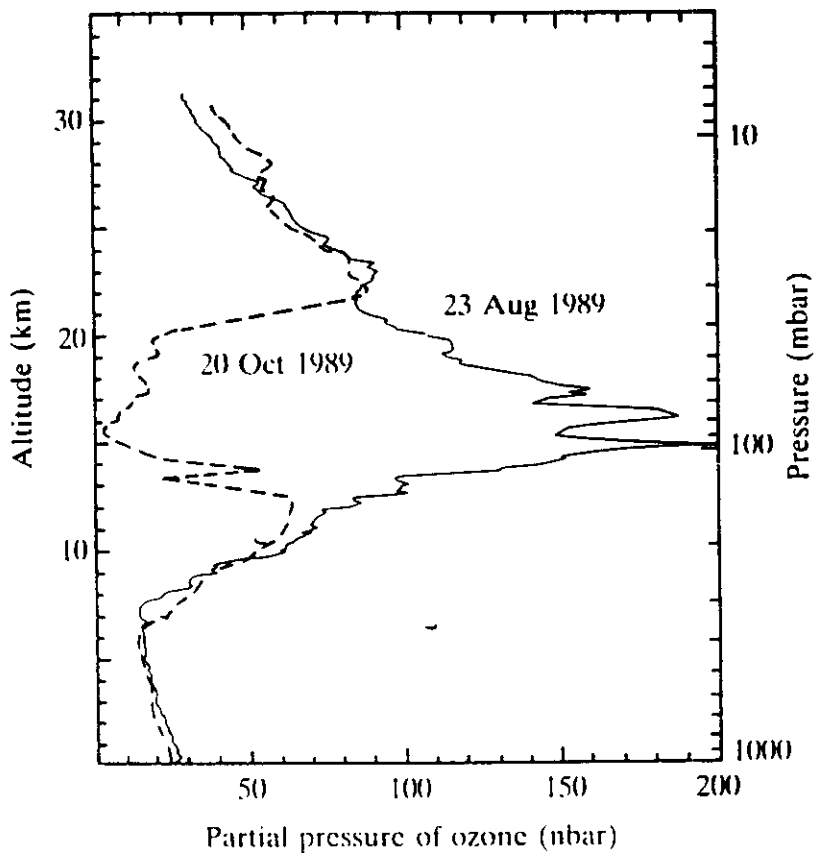

Fig. 4.28. Ozone concentrations over McMurdo Station in August and in October, 1989. These altitude profiles show that the concentrations dropped drastically in the layer between 14 and 22 km, the reduction in ozone being 98% at 15 km. Source: Deshler, T., Hoffmann, D. J., Hereford, J. V., and Sutter, C. B., *Geophys. Res. Letts.* **17**, 151 (1990).

1985. One worrying feature was that rather more sophisticated ozone instruments (see Section 4.6 and Fig. 4.26) such as the Total Ozone Mapping Spectrometer (TOMS) and the Solar Backscattered UltraViolet (SBUV) instrument on the Nimbus 7 satellite had apparently not detected the ozone depletion. However, it subsequently emerged that ozone concentrations as low as those observed by BAS were being rejected from the satellite data on the grounds that they lay outside what was thought to be a 'reasonable' range. When the error was recognized the satellite results were reprocessed. and they confirm the BAS findings.

The satellite TOMS results give a better overall view of ozone over the

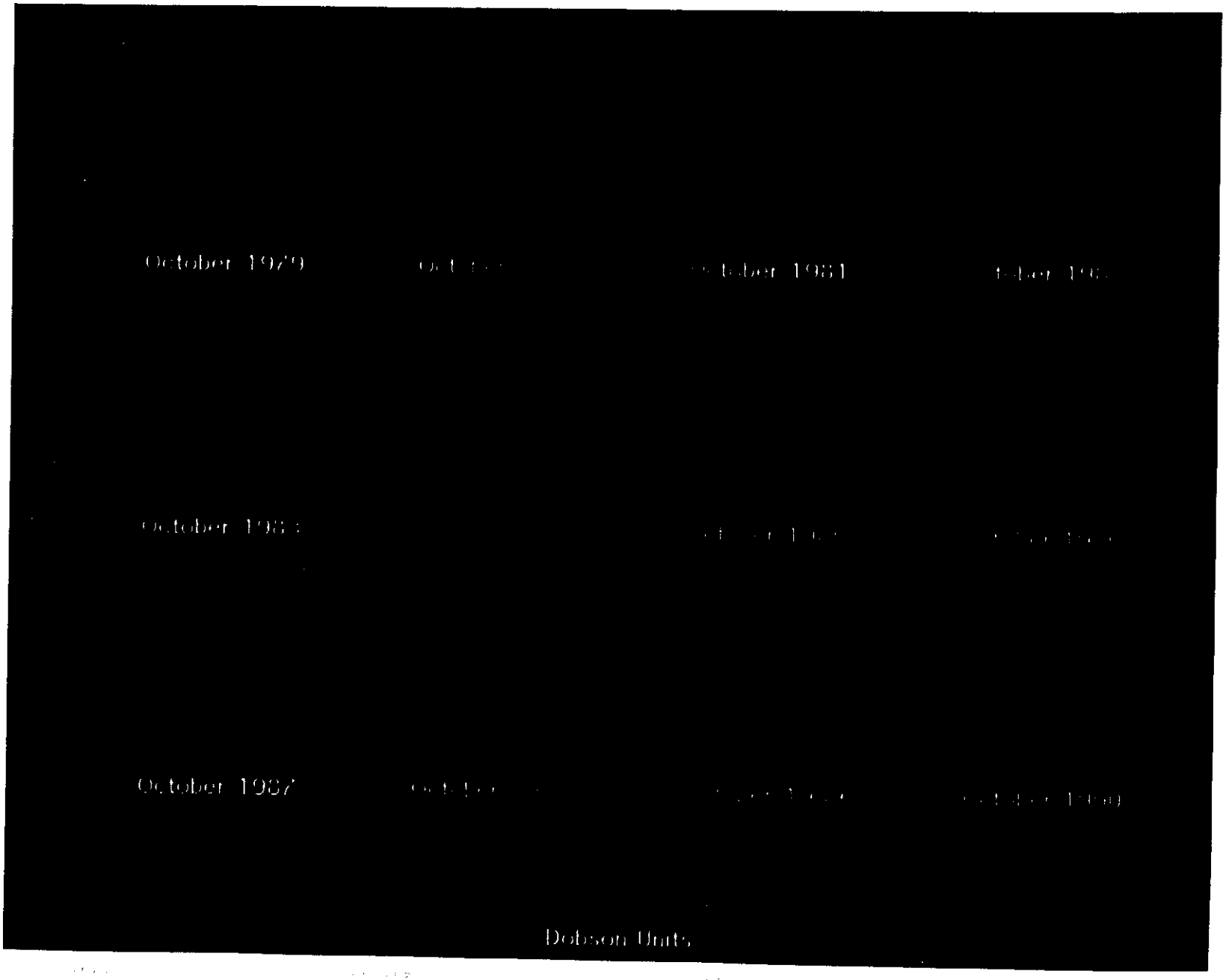
October 1979
October 1981
October 1983
October 1987
Dobson Units

Day 3

(6) REVIEW OF QUANTUM MECHANICS AND SPECTROSCOPY

We consider transitions among molecular states induced by electric dipole moment matrix elements. Weaker transitions (magnetic dipole, electric quadrupole) are due to higher order interactions between the molecules and radiation. A complete derivation of the dipole moment interaction can be found in (e.g.) Bernath; for higher moments see, e.g., Condon and Shortley, Radiation.

Transitions are induced by the perturbation from the interaction of the electric dipole moment vector with the electric field from the radiation:

H' = ... = ... $H' = -\bar{\mu}\cdot\bar{E} = -\bar{\mu}\cdot E_0 \cdot e^{(ikz - i\omega t)}$

where mu = x, y, z

So we solve equations of the form

| |**2 $\left| \int d\tau \, \psi_a \left(-\bar{\mu}\cdot\bar{E}_0 \, e^{(ikz - i\omega t)} \right) \psi_b \right|^2$

By the usual quantum mechanical methods. If you are not familiar with such derivations, I recommend it as a reading exercise. The important quantities are the dipole moment matrix elements; intensities are proportional to:

| |**2 == |<>|**2 = muab**2 $\left| \int d\tau \, \psi_a \mu \psi_b \right|^2 \equiv |\langle a|\mu|b\rangle|^2 = \mu_{ab}^2$

This is the square of the dipole moment matrix element allowing the transition. The matrix element has the dimensions of cm^5 g s_2 (or erg cm^3); (1 debye)**2 = 10-36 erg cm^3

(1 Bohr magneton)**2 = 8.600736e-41 erg cm3

Magnetic dipole moment induced transitions are generally substantially smaller than electric dipole moment transition (they are important in the special cases when the electric dipole moment is 0 by symmetry, and when the molecule possesses a net electronic angular momentum - e.g., O2).

Rotational transitions

For rotational transitions, without complication from electronic or nuclear interactions,

|mu u>l|**2 = mu0**2 * Ju / (2Ju + 1) $\mu_{ul}^2 = \mu_0^2 \frac{J_u}{2J_u + 1}$

Where mu0 is the static dipole moment and the selection rule is DJ = +-1. Remember that the degeneracies of these rotational transitions are 2J+1. Detailed balance requires that g_l |lu|**2 = g_u |ul|**2

|mu|**2 (do u>l and l>u) to illustrate detailed balance:

$(2J+1)\mu^2 I_u = (2J+1)\mu_u^2 I$

$\mu^2 I_u = \mu_0^2 \frac{(J+1)}{(2J+1)}$

For this simple example, the rotational energy levels (ignoring centrifugal distortion effects) are B*J*(J+1), where B is the rotational constant, proportional to the inverse of the moment of inertia: B = h_bar**2 / 2*I $B = \hbar^2/2I$

The spacing of the rotational transitions is thus 2B (illustrate with ladder).

Rotational constants vary from substantially less than 1 cm-1, for heavier molecules, to 20+ cm-1 for the lightest (hydrogenic) molecules.

Needless to say, rotational spectra (positions and intensities) get much more complicated very quickly: show example of the term values for HO2 and mention that it is an asymmetric top with electronic spin angular momentum.

The important concepts to carry away are that rotational transitions are important in atmospheric spectra in the microwave through far infrared regions (less than about 200 cm-1); that they are fairly well characterized in terms of positions and intensities for the important atmospheric species.

Vibrational transitions

These are vibrations along the bond axes of the molecules. Their study is an immensely complicated field which we won't broach except for a few convenient topics. For the simplest case - again, a diatomic molecule - the vibrations occur in a potential well describing the energy versus the separation of the two atoms:

draw a potential well, energy levels, and note fundamental, overtone and hot band transitions.

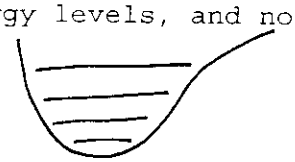

Vibrational transitions are almost synonymous with the infrared. They range in energies from, usually, several hundred to several thousand cm-1. Note that when I construct a ladder of infrared term values and transitions, I must put in the rotational sub-levels; each vibrational state has a full manifold of rotational states included. Transitions almost always include a change in rotational state along with a change in vibrational state.

draw the ladder; indicate for polar diatomic the selection rules (P, R, no Q)

draw the resulting spectrum of the fundamental band, with regular P, R spacing.

Electronic transitions

These are transitions among different electronic states of the molecules; they occur at higher energies than rotations or vibrations - generally in the visible and UV, with some occurring down into the infrared. Electronic transitions each have a set of vibrational sublevels, each of which has a set of rotational sublevels.

Example of potential curves - O2 - showing atmospheric bands. Also show synthesis (mention clouds) and the bands in a GOME spectrum.

We need to mention a process often seen in electronic transitions that often affects their atmospheric spectra - predissociation. Copy figure from BS p. 26; the excited state can decay back to the ground state or it can cross nonradiatively into the repulsive state, falling apart as separated atoms. The effect of this extra decay channel shortens the lifetime of the excited state which, as we shall see, broadens the spectrum. Predissociation can smooth out the rotational structure and even the vibrational structure of an electronic state.

BS

* ~~show example of predissociation in the ClO spectrum~~ not predissociation!

So, we have these transition types, and a vast, complex field of spectroscopy describing how and where they occur. We need to unify the situation so that we can address how molecules are measured quantitatively in the atmosphere.

Quantitative Spectroscopy $S(cm) = \frac{8\pi^3}{3hc} \sigma \left(e^{-E_l/kT} - e^{-E_u/kT}\right) \frac{g_u}{Q} |\mu_{ul}|^2$

Intensity - the basic amount of absorbing or emitting per molecule:

S (cm) = ... n versions of equation, see other sheet.

This is the basic and appropriate unit for intensities in most applications of atmospheric spectroscopy, from microwave through UV as long as we are describing separate spectroscopic lines. Any other creatures, such as oscillator strengths, Einstein A coefficient, or dipole moments should immediately be converted. For example:

Einstein A coefficients - other sheet

Aside on population fractions and partition functions:

Remember that Q = sum .... and Q_tot = Q_rot * Q_vib * Q_el * ....

Line intensities are tabulated at standard temperatures (often 296 K or 300 K); they need to be converted to intensities at different temperatures for use in atmospheric calculations.

For rotational transitions of linear molecules, the approximation Q_rot = T / (c2 * B) is often useful for conversion, when re-summing is inappropriate.

For asymmetric top molecules - see sheet,

where gamma is the "symmetry number" (=1 if no obvious symmetry is present in the molecule). gamma = the number of values of he rotational coordinates corresponding to indistinguishable orientations of the molecule.

Now that we have intensities, we need to see how they manifest themselves in the spectrum - how they are related to optical depth and lineshapes and ultimately the spectrum itself.

Go back to our picture of propagation through a gas cell:

I = I0exp.... $I = I_0 e^{-\tau} + R(T)(1 - e^{-\tau})$

and note that, in the limit of pure absorption (emission contribution negligible)

I/I0 = exp (-tau) - and draw an absorption spectrum

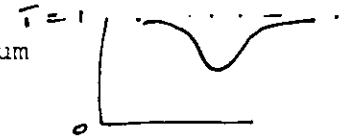

in the limit of pure emission: draw emission spectrum normalized to blackbody radiance.

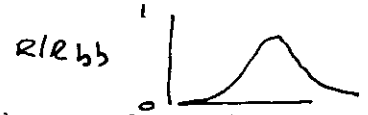

Note that they are inverses. I will now show how to determine optical depths from intensities, concentrations of molecules, and normalized lineshape functions.

First consider lineshape functions - the shape of an absorption or emission line at a given pressure and temperature (we will get into details in a few minutes):

draw lineshape function - note it is normalized to 1, so it is in units of cm:

(note other units need if using ν instead of σ

The product of the intensity (in cm) and the lineshape function versus cm-1 (in cm) is a cross section in cm^2. The product of the cross sections in cm^2 and the column density of molecules in cm-2 is the optical thickness (dimensionless).

Thus, the radiative transfer through the line at wavenumber sigma depends on tau (sigma) just as before:

I (sig) = I0e(-tau) + R(sig, T)(1 - e(-tau))

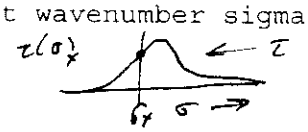

And that's it! except for a few details. Like what the lineshape functions are and how they depend on pressure, temperature, and wavenumber (frequency).

Lineshapes

Normalized Lorentzian:

L_l = $$L_l = \frac{b_l}{\pi} \frac{1}{(\sigma-\sigma_0)^2 + b_l^2}$$

where bl is the half-width of the line at half-maximum intensity. The natural width of the line (which we usually do not see in the infrared, but do see in predissociated UV spectra) gives rise to a Lorentzian lineshape with HWHM = 1/(4*pi*tau). Pressure (collisional) broadening is Lorentzian with HWHM = 1/(2*pi*tau), tau = average time between collisions:

bl = gamma (cm-1 atm-1, usually) * P(atm) or MHz/Torr, or ....

The pressure broadening coefficients are ~0.05 cm-1 atm-1 (0. is large, 0.03 is small - larger is for polar species, low rotational levels - dipole-quadrupole interactions; smaller ~ hard sphere), with substantial dependence on rotational state but little dependence on vibrational state (i.e., a vibrational and rotational transition with the same rotational quanta involved are within ~10% of being the same). More on this later. Note that Lorentz widths add directly:

b (air) ≅ 0.79 b (N2) + 0.21 b (O2).

Normalized Gaussian - Doppler broadening of lines:

L_g = $$L_g = \frac{\pi^{-1/2}}{b_g} e^{-\left[\frac{(\sigma-\sigma_0)^2}{b_g^2}\right]}$$

where bg is the HW1/e

bg = $$b_g = \left(\frac{2kT}{mc^2}\right)^{1/2} \sigma_0 = 4.30140 \times 10^{-7} \times \sigma_0 \times \sqrt{\frac{T(K)}{m(amu)}}$$

Gaussian linewidths add in quadrature: bg = SQRT (b1^2 + b2^2)

Note that pressure broadening depends strongly on the atmospheric pressure (and thus altitude) but only weakly on frequency, while Doppler broadening depends directly on frequency but only weakly on altitude (via the temperature dependence). Thus, for a given transition, pressure broadening will tend to dominate the overall linewidth at lower altitudes and Doppler broadening at higher altitudes.

* show slide of stratospheric FIR example., note change for mid-IR
* show FIRS-2 examples of cusp-shaped lines

The actual shape of a line at a given pressure and temperature in the atmosphere is a convolution of Lorentz (pressure/lifetime) and Gaussian (Doppler) broadening - the Voigt profile:

L_v = L_g X L-l $$L_v = L_g * L_l$$

The Voigt is a function with some wonderful symmetry properties; its calculation with tradeoffs between speed and accuracy could be the

subject of a whole course. I will be glad to discuss it off-line with anyone who is interested. I have put an extremely accurate subroutine for calculating Voigt functions (and their first and second derivatives) on the ftp site.

Aside: often in electronic transitions, especially those that are significantly predissociated, pressure and Doppler broadening are negligible compared to the lifetime broadening.

Now we can see how a line saturates over its profile:

For emission:

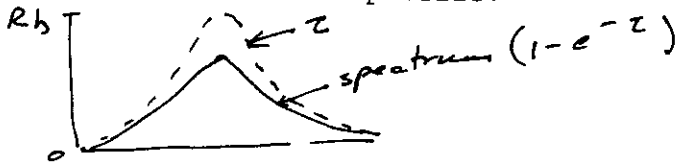

i.e., the center of the line saturates more than the wings.

For absorption:

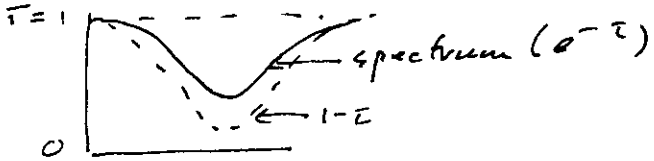

i.e., the same. Note that the term "equivalent width" (W) of a line is used to denote the area under (or over) a line - it simply means that if a line of the same area was completely black, it would have such a width.

The effect of saturation on a line (the fact that e-tau =/= 1-tau) decreases the areas under the line. The broader the line, the less saturation, and the stronger the line, the more saturation. We are more often than not in a situation where we measure lines with instruments (FTS instruments, array spectrometers) that do not have the resolution to see the lineshape - basically, we measure the equivalent width of the line. We need to be able to model back from the line parameters to determine how much gas corresponds to the measured line area or equivalent width. The situation for Lorentzian lines (the dominant broadened for many important atmospheric cases) is discussed in detail in Penner. The equivalent width of a line lies between two limits:

saturated limit unsaturated limit

2 SQRT (S*N*b) <= W <= S*N $2\sqrt{S \cdot N \cdot b} \leq W \leq S \cdot N$

This relationship (in detail) is known as the "curve of growth". For weak lines (HO2 in the far infrared) we only need to know the intensities; intensities are generally better known that pressure broadening coefficient (especially in the far infrared, because of the Stark effect); For strong lines, the line width is as important as the intensity in determining the area under the line. Needless to say, when Voigt profiles are needed it becomes quite complex!

I have some additional material on pressure broadening coefficients and how they vary with transition and (significantly) with temperature, but I will save that to discuss off-line with anyone who wants more detail.

There are many additional complexities in line shapes as well as intensities, such as speed dependence of the lineshapes, collisional narrowing, line mixing through elastic collisions - none of which I

will touch on here.

Note that if there are several gases in a cell, or an atmosphere, they can interfere with absorption among them. This is why the calculation of "global warming potentials" of IR active gases requires careful modeling of the spectral interference and the amounts of the various species.

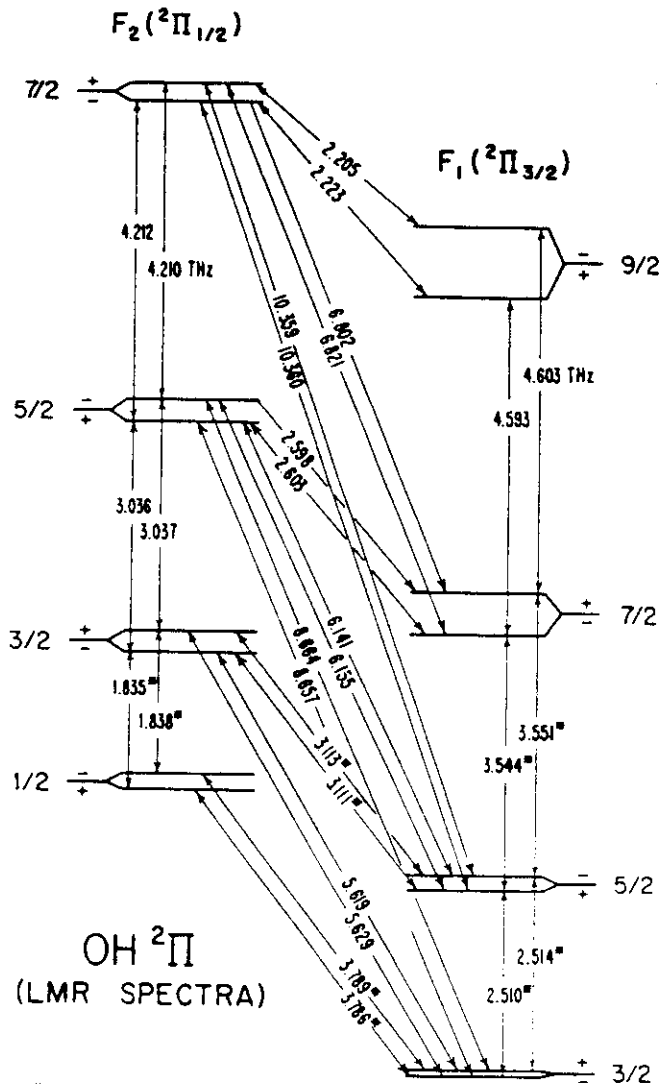

FIG. 1. — The low lying energy levels of the OH radical, connected by electric dipole transitions ($+ \leftrightarrow -$) in the far infrared. The parity doubling (or lambda doubling) has been exaggerated for the sake of clarity. The transition frequencies are given in THz.

THE ASTROPHYSICAL JOURNAL, 258:899–903, 1982 July 15
1982 The American Astronomical Society. All rights reserved. Printed in U.S.A.

THE FAR-INFRARED SPECTRUM OF THE OH RADICAL[1]

J. M. BROWN AND J. E. SCHUBERT
Department of Chemistry, Southampton University
K. M. EVENSON
National Bureau of Standards
AND
H. E. RADFORD
Harvard-Smithsonian Center for Astrophysics
Received 1982 January 4; accepted 1982 February 8

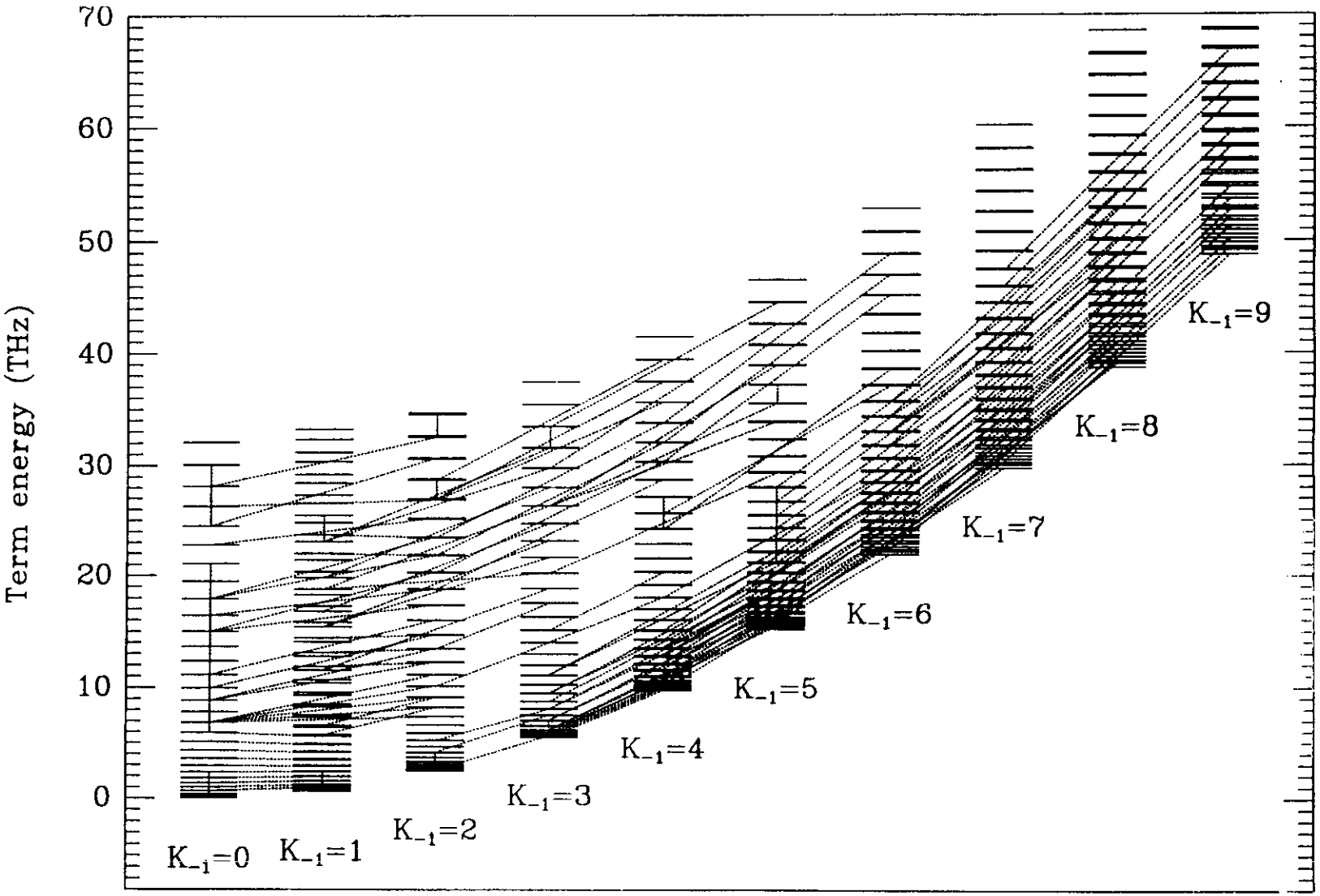

HO_2 energy levels, transitions, and combination differences

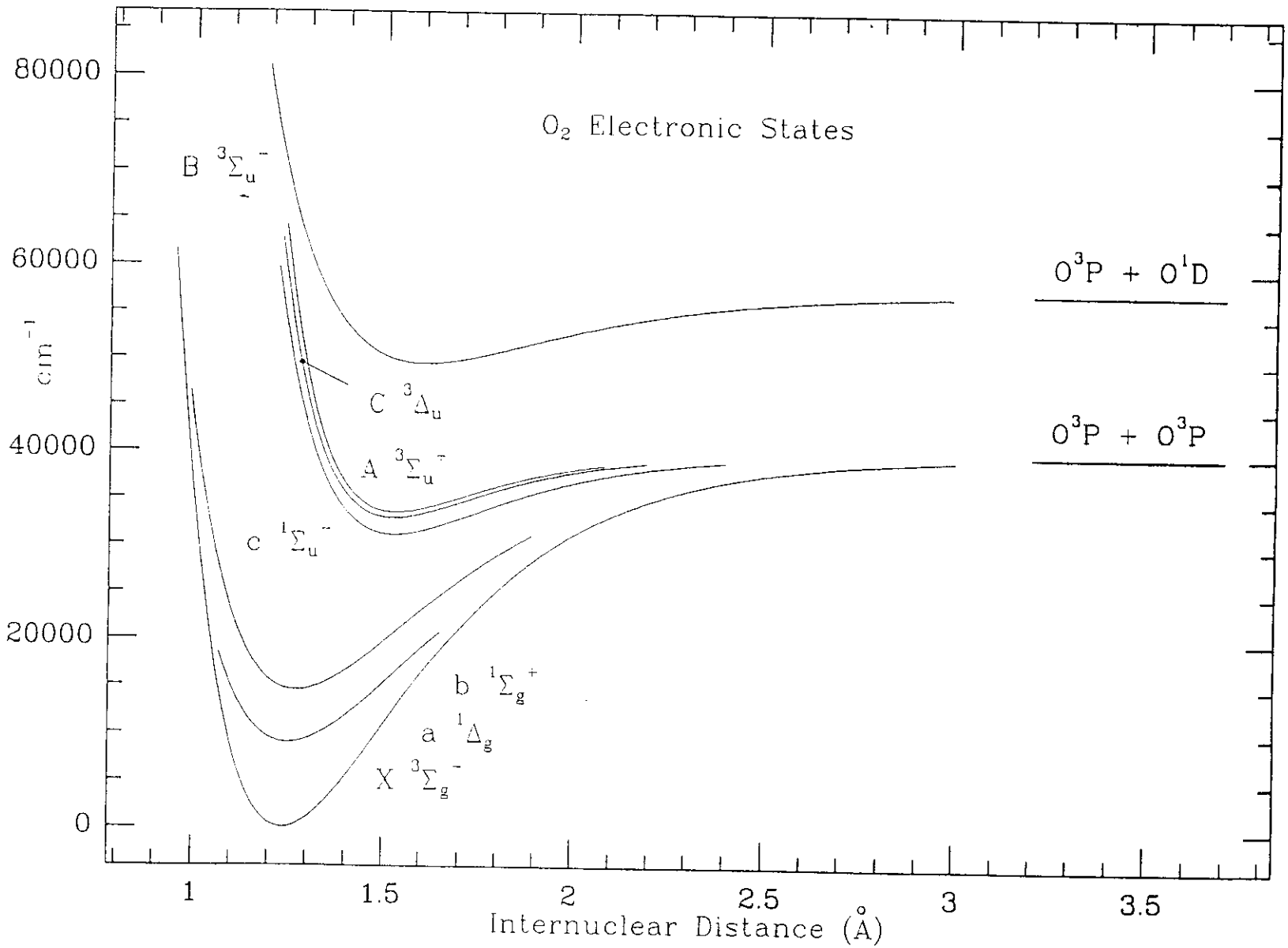
O2 Electronic States
80000
60000
40000
20000
0
cm-1
B 3Σu-
C 3Δu
A 3Σu+
c 1Σu-
b 1Σg+
a 1Δg
X 3Σg-
O3P + O1D
O3P + O3P
1
1.5
2
2.5
3
3.5
Internuclear Distance (Å)

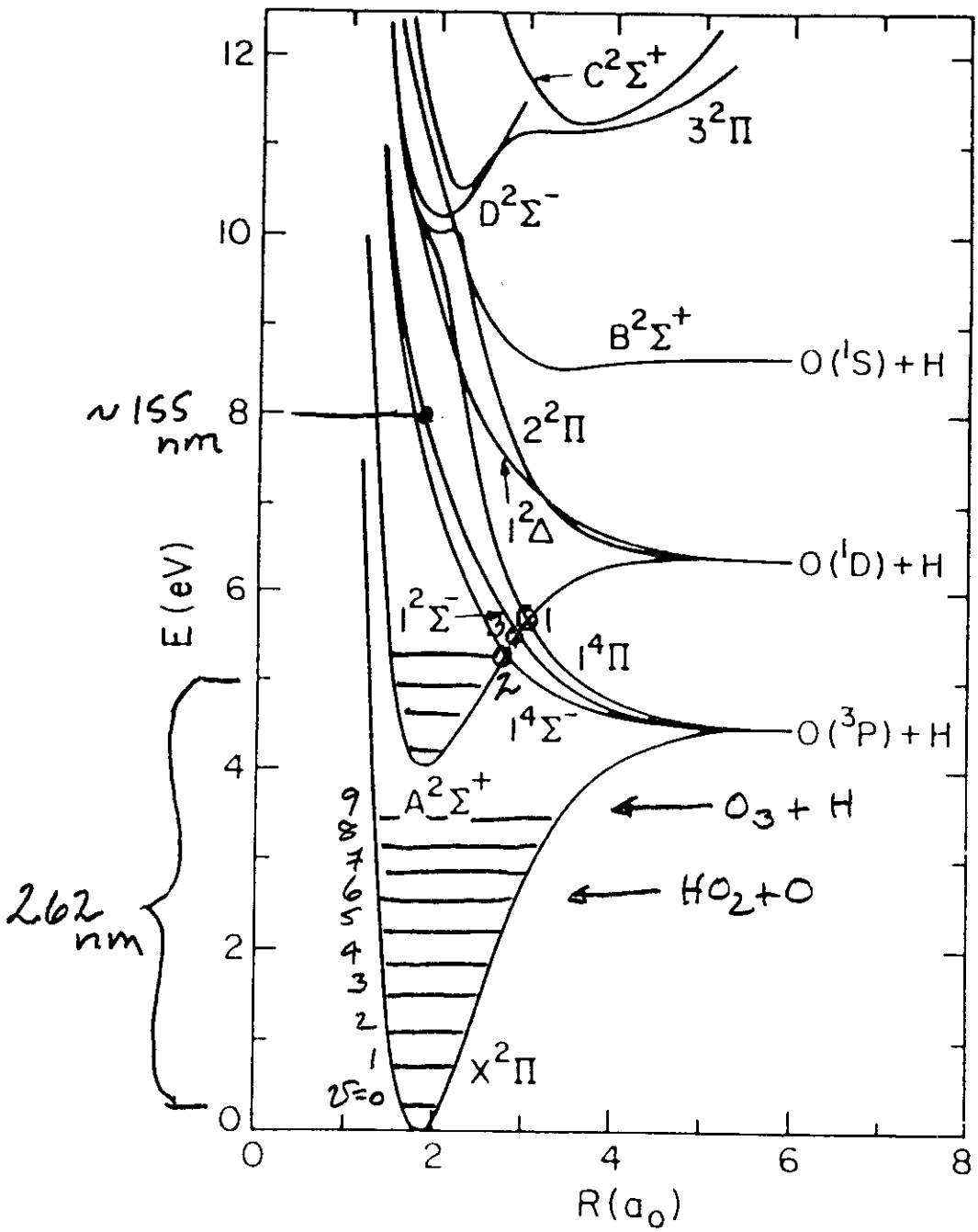

Potential energy curves of the OH molecule.

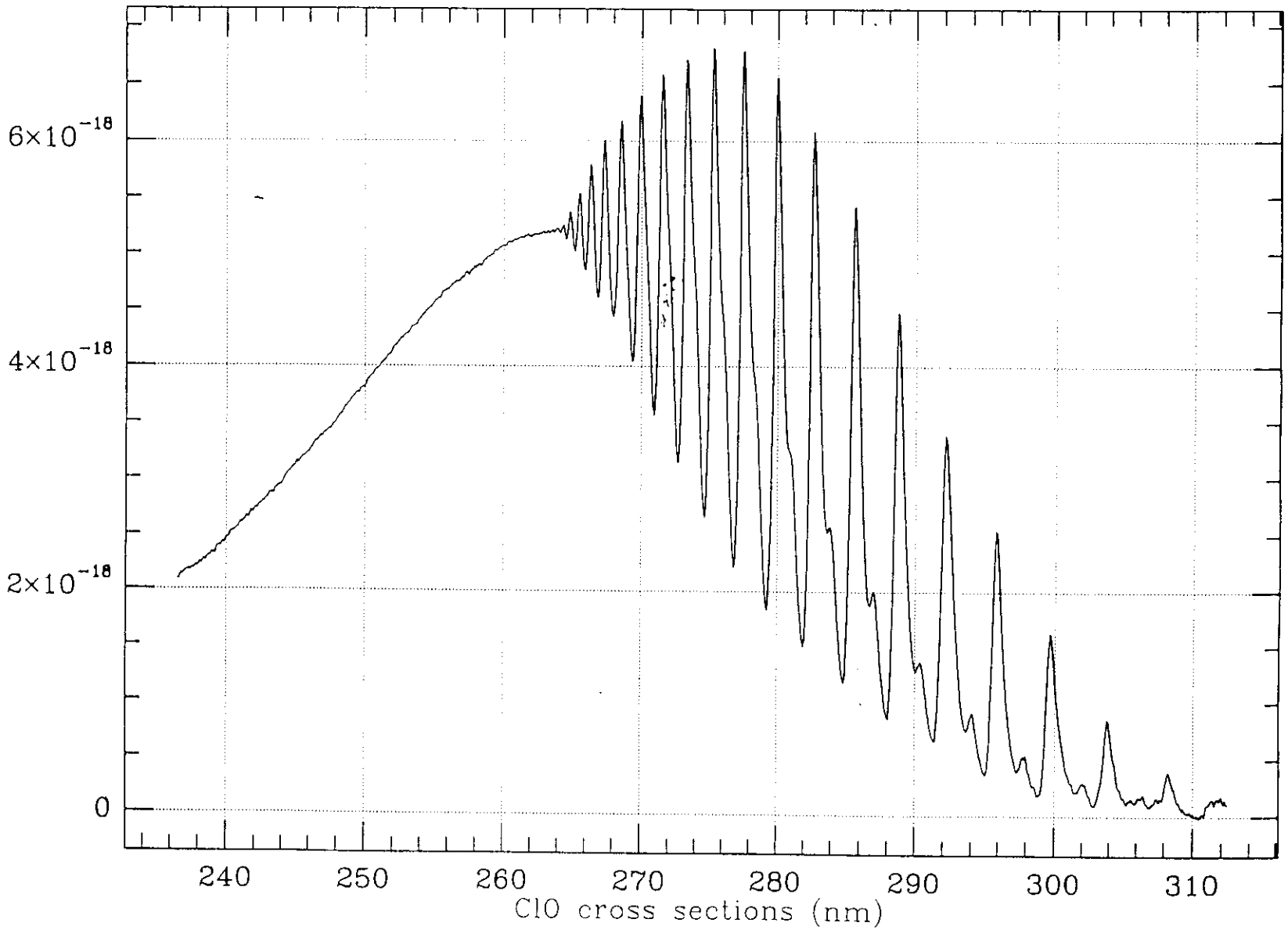
6×10⁻¹⁸
4×10⁻¹⁸
2×10⁻¹⁸
0
240
250
260
270
280
290
300
310
ClO cross sections (nm)

$b_p = b_l$ for

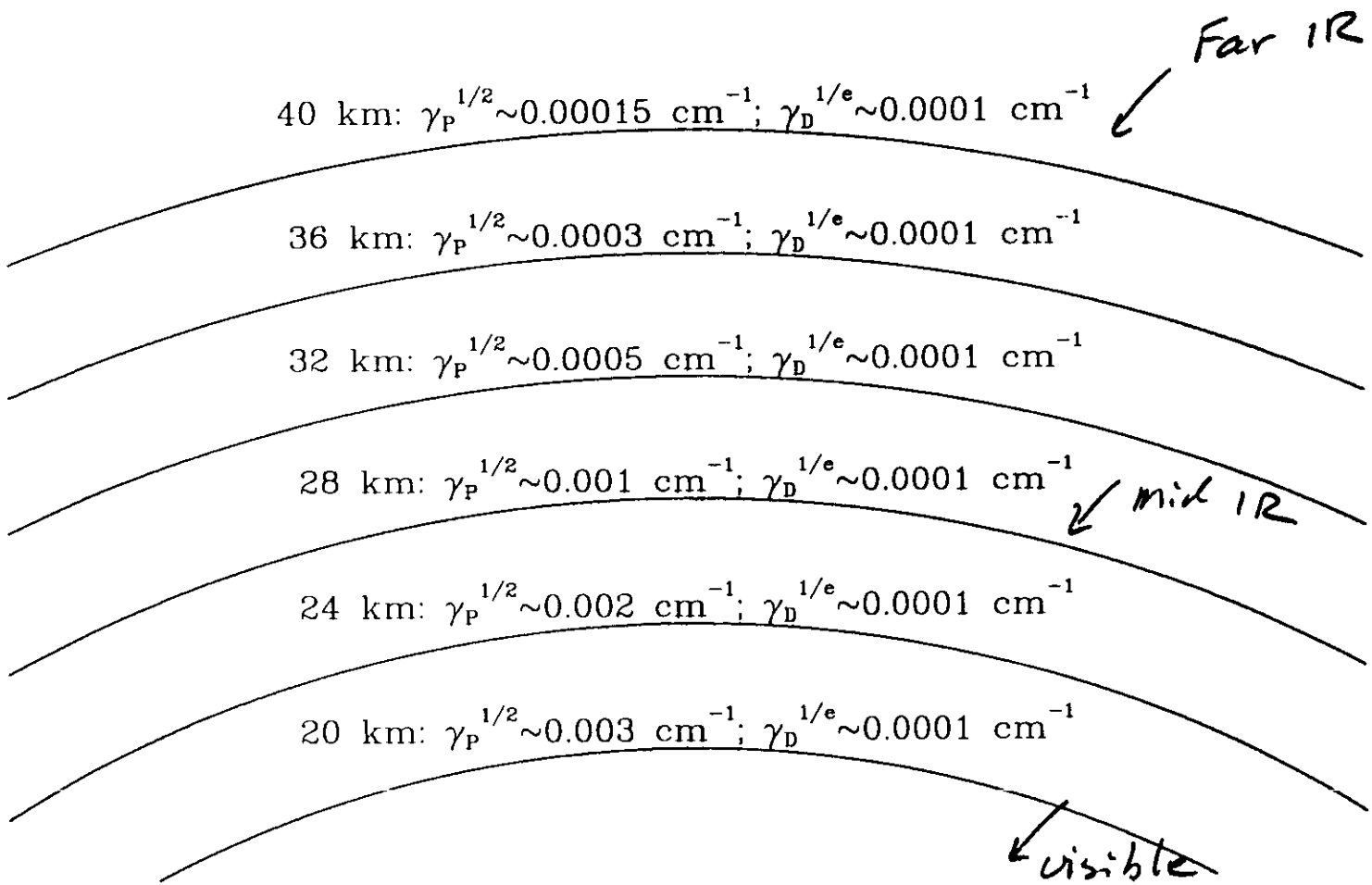
Far IR
40 km: $\gamma_P^{1/2}$~0.00015 cm^{-1}; $\gamma_D^{1/e}$~0.0001 cm^{-1}
36 km: $\gamma_P^{1/2}$~0.0003 cm^{-1}; $\gamma_D^{1/e}$~0.0001 cm^{-1}
32 km: $\gamma_P^{1/2}$~0.0005 cm^{-1}; $\gamma_D^{1/e}$~0.0001 cm^{-1}
28 km: $\gamma_P^{1/2}$~0.001 cm^{-1}; $\gamma_D^{1/e}$~0.0001 cm^{-1}
mid IR
24 km: $\gamma_P^{1/2}$~0.002 cm^{-1}; $\gamma_D^{1/e}$~0.0001 cm^{-1}
20 km: $\gamma_P^{1/2}$~0.003 cm^{-1}; $\gamma_D^{1/e}$~0.0001 cm^{-1}
visible

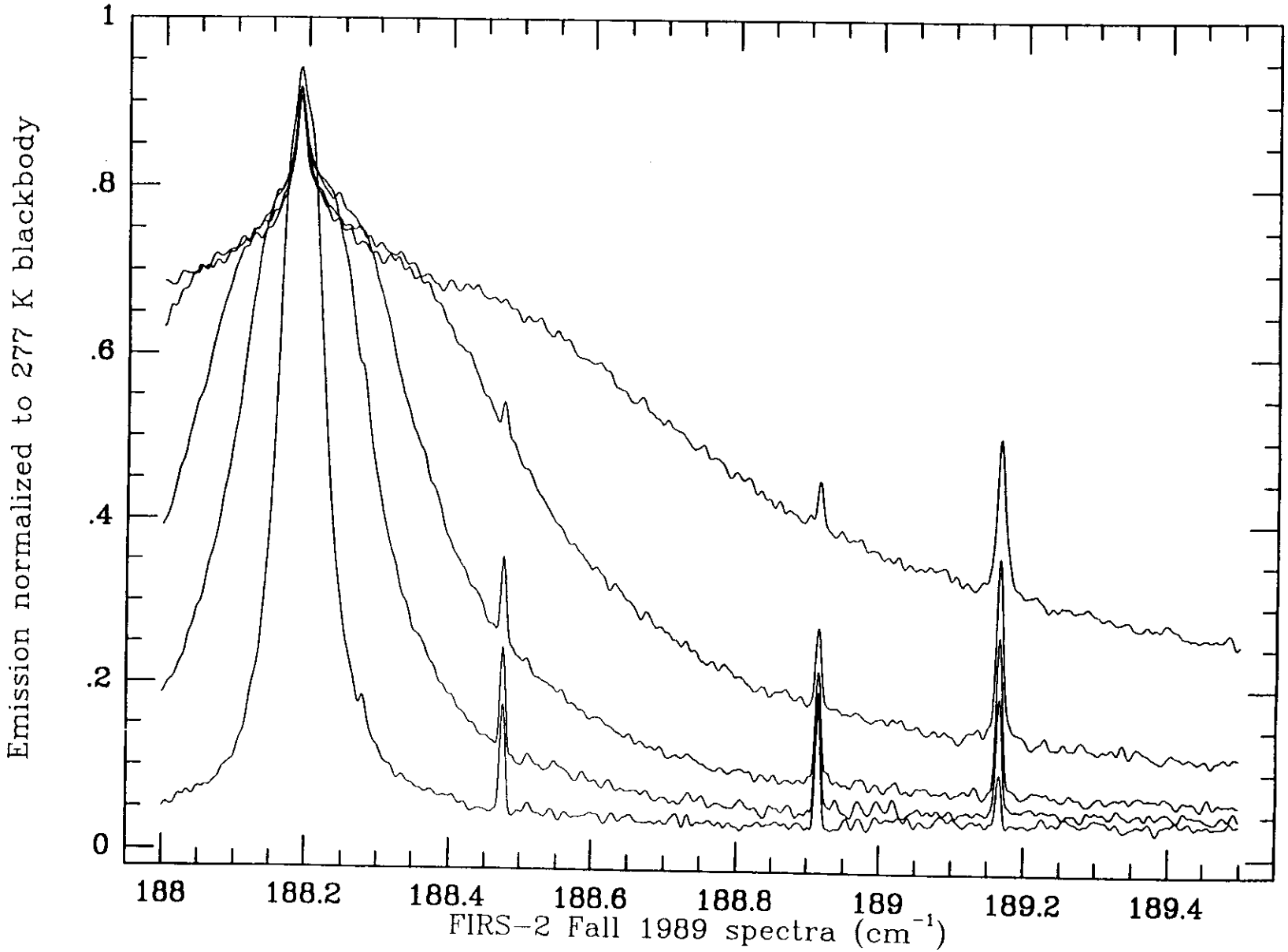
Emission normalized to 277 K blackbody
1
.8
.6
.4
.2
0
188
188.2
188.4
188.6
188.8
189
189.2
189.4
FIRS-2 Fall 1989 spectra (cm^{-1})

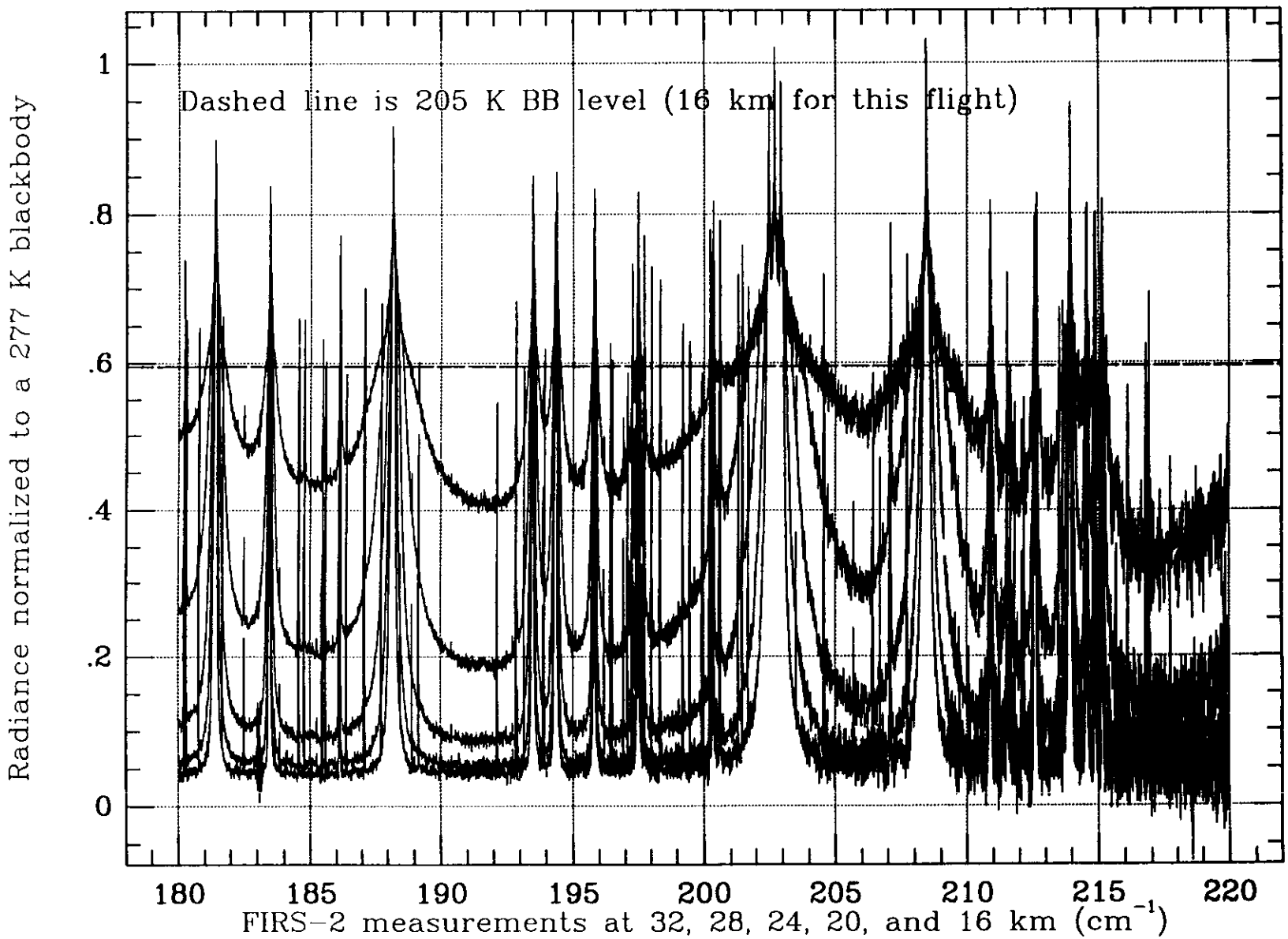
Dashed line is 205 K BB level (16 km for this flight)
Radiance normalized to a 277 K blackbody
1
.8
.6
.4
.2
0
180
185
190
195
200
205
210
215
220
FIRS-2 measurements at 32, 28, 24, 20, and 16 km (cm^{-1})

Day 4

(8) continued

(9) Spectroscopic databases

web sites for HITRAN, JPL, Geisa are on the ftp server

Review tables describing HITRAN and JPLSMM

Pick a section of HITRAN database and go over; suggest that students chase down some of the primary references to see if they can duplicate the numbers and their uncertainties. (I will suggest molecules and bands to try, for those interested.)

There has been a shift over how parameters are determined; ~90% of HITRAN is now FTS-derived.

HITRAN includes cross section files for some IR molecules with too many lines to practically include in a line database (table from paper)

HITRAN also now includes some UV/visible cross sections (our abstract and slide of poster); these will grow in the future due to their importance in satellite measurements of the atmosphere.

Go over a section of the JPLSMM to describe numbers as well.

new: O_3, OClO, BrO, H_2CO, ClO, NO_2

N_2O

SO_2

Preach about how these databases are NOT fundamental - they are secondary references; any published fittings of atmospheric measurements MUST use primary sources!

SCATTERING

I am operating under the assumption that Mie (particle) scattering is being addressed by other teachers. I will discuss Rayleigh (molecular) scattering.

Molecules (such as N2 and O2) are polarizable. That is, an applied electric field will induce a dipole moment in an otherwise nonpolar molecule. This polarizability varies weakly with the frequency of the electric field, at least until the frequency becomes comparable to that of an accessible electronic state of the molecule, where resonant effects must be considered.

The induced dipole moment is mu = alpha * E (tensor product)

$$\mu = \bar{\alpha} \cdot \bar{E}$$

and the energy of interaction is 1/2 alpha * E^2

$$\text{Energy} = 1/2 \alpha E^2$$

The induced dipole then may re-radiate, giving a cross sections for the entire process proportional to E^4 (see Goody and Yung, e.g., for details). The cross section for Rayleigh scattering per molecule is

Qr = 128*pi^5*alpha^2/3*lambda^4

$$Q_r = \frac{128 \pi^5 \alpha^2}{3 \lambda^4}$$

[Aside - if time - Poynting vector example of near-Rayleigh]
We can make use of the geometric identity

alpha = (n-1)/2*pi*N (N = gas density)

$$|\alpha| = (n-1)/2\pi N_0$$

where n is the index of refraction (it is the interaction with the polarizabilities which causes refraction!) to give the usual expression for the Rayleigh cross section:

Qr = 32*pi^3(n-1)^2/3*N0*lambda^4 (N0 now Loschmidt's number, density at STP)

$$Q_r = \frac{32\pi^3 (n-1)^2}{3 N_0 \lambda^4}$$

* example of GOME spectrum with low albedo - Rayleigh source of short wavelength light.

It can also be readily shown that the phase function for Rayleigh scattering is (3/16*pi)*(1+cos^2theta)

$$\Phi = \frac{3}{16\pi}(1+\cos^2\Theta)$$

The (strong) polarization of the scattering can also be determined.

Thus, if we know the dynamic polarizabilities of N2 and O2 we can completely describe Rayleigh scattering events in the atmosphere. Fortunately, these are quite well known to at least 200 nm, and the scattering has been fully characterized. The dynamic polarizabilities and their anisotropies have been analyzed by Bates [1984], which remains the best review of the available data.

D.R. Bates, Planet. Space Sci. 32, 785-790 (1984).

There is, however a complication: The polarizabilities of N2 and O2 are anisotropic; they are different along the molecular axes than across. The effect of the polarizability anisotropy is to allow for the inducing of transitions among the rotational (and, weakly, vibrational) states of the molecules. This means that some fraction (several percent for scattering through one atmosphere at 300-350 nm) of the Rayleigh scattering is inelastic. A fraction of the Fraunhofer light incident upon the scatterers is scattered out into an envelope of the Raman spectra centered at the incident wavelength. This effect in atmospheric spectra is known as the "Ring effect" (after Grainger and Ring) who first observed it in ground-based measurements of scattered solar light.

$$\gamma = \alpha^{\parallel} - \alpha^{\perp} \qquad \bar{\alpha} = [\alpha^{\parallel} + 2\alpha^{\perp}]/3$$

This inelastic scattering has its own spectrum, which substantially interferes with the measurement of trace atmospheric species in the UV (remember 1/lambda^4). We must be able to correct for it quantitatively in order to make reasonable measurements of, for example, NO2, BrO, OClO, H2CO, and SO2 - correction also helps improve O3 measurements.

Fortunately, the anisotropies of the polarizabilities of N2 and O2 have also been quite well determined for the UV/visible and IR, for at least 200-1000 nm (for longer wavelengths, Rayleigh scattering, including this inelastic component, is usually negligible - remember

1/lambda^4 dependence).

With these anisotropies and the quantum mechanical solution to cross sections for the Raman scattering (here is the dominant rotational Raman part) we can calculate accurate cross sections for the inelastic scattering component for O2 and for N2 for any wavelength in this range. Here is an example at 440 nm, in the region where NO2 is fitted in visible atmospheric spectra.

* N2 and O2 scattering at 440 nm

The input to the atmosphere is the solar Fraunhofer spectrum - here is an example of a measurement of it:

* Kurucz spectrum

Looking again at the 440 nm sample window, these panels show the whole process, as developed for fitting of GOME spectra:

* 4-panel figure with explanation and BOAS/DOAS distinction

To demonstrate how important proper inclusion of the Ring effect is on atmospheric UV measurements, here is an example of fitting a GOME spectrum for BrO, showing that the Ring component is an order of magnitude larger:

* BrO and Ring comparison

This anisotropic component has an effect on the overall Rayleigh scattering cross section:

QR = (3) $$Q_R = \frac{32\pi^3 (n-1)^2 F_K}{3 N_0^2 \lambda^4}$$

where Fk is the King factor, given by:

Fk = (4) $$F_K = 1 + 2\left(\frac{\gamma}{3\bar{\alpha}}\right)^2 = \frac{6+3\rho_0}{6-7\rho_0} = 1 + \frac{2\epsilon}{9}$$

We give the best current parameterization of it for 200-1000 nm in our Chance and Spurr paper.

The intensities for the elastic and inelastic components, there polarization dependences and phase functions, are all now well-determined:

* Table of intensities and phase functions

The index of refraction versus wavelength is also very well determined, so that we can calculate refractive ray tracing (using Snell's Law) through the atmosphere, which is a necessity for many atmospheric measurement geometries. We also give the best current representation of it, from parameterization of Bates' data:

* (6) $$(n-1) \times 10^4 = 0.7041 + \frac{315.90}{157.39 - \sigma^2} + \frac{8.4127}{50.429 - \sigma^2}$$ σ in $(\mu m)^{-1}$

* Snell's law - n1*sin(theta1) = n2*sin(theta2)

Lastly for this topic, note that there is often some confusion and indeterminacy in wavelength assignments due to the air/vacuum index of refraction correction. Dispersion (e.g., grating) instruments often measure wavelengths, which are often measured in air (at what density? sometimes not apparent) and they are sometimes corrected in an untraceable fashion. Reference spectra are sometimes reported without explicitly saying whether the wavelengths are air or vacuum - it makes a substantial difference!

FTS instruments measure wavenumbers (cm-1) which are frequencies! (no "1/cm" or "reciprocal centimeters", please). By definition, they do not need to be corrected for the index of refraction. However, one does occasionally see "air wavenumbers" (presumably from partial correction of wavelengths), which should never be used.

The HITRAN Database

HITRAN is an acronym for high resolution transmission molecular absorption database. HITRAN is a compilation of spectroscopic parameters which a variety of computer simulation codes use to predict the transmission and emission of light in the atmosphere. The database is a long-running project started by the Air Force Cambridge Research Laboratories (AFCRL) in the late 1960's in response to the need for detailed knowledge of the infrared properties of the atmosphere. The HITRAN compilation, and its analogous database HITEMP (high-temperature spectroscopic absorption parameters), are now being developed at the Atomic and Molecular Physics Division, Harvard-Smithsonian Center for Astrophysics under the continued direction of Dr. Laurence S. Rothman.

The current edition of the HITRAN molecular spectroscopic database is available on CD-ROM. It is included in a compilation called HAWKS (HITRAN Atmospheric Workstation). HAWKS represents more fully a "matter" database.

In addition to the 1,000,000 line HITRAN96 database, there are files containing aerosol indices of refraction, UV line-by-line and cross-section parameters, supplemental files of gases such as ionic species and high-vibrational calculations, and more extensive IR cross-sections. In addition, there is the software handling of the data in both Windows and UNIX platforms, all available on a CD-ROM.

The database is currently distributed on a single CD-ROM. A free copy may be obtained by researchers using their institutional addresses by completing the HITRAN Request Form. Special questions should be addressed to Dr. Laurence Rothman at LRothman@CfA.Harvard.edu.

Last updated: October 8, 1999

Table 2. Summary of species represented in HITRAN

Mol. no.	Molecule	Number of isotopomers	Number of bands	Number of lines	Spectral coverage (cm^{-1})
1	H_2O	4	137	49 444	0–22 657
2	CO_2	8	589	60 802	442–9649
3	O_3	5	106	275 133	0–4033
4	N_2O	5	164	26 174	0–5132
5	CO	6	47	4 477	3–6418
6	CH_4	3	51	48 032	0–6185
7	O_2	3	19	6 292	0–15 928
8	NO	3	50	15 331	0–3967
9	SO_2	2	9	38 853	0–4093
10	NO_2	1	12	100 680	0–2939
11	NH_3	2	40	11 152	0–5295
12	HNO_3	1	13	165 426	0–1770
13	OH	3	103	8 676	0–9997
14	HF	1	6	107	41–11 536
15	HCl	2	17	533	20–13 458
16	HBr	2	16	576	16–9759
17	HI	1	9	237	12–8488
18	ClO	2	12	7 230	0–1208
19	OCS	4	7	858	0–2089
20	H_2CO	3	10	2 702	0–2999
21	HOCl	2	6	15 565	0–3800
22	N_2	1	1	120	1922–2626
23	HCN	3	8	772	2–3422
24	CH_3Cl	2	8	9 355	679–3173
25	H_2O_2	1	2	5 444	0–1500
26	C_2H_2	2	11	1 668	604–3375
27	C_2H_6	1	2	4 749	720–3001
28	PH_3	1	2	2 886	708–1411
29	COF_2	1	7	54 866	725–1982
30	SF_6	1	1	11 520	940–953
31	H_2S	3	15	7 151	2–2892
32	HCOOH	1	1	3 388	1060–1162
33	HO_2	1	4	26 963	0–3676
34	O	1	1	2	68–159
35	$ClONO_2$	2	3	32 199	763–798
36	NO^+	1	6	1 206	1634–2531
37	HOBr	2	2	4 358	0–316

Table 3. Example of HITRAN line-transition format.

Mol/Iso	ν_{nn}	S_{nn}	$\mathfrak{R}_{nn}$	γ_{air}	γ_{self}	E"	n	δ	iv'	iv"	q'	q"	ierr	iref
21	800.451076	3.197E-26	6.579E-05	0.0676	0.0818	2481.5624	0.78	0.000000	14	6		P 37	465	2 2 1
291	800.454690	9.724E-22	1.896E-02	0.0845	0.1750	369.6303	0.94	0.000000	9	1	341619	331519	000	4 4 1
291	800.454690	3.242E-22	2.107E-03	0.0845	0.1750	369.6303	0.94	0.000000	9	1	341519	331419	000	4 4 1
121	800.455380	1.037E-22	1.657E-03	0.1100	0.0000	530.3300	0.75	0.000000	32	14	46 640	45 540	000	4 4 1
121	800.455380	1.037E-22	1.657E-03	0.1100	0.0000	530.3300	0.75	0.000000	32	14	46 740	45 640	000	4 4 1
101	800.456743	1.680E-23	1.659E-04	0.0670	0.0000	851.0494	0.50	0.000000	2	1	45 244 0–	44 143 0–	301	6 6 1
101	800.457045	1.710E-23	1.689E-04	0.0670	0.0000	851.0469	0.50	0.000000	2	1	45 244 1–	44 143 1–	301	6 6 1
101	800.457310	1.740E-23	1.718E-04	0.0670	0.0000	851.0442	0.50	0.000000	2	1	45 244 2–	44 143 2–	301	6 6 1
121	800.457760	4.726E-23	4.614E-03	0.1100	0.0000	920.0900	0.75	0.000000	32	14	502922	492822	000	4 4 1
121	800.457760	4.726E-23	4.614E-03	0.1100	0.0000	920.0900	0.75	0.000000	32	14	502822	492722	000	4 4 1
24	800.465942	9.792E-27	6.063E-04	0.0754	0.1043	1341.2052	0.69	0.000000	8	3		R 13	425	2 2 1
121	800.466160	1.061E-22	2.720E-03	0.1100	0.0000	632.1200	0.75	0.000000	32	14	471236	461136	000	4 4 1
121	800.466160	1.061E-22	2.720E-03	0.1100	0.0000	632.1200	0.75	0.000000	32	14	471136	461036	000	4 4 1
35	800.472900	3.878E-26	6.919E-04	0.0686	0.0871	629.0354	0.76	0.000000	2	1	1814 4	1713 5	455	5 5 1
101	800.473083	1.270E-23	1.254E-04	0.0670	0.0000	851.0095	0.50	0.000000	2	1	45 244 0 –	44 143 0 –	301	6 6 1
101	800.474860	1.210E-23	1.195E-04	0.0670	0.0000	851.0064	0.50	0.000000	2	1	45 244–1 –	44 143–1 –	301	6 6 1
31	800.475500	1.680E-24	3.617E-05	0.0653	0.0890	1092.4340	0.76	0.000000	2	1	51 547	50 248	002	1 1 2
291	800.476220	9.597E-22	6.010E-03	0.0845	0.1750	361.9747	0.94	0.000000	9	1	341420	331320	000	4 4 1
291	800.476220	3.199E-22	6.010E-03	0.0845	0.1750	361.9747	0.94	0.000000	9	1	341520	331420	000	4 4 1
101	800.476937	1.160E-23	1.145E-04	0.0670	0.0000	851.0037	0.50	0.000000	2	1	45 244–2 –	44 143–2 –	301	6 6 1
101	800.484334	1.740E-23	2.153E-05	0.0670	0.0000	106.0760	0.50	0.000000	2	1	8 4 4–1 –	9 3 7–1 –	301	6 6 1

Note: FORTRAN Format (I2,I1,F12.6,1P2E10.3,0P2F5.4,F10.4,F4.2,F8.6,2I3,2A9,3I1,3I2) corresponding to the following:

Mol	I2	molecule number
Iso	I1	isotope number (1 = most abundant, 2 = second most abundant, etc.)
ν_{nn}	F12.6	frequency in cm^{-1}
S_{nn}	E10.3	intensity in $cm^{-1}/(molecule \cdot cm^{-2})$ @ 296 K
$\mathfrak{R}_{nn}$	E10.3	weighted transition moment-squared in $Debye^2$
γ_{air}	F5.4	air-broadened halfwidth (HWHM) in cm^{-1}/atm @ 296 K
γ_{self}	F5.4	self-broadened halfwidth (HWHM) in cm^{-1} atm @ 296 K
E"	F10.4	lower state energy in cm^{-1}
n	F4.2	coefficient of temperature dependence of air-broadened halfwidth
δ	F8.6	airbroadened pressure shift of line transition in cm^{-1}/atm @ 296 K
iv',iv"	2I3	upper state global quanta index, lower state global quanta index
q',q"	2A9	upper state local quanta, lower state local quanta
ierr	3I1	accuracy indices for frequency, intensity, and air-broadened halfwidth
iref	3I2	indices for table of references corresponding to frequency, intensity, and halfwidth

UV Spectral Data for HITRAN 2000

K. Chance, T.P. Kurosu, K. Yoshino
W. Parkinson, L.S. Rothman
Harvard–Smithsonian Center for Astrophysics
Atomic and Molecular Physics Division

A. Goldman
University of Denver
Department of Physics

J. Orphal
University of Bremen
Institute of Remote Sensing

Tables of Molecules, Bands and Spectral Ranges

Table 1. UV cross-sections represented in HITRAN

Molecule	Band System	Spectral Range (cm^{-1})	Temperature (K)
N_2O	$A\,^1\Sigma^+ \leftarrow X\,^1\Sigma^+$	44925 – 49504	298
SO_2	$\tilde{B}\,^1B_1 \leftarrow \tilde{X}\,^1A_1$	31847 – 36452	213
		45455 – 50000	295
	$^1B_1 \leftarrow \tilde{X}\,^1A_1$ (Hartley–Huggins)	34870 – 42190	203–293
O_3	$^1B_1 \leftarrow \tilde{X}\,^1A_1$ (Chappuis – Wulf)		
H_2CO	$\tilde{A}\,^1A_2 \leftarrow \tilde{X}\,^1A_1$	27591 – 33311	223, 293
BrO	$A\,^2\Pi \leftarrow X\,^2\Pi$	25784 – 33813	228, 298
OClO	$A^2A_2 \leftarrow X\,^2B_1$	30992 – 41220	228
ClO	$B \leftarrow X\,^2\Pi_i$	32000 – 37700	220
N_2O	$A^1\Sigma^+ \leftarrow X^1A_1$	17540 – 52360	213, 298

Table 2. UV line-by-line data represented in HITRAN

Molecule	Band System	Spectral Range (cm^{-1})
O_2	$A\,^3\Sigma_u^+ \leftarrow X\,^3\Sigma_g^-$ (Herzberg I)	57000 – 65000
	$c\,^1\Sigma_u^- \leftarrow X\,^3\Sigma_g^-$ (Herzberg II)	38400 – 43400
	$A'\,^3\Delta_u \leftarrow X\,^3\Sigma_g^-$ (Herzberg III)	34000 – 49400
OH	$A\,^2\Sigma^+ \leftarrow X\,^2\Pi_i$	31000 – 36000
NO	$A\,^2\Sigma^+, B\,^2\Pi, C\,^2\Pi, D\,^2\Sigma^+ \leftarrow X\,^2\Pi_r$ ($\gamma, \beta, \delta, \alpha$-bands)	44300 – 63000

Introduction

The current edition of the HITRAN compilation [1] of 1996 extended into the ultraviolet region for the first time with the inclusion of UV cross-sections for N_2O at 296K in the wavelength region 170–222 nm, and SO_2 at 213K in the wavelength region 172–240 nm. The cross-section data employ the identical format as adopted for the IR cross-sections, namely a table of cross-sections at equal wavenumber interval. These sets of cross-sections are introduced with a standardized header providing essential information about each pressure-temperature set.

High-resolution data for the O_2 Schumann-Runge system were also added to the compilation with line-transition parameters similar in format to the main body of HITRAN. The UV data are kept in a separate directory in the HITRAN compilation and further segmented by (two) sub-directories, one for the cross-section data and the other for line parameter data.

New Data above 20000 cm^{-1}

For the upcoming edition of the database, HITRAN2000, we anticipate adding high-resolution cross-sections for several molecular band systems: O_3, OClO, BrO, H_2CO, ClO, and NO_2. In addition, there will be line-by-line data for O_2, NO, and OH. The spectra of these gases have applications to a number of programs, including the ESA Global Ozone Monitoring Experiment (GOME) [2], and the NASA EOS (Earth Observing System) program [3].

Format

File structure & format (in FORTRAN) for cross-section files

Molecule	$\nu_{1,line}$ / $\nu_{1,step}$ (cm^{-1})	# of points	T_1 (K)	P_1 (torr)	σ_{max}	Reference / Resolution, etc
A10	F10.4	F10.4	I10	F10.4	F10.4	3A10
	Cross-sections (10 per line) (cm^2/molecule at T_1, P_1) (10E10.3)					
Molecule	$\nu_{1,line}$ / $\nu_{1,step}$ (cm^{-1})	# of points	T_2 (K)	P_2 (torr)	σ_{max}	Reference / Resolution, etc
A10	F10.4	F10.4	I10	F10.4	F10.4	3A10
	Cross-sections (10 per line) (cm^2/molecule at T_2, P_2) (10E10.3)					
⋮						
Molecule	$\nu_{1,line}$ / $\nu_{1,step}$ (cm^{-1})	# of points	T_i (K)	P_i (torr)	σ_{max}	Reference / Resolution, etc
A10	F10.4	F10.4	I10	F10.4	F10.4	3A10
	Cross-sections (10 per line) (cm^2/molecule at T_i, P_i) (10E10.3)					
Molecule	$\nu_{1,line}$ / $\nu_{1,step}$ (cm^{-1})	# of points	T_1 (K)	P_1 (torr)	σ_{max}	Reference / Resolution, etc
A10	F10.4	F10.4	I10	F10.4	F10.4	3A10
	Cross-sections (10 per line) (cm^2/molecule at T_1, P_1) (10E10.3)					

Potential Curves for Oxygen

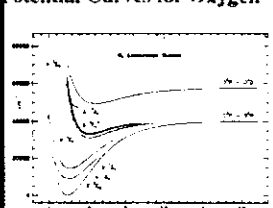

O_3 Cross-Sections

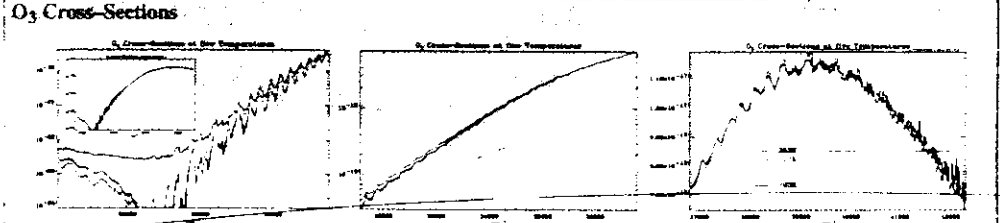

Other Molecules

The choice of other molecules to include for HITRAN2000 is based upon current needs for the analysis of satellite- and ground-based measurements of the atmosphere. The European Space Agency's Global Ozone Monitoring Experiment (GOME), for example, can measure BrO, OClO, SO_2, H_2CO, and H_2O as well as O_3 and NO_2. While the choices of cross sections used in analysis of field measurements is currently evolving, HITRAN2000 includes spectra that have been demonstrated to provide reasonable fitting.

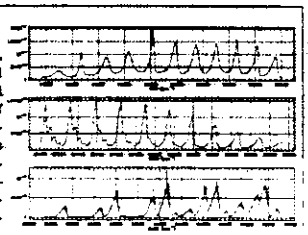

Summary

Tables 1 and 2 summarize the UV data to be included in the next edition of the HITRAN compilation. The improvement of quantitative spectroscopy in the UV and its cataloguing in HITRAN will substantially improve the state of global measurements of these gases. Improvements are intended to include FTS-based measurements of cross sections and their temperature dependences for the complete set of molecules included in HITRAN2000, as well as extension to other species. These might include, for example, OBrO and NO_3, and line-by-line UV parameters for ClO.

L.S. Rothman et al., "The HITRAN Molecular Spectroscopic Database and HAWKS (HITRAN Atmospheric Workstation: 1996 Edition," J. Quant. Spectrosc. and Rad. Transfer 60, 665-710 (1998).

K.V. Chance et al., "Retrieval and assimilation algorithms for the Global Ozone Monitoring Experiment and the SCIAMACHY Imaging Absorption spectrometer for Atmospheric CHartography," Proc. S.P.I.E., Remote Sensing of Atmospheric Chemistry 1491, 151-166 (1991).

M.D. King et al., "The Earth Observing System (EOS): A space-based program for studying mankind's impact on the global environment," Opt. Photonics News 6, 34-39 (1995).

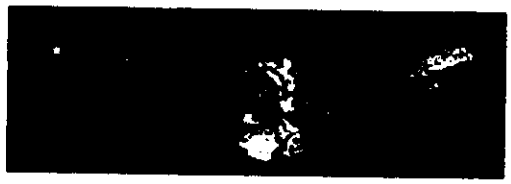

JPL Molecular Spectroscopy

Molecular spectroscopy is the study of absorption of light by molecules. In the gas phase at low pressures, molecules exhibit absorption in narrow lines which are very characteristic of the molecule as well as the temperature and pressure of its environment. In the microwave and long-wavelength infrared regions of the spectrum, these lines are due to quantized rotational motion of the molecule. At shorter wavelengths similar lines are due to quantized vibration and electronic motion as well as rotational motion. The precise frequencies of these lines can be fit to quantum mechanical models which can be used both to determine the structure of the molecule and to predict the frequencies and intensities of other lines. Because this absorption is so characteristic, it is very valuable for detecting molecules in the Earth's stratosphere, planetary atmospheres, and even the interstellar medium. *This home page contains very specialized technical information. While the general user is welcome to browse its contents, the descriptions assume a knowledge of spectroscopy and quantum mechanics.*

The JPL Molecular Spectroscopy Team supports NASA programs in Astrophysics, Atmospheric Science, and Planetary Science. Its activities include measurement of rotational lines, fitting the lines, and preparing a catalog of line positions and intensities. The members of the team include Edward A. Cohen, Timothy J. Crawford, Brian J. Drouin, John C. Pearson, and Herbert M. Pickett.

Features

- Catalog Directory with links
- Catalog Browser Form
- New Catalog Additions
- What's New with Fitting Programs

Guide to anonymous ftp file system for spec.jpl.nasa.gov

- The sub-directory calpgm contains programs for fitting spectra. These programs are copyrighted, but made freely available as a service to the spectroscopic community. Some of the details of the program are described in *H. M. Pickett, "The Fitting and Prediction of Vibration-Rotation Spectra with Spin Interactions," **J. Molec. Spectroscopy 148**, 371-377 (1991).*
- The sub-directory catalog contains files related to the JPL spectral line catalog. The file catdir.cat contains the current catalog directory in a format described in the written catalog description. Line files are designated as ctttttt.cat, where ttttt is the zero-filled catalog tag number (the first entry in each line of the catdir.cat file). For example, the H atom line list is in file c001001.cat. The line files and the directory file are text files readable with usual text file system utilities. It is recommended that they be transferred under ftp using the ASCII option, although binary should work with UNIX hosts. The file README contains a short description of the format of catdir.cat and the catalog files. A html catalog directory is available which provides links to the catalog

entries and the associated documentation (in either pdf or Tex format). The current literature reference for the catalog is *H. M. Pickett, R. L. Poynter, E. A. Cohen, M. L. Delitsky, J. C. Pearson, and H. S. P. Muller, "Submillimeter, Millimeter, and Microwave Spectral Line Catalog," J. Quant. Spectrosc. & Rad. Transfer 60, 883-890 (1998).*

- The sub-directory catalog/doc contains the documentation for the line files. Documentation for a particular species follows the line file naming convention except that the first character is 'd' rather than 'c'. These files are text files in LATeX format. The files catdoc.tex, catintro.tex, catdir.tex, and moldoc.tex are the files used to generate the catalog descriptive report. The file pretex.tex can be used to prepare a single document page. Processing the full documentation will generate a document of over 300 pages! This documentation is also available in postscript form as catdoc.ps (734 kbytes). If you have the free Adobe Acrobat reader, you can read the document catdoc.pdf (707 kbytes). A pdf version of the introductory information about formats, etc., is available as catintro.pdf (166 kbyes).
- The sub-directory catalog/pgm contains utility programs for catalog access. The subroutine set catread.f contains code for reading files into a FORTRAN program. These routines use random access, and assume that the files have a fixed line length within the file. Some modification of path names and file open options will be required for operating systems other than UNIX. The program catlist.f uses catread.f to provide listing of lines for selected molecules over a selected frequency range.
- The sub-directory catalog/archive contains the some of the input files for calculating the catalog files

WARNING: this file system is the living repository of the JPL catalog. Recently added files may still be in a preliminary state. Caution should be used for species which have a catdir.cat line ending with '*', which have been modified since the last published edition of the catalog.

Herb Pickett, e-mail: hmp@spec.jpl.nasa.gov

The catalog data files are composed of 80-character card images, with one card image per spectral line. The format of each card image is:

```
  FREQ, ERR, LGINT, DR,  ELO, GUP, TAG, QNFMT,  QN',  QN"
(F13.4,F8.4, F8.4,  I2,F10.4,  I3,  I7,    I4,  6I2,  6I2)
```

FREQ: Frequency of the line in MHz.
ERR: Estimated or experimental error of FREQ in MHz.
LGINT: Base 10 logarithm of the integrated intensity in units of nm^2 MHz at 300 K.
DR: Degrees of freedom in the rotational partition function (0 for atoms, 2 for linear molecules, and 3 for nonlinear molecules).
ELO: Lower state energy in cm^(-1) relative to the ground state.
GUP: Upper state degeneracy.
TAG: Species tag or molecular identifier.
A negative value flags that the line frequency has been measured in the laboratory. The absolute value of TAG is then the species tag and ERR is the reported experimental error. The three most significant digits of the species tag are coded as the mass number of the species.
QNFMT: Identifies the format of the quantum numbers
QN': Quantum numbers for the upper state.
QN": Quantum numbers for the lower state.

The on-line version of the catalog contains individual files for each molecular species. Line files are designated as cttttttt.cat, where tttttt is the zero-filled catalog tag number. For example, the H atom line list is in file c001001.cat.

A directory of the catalog is found in a file called 'catdir.cat.' Each element of this directory is an 80-character record with the following format:

```
TAG,  NAME, NLINE,  QLOG,  VER
(I6,X, A13,    I6, 7F7.4,  I2)
```

TAG: The species tag or molecular identifier.
NAME: An ASCII name for the species.
NLINE: The number of lines in the catalog.
QLOG: A seven-element vector containing the base 10 logorithm of the partition function for temperatures of 300 K, 225 K, 150 K, 75 K, 37.5 K, 18.75 K, and 9.375 K, respectively.
VER: The version of the calculation for this species in the catalog. The version number is followed by * if the entry is newer than the last edition of the catalog.

1899669.5047	1.4667	-2.9898	3	544.8301	11	17001	224	5	-1	5	5	5	1	6	6
1936721.9519	1.4656	-3.0416	3	543.5972	9	17001	224	5	1	5	4	5	-1	6	5
1936750.1521	1.4656	-4.7737	3	543.5972	11	17001	224	5	1	5	5	5	-1	6	5
1936781.0722	1.4656	-2.9610	3	543.5961	11	17001	224	5	1	5	5	5	-1	6	6
1980887.6145	0.4725	-13.0636	3	289.0466	9	17001	224	4	1	5	4	3	-1	3	3
2012894.8189	0.4725	-11.5179	3	288.7734	9	17001	224	4	-1	5	4	3	1	3	3
2204853.1253	0.6351	-2.4517	3	355.9163	7	17001	224	4	1	4	3	4	-1	5	4
2204927.1246	0.6352	-3.9957	3	355.9163	9	17001	224	4	1	4	4	4	-1	5	4
2204939.4420	0.6352	-2.3523	3	355.9159	9	17001	224	4	1	4	4	4	-1	5	5
2223197.7071	0.6350	-2.4328	3	355.1219	7	17001	224	4	-1	4	3	4	1	5	4
2223221.3025	0.6350	-3.9767	3	355.1219	9	17001	224	4	-1	4	4	4	1	5	4
2223242.6257	0.6350	-2.3334	3	355.1212	9	17001	224	4	-1	4	4	4	1	5	5
2509935.4400	0.5000	-0.7986	3	0.0018	5	-17001	224	2	1	3	2	1	-1	2	2
2509949.0100	0.3000	0.3475	3	0.0018	7	-17001	224	2	1	3	3	1	-1	2	2
2509988.1500	0.3000	0.1556	3	0.0000	5	-17001	224	2	1	3	2	1	-1	2	1
2514298.7300	0.5000	-0.7974	3	0.0574	5	-17001	224	2	-1	3	2	1	1	2	2
2514316.7050	0.3000	0.3487	3	0.0574	7	-17001	224	2	-1	3	3	1	1	2	2
2514353.4900	0.3000	0.1568	3	0.0556	5	-17001	224	2	-1	3	2	1	1	2	1
2598103.5574	0.2436	-1.9173	3	202.3808	5	17001	224	3	-1	3	2	3	1	4	3
2598175.0856	0.2436	-3.2183	3	202.3808	7	17001	224	3	-1	3	3	3	1	4	3
2598175.7820	0.2436	-1.7869	3	202.3808	7	17001	224	3	-1	3	3	3	1	4	4
2603402.3275	0.2436	-1.9049	3	201.9327	5	17001	224	3	1	3	2	3	-1	4	3
2603420.1376	0.2436	-3.2058	3	201.9327	7	17001	224	3	1	3	3	3	-1	4	3
2603427.6140	0.2436	-1.7746	3	201.9324	7	17001	224	3	1	3	3	3	-1	4	4
3036258.8200	0.5000	-0.8812	3	187.4941	5	-17001	224	3	1	3	2	2	-1	2	2
3036270.6600	0.5000	0.0730	3	187.4937	5	-17001	224	3	1	3	2	2	-1	2	1
3036276.6300	0.5000	0.2649	3	187.4941	7	-17001	224	3	1	3	3	2	-1	2	2
3036574.5600	0.5000	-0.8815	3	187.7550	5	-17001	224	3	-1	3	2	2	1	2	2
3036644.7800	0.5000	0.0727	3	187.7526	5	-17001	224	3	-1	3	2	2	1	2	1
3036646.1000	0.5000	0.2646	3	187.7550	7	-17001	224	3	-1	3	3	2	1	2	2
3110930.1167	0.1254	-1.2960	3	83.7247	5	17001	224	2	-1	2	2	2	1	3	3
3110932.2811	0.1254	-1.4878	3	83.7242	3	17001	224	2	-1	2	1	2	1	3	2
3110944.1138	0.1254	-2.4420	3	83.7242	5	17001	224	2	-1	2	2	2	1	3	2

Ring effect studies: Rayleigh scattering, including molecular parameters for rotational Raman scattering, and the Fraunhofer spectrum

Kelly V. Chance and Robert J. D. Spurr

Improved parameters for the description of Rayleigh scattering in air and for the detailed rotational Raman scattering component for scattering by O_2 and N_2 are presented for the wavelength range 200–1000 nm. These parameters enable more accurate calculations to be made of bulk molecular scattering and of the Ring effect for a variety of atmospheric radiative transfer and constituent retrieval applications. A solar reference spectrum with accurate absolute vacuum wavelength calibration, suitable for convolution with the rotational Raman spectrum for Ring effect calculations, has been produced at 0.01-nm resolution from several sources. It is convolved with the rotational Raman spectra of O_2 and N_2 to produce an atmospheric Ring effect source spectrum. © 1997 Optical Society of America

Applied Optics 36, 5224-5230, 1997.

Rayleigh Scattering Cross Section

$$Q^R(\mathrm{cm}^2) \;=\; \frac{128\pi^5}{3\lambda^4}\alpha^2$$

Rotational Raman Cross Sections

$$Q^W_{N,N'}(\mathrm{cm}^2) \;=\; \frac{256\pi^5}{27(\lambda')^4}\gamma^2 f_N b_{N',J',N,J},$$

where f_N is the fractional population in the initial state, and the Placzek-Teller coefficients are given in a Hund's case b coupling scheme by

$$b_{N',J',N,J} = (2N+1)(2N'+1)(2J'+1)\begin{pmatrix} N & L & N' \\ 0 & 0 & 0 \end{pmatrix}^2 \begin{Bmatrix} N & L & N' \\ J' & S & J \end{Bmatrix}^2.$$

J is the total angular momentum, S is the electronic spin angular momentum (1 for O_2 and 0 for N_2), and L is the component of the 2nd rank polarizability tensor. $L = 0$ for average polarizability (Rayleigh scattering) and $L = 2$ for the present Raman scattering. O_2 eigenvectors must be expanded in terms of the Hund's case b basis set.

Index of Refraction

$$(n_{air} - 1) \times 10^4 = 0.7041 + \frac{315.90}{157.39 - \sigma^2} + \frac{8.4127}{50.429 - \sigma^2}$$

$$\sigma\ (\mu m^{-1}) = 1/\lambda\ (\mu m)$$

Rayleigh Scattering Cross Section at STP (cm^2)

$$Q_R \times 10^{24} = \frac{3.9993 \times 10^{-4}\sigma^4}{1 - 1.069 \times 10^{-2}\sigma^2 - 6.681 \times 10^{-5}\sigma^4}$$

Rayleigh Scattering Phase Functions

$$\begin{aligned}
\Phi_0^C &= \frac{3}{160\pi}\left[\frac{(180 + 13\epsilon) + (180 + \epsilon)\cos^2\theta}{18 + \epsilon}\right] \\
\Phi_0^W &= \frac{3}{160\pi}(13 + \cos^2\theta) \\
\Phi_0^T &= \frac{3}{80\pi}\left[\frac{(45 + 13\epsilon) + (45 + \epsilon)\cos^2\theta}{9 + 2\epsilon}\right]
\end{aligned}$$

$\epsilon = (\gamma/\overline{\alpha})^2$, γ is the anisotropy of the polarizability, and $\overline{\alpha}$ is the average polarizability. In each case, the phase function is given in terms of the *respective* depolarization ratio ρ_0^X $(X = C, W, T)$ by:

$$\Phi_0^X = \frac{3}{8\pi}\left[\frac{(1 + \rho_0^X) + (1 - \rho_0^X)\cos^2\theta}{2 + \rho_0^X}\right]$$

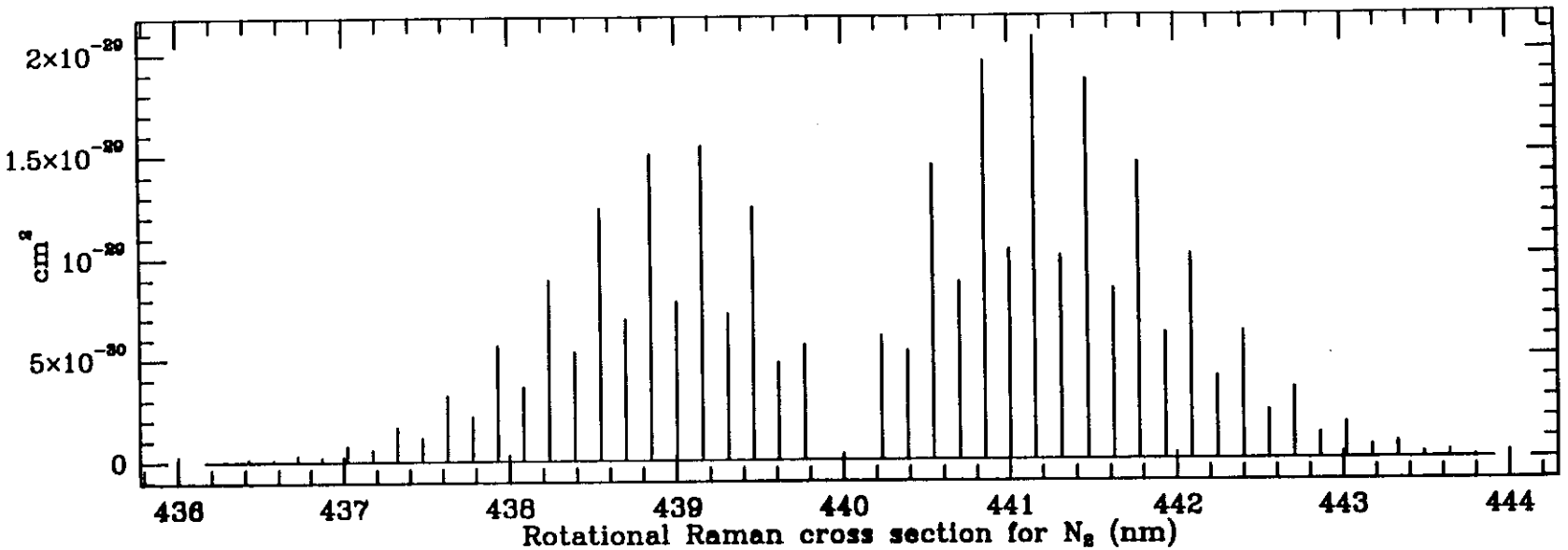
2×10⁻²⁹
1.5×10⁻²⁹
10⁻²⁹
5×10⁻³⁰
0
cm²
436
437
438
439
440
441
442
443
444
Rotational Raman cross section for N₂ (nm)

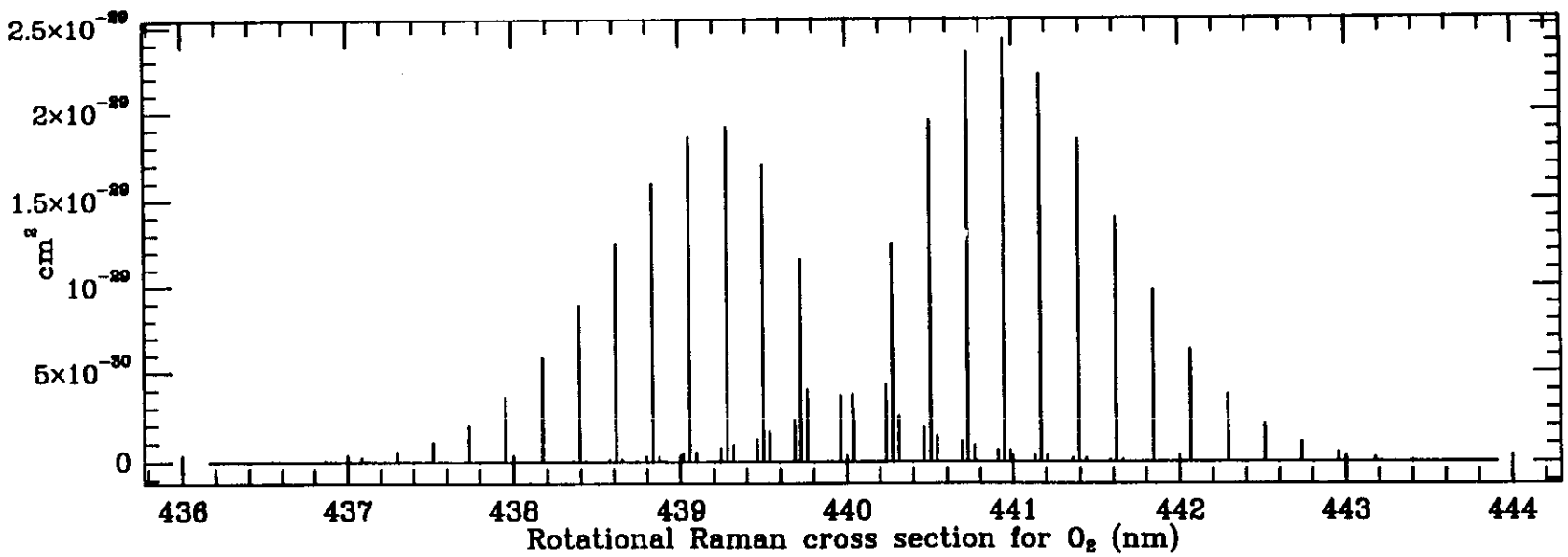
2.5×10⁻²⁹
2×10⁻²⁹
1.5×10⁻²⁹
10⁻²⁹
5×10⁻³⁰
0
cm²
436
437
438
439
440
441
442
443
444
Rotational Raman cross section for O₂ (nm)

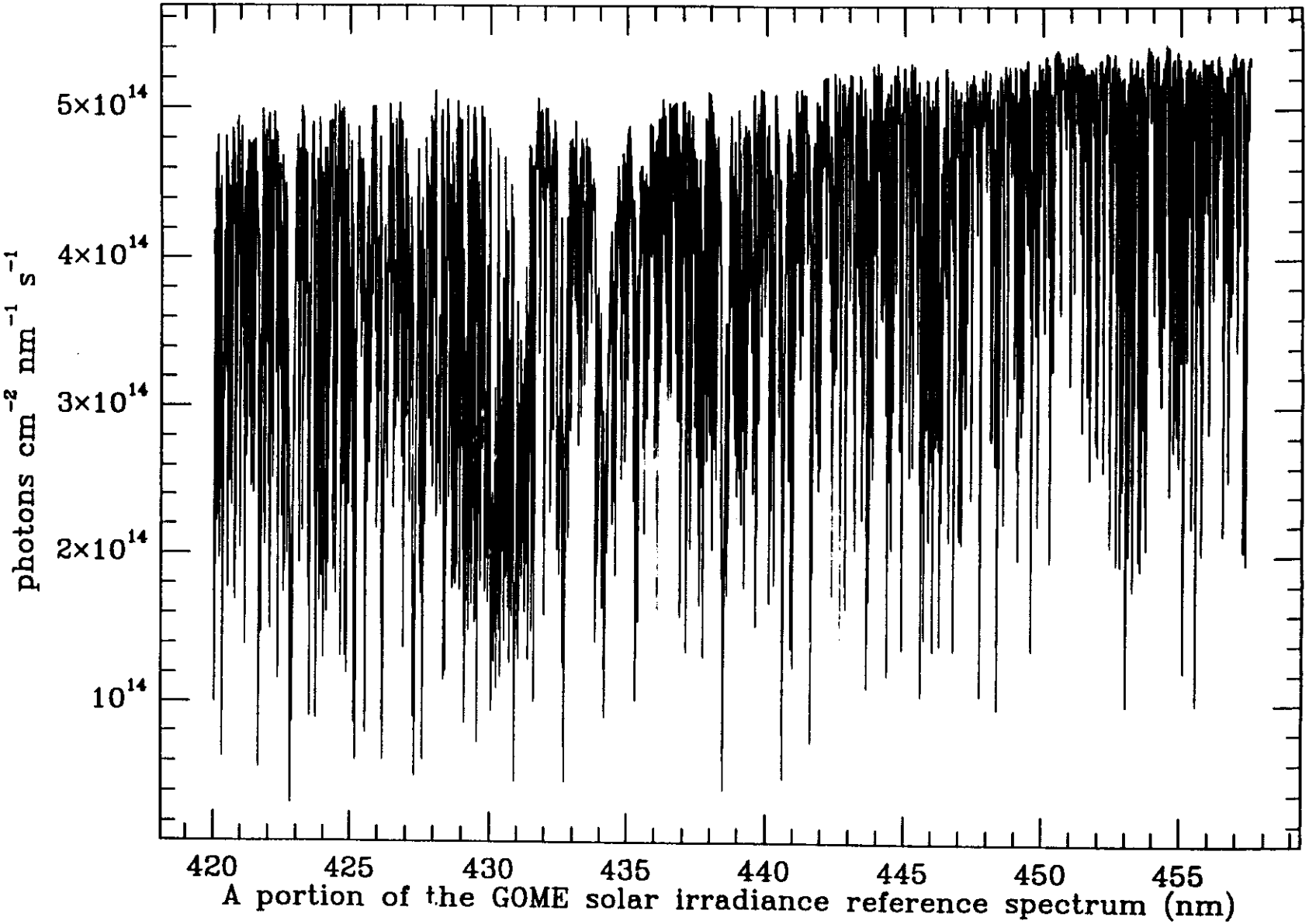
5×10^14
4×10^14
3×10^14
2×10^14
10^14
photons cm^-2 nm^-1 s^-1
420
425
430
435
440
445
450
455
A portion of the GOME solar irradiance reference spectrum (nm)

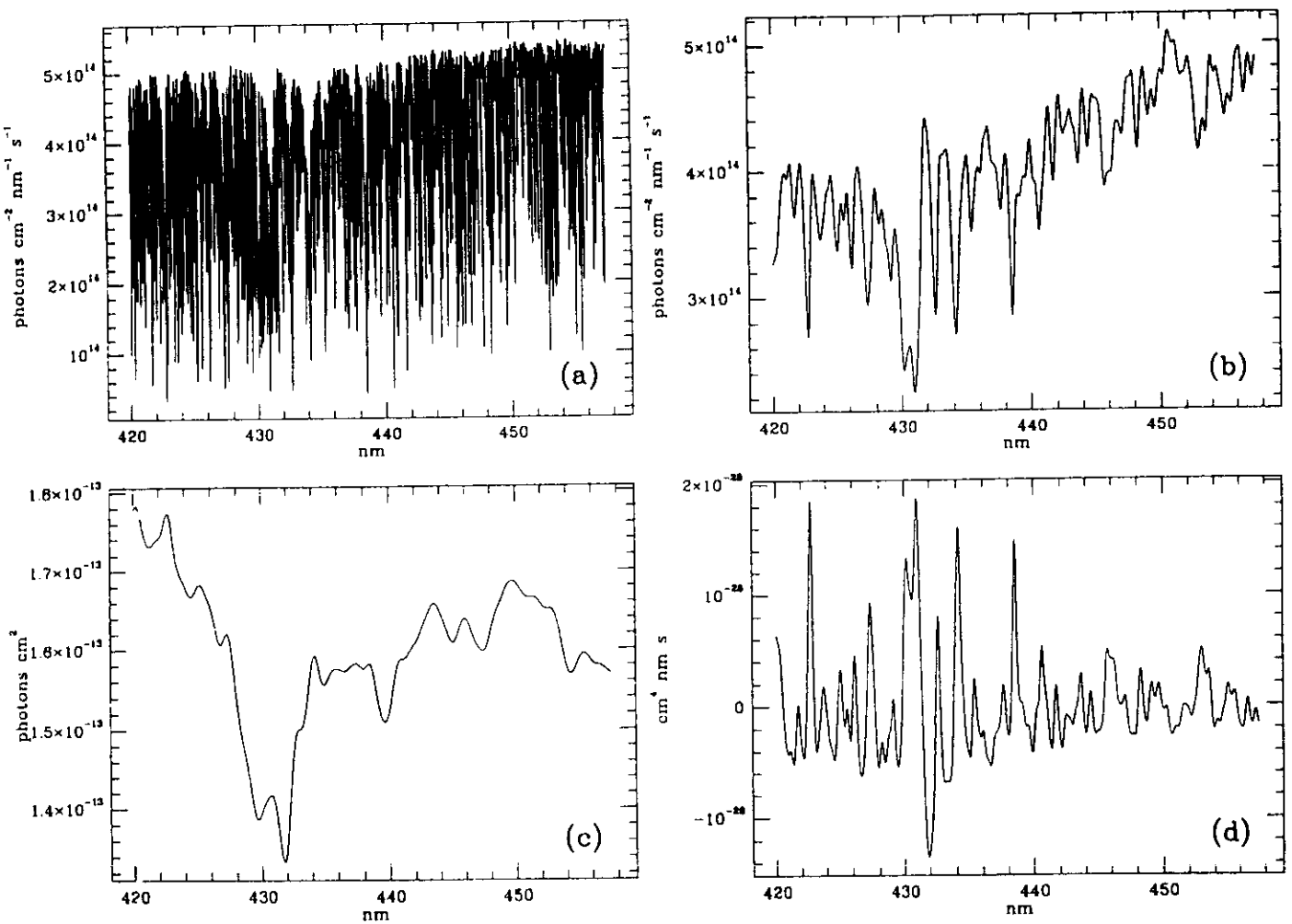

Fig. 2. (a) Sample of the Fraunhofer reference spectrum determined in this study. (b) The same Fraunhofer spectrum, convolved with a Gaussian slit function having a half-width at $1/e$ intensity of 0.212 nm, appropriate to the GOME instrument in this wavelength range. (c) The Fraunhofer spectrum of (b), convolved with the rotational Raman cross sections to create a Ring effect source spectrum. The units are those of cross section × photons, corresponding to the Ring effect scattering source per air molecule at 250 K. (d) The ratio of the Ring effect source spectrum given in (c) to the Fraunhofer spectrum of (b), with a cubic polynomial subtracted off. This spectrum closely corresponds to the Ring effect spectrum used in previous studies for atmospheric spectrum correction, as discussed in the text.

Relative Rayleigh and Raman Scattering Intensities, Mostly from Kattawar *et al.*, 1981

V polarization in	H polarization in	Sum (natural light in)
	Rayleigh-Brillouin	
${}^{V}C_V = 180 + 4\epsilon$	${}^{H}C_V = 3\epsilon$	${}^{0}C_V = 180 + 7\epsilon$
${}^{V}C_H = 3\epsilon$	${}^{H}C_H = 3\epsilon + (180 + \epsilon)cos^2\theta$	${}^{0}C_H = 6\epsilon + (180 + \epsilon)cos^2\theta$
${}^{V}C_0 = 180 + 7\epsilon$	${}^{H}C_0 = 6\epsilon + (180 + \epsilon)cos^2\theta$	${}^{0}C_0 = (180 + 13\epsilon) + (180 + \epsilon)cos^2\theta$
		$\rho_0^C = 6\epsilon/(180 + 7\epsilon)$
	Raman	
${}^{V}W_V = 12\epsilon$	${}^{H}W_V = 9\epsilon$	${}^{0}W_V = 21\epsilon$
${}^{V}W_H = 9\epsilon$	${}^{H}W_H = 9\epsilon + 3\epsilon cos^2\theta$	${}^{0}W_H = 18\epsilon + 3\epsilon cos^2\theta$
${}^{V}W_0 = 21\epsilon$	${}^{H}W_0 = 18\epsilon + 3ccos^2\theta$	${}^{0}W_0 = 39\epsilon + 3\epsilon cos^2\theta$
		$\rho_0^W = 6/7$
	Sum	
${}^{V}T_V = 180 + 16\epsilon$	${}^{H}T_V = 12\epsilon$	${}^{0}T_V = 180 + 28\epsilon$
${}^{V}T_H = 12\epsilon$	${}^{H}T_H = 12\epsilon + (180 + 4c)cos^2\theta$	${}^{0}T_H = 24\epsilon + (180 + 4\epsilon)cos^2\theta$
${}^{V}T_0 = 180 + 28\epsilon$	${}^{H}T_0 = 24\epsilon + (180 + 4\epsilon)cos^2\theta$	${}^{0}T_0 = (180 + 52\epsilon) + (180 + 4\epsilon)cos^2\theta$
		$\rho_0^T = 6\epsilon/(45 + 7c)$

$$\epsilon = (\gamma/\overline{\alpha})^2$$

$$\Phi_0^X = \frac{3}{8\pi}\left[\frac{(1+\rho_0^X) + (1-\rho_0^X)cos^2\theta}{2+\rho_0^X}\right]$$

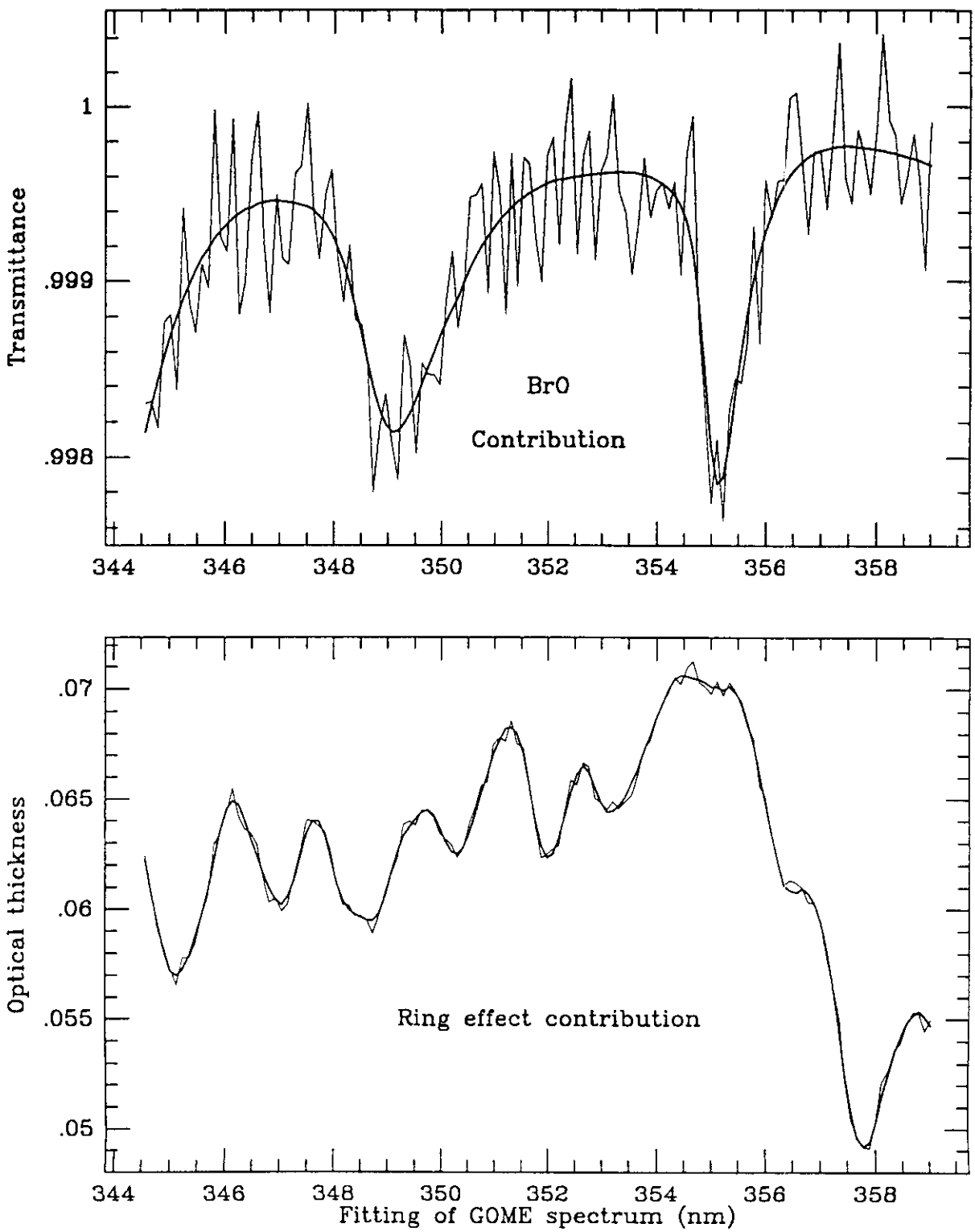
Transmittance
1
.999
.998
BrO
Contribution
344
346
348
350
352
354
356
358
Optical thickness
.07
.065
.06
.055
.05
Ring effect contribution
Fitting of GOME spectrum (nm)

Day 5

First, let us consider the Curtis Godson (or van de Hulst Curtis Godson approximation for inhomogeneous atmospheres. In the approximation of an atmosphere that is exponential in pressure. In such a case, the total abundance is shown by simple integration to be equivalent to that of a layer of the base pressure, with thickness equal to that of the exponential scale height. However, H-C-G showed that a best overall single layer representation for calculation of spectra of such atmospheres is one where the representative pressure is 1/2 the base pressure. For an atmospheric shell with pressure boundaries P1 and P2, the best choice is (P1+P2)/2. This can readily be4 demonstrated by integration over P(z)dz to determine the pressure-weighted average.

The general procedure for constructing an atmospheric model is then to:

construct layered atmosphere appropriate to geometry;
determine whether refraction needed;
recursive tests for layering (are the layers small enough?) - OH (z) -
        % changes
        cloud complications in M-S (change in OD)

assemble databases ....

model spectrum
        line-by-line (approximations to speed up; correlated k)
        adding ODs, perhaps (for emission, with respect to a standard
        temperature; using the blackbody formulation)
        model transmission or emission
        adjust for i), albedo, closure terms

perform fitting - nlls
        onion peeling or global fitting for limb
        statistical regularization (e.g., optimal estimation or
        Philips-Tikhonov) for under-constrained problems
        linear vs. nonlinear fitting models (DOAS versus BOAS)

It is very important for the serious student to realize that it is the retrieval that matters, and that the way to participate meaningfully is to investigate relevant retrieval issues down to bedrock. We do have an unfortunate tendency in our community to operate by reputation and by acronym (as a way to obtain credit that is not always due) - atmospheric measurements is not nearly as rigorous a field as, for example, laboratory spectroscopy. So, when anyone (even myself or your other teachers in this course) tells you that such-and-such a method, described by this-or-that acronym is the best, you should always remain skeptical. The best way to contribute yourself is to learn the details (which many atmospheric measurers do not), question everything, and experiment endlessly. Library research, which I feel in under-utilized in our field, can also help to improve retrievals. If you take my challenge and trace line parameters to there source you can find some very interesting things. Also, if you track down fitting techniques which are supposed to be very well validated, you may find some surprises - like they are mainly validated by old age.

FIRS-2 Measurement Applications

- Atmospheric modeling: FIRS-2 determines details of stratospheric photochemistry, improving predictive capability of models.
- Global warming studies: FIRS-2 determines details of the atmospheric radiative properties of greenhouse gases, especially CO_2.
- Industrial processes: FIRS-2 measures effects of chlorofluorocarbons and halons on the ozone layer.
- Agricultural processes: FIRS-2 measures gaseous by-products of agriculture; nitrous oxide, bromine species resulting from methyl bromide use.

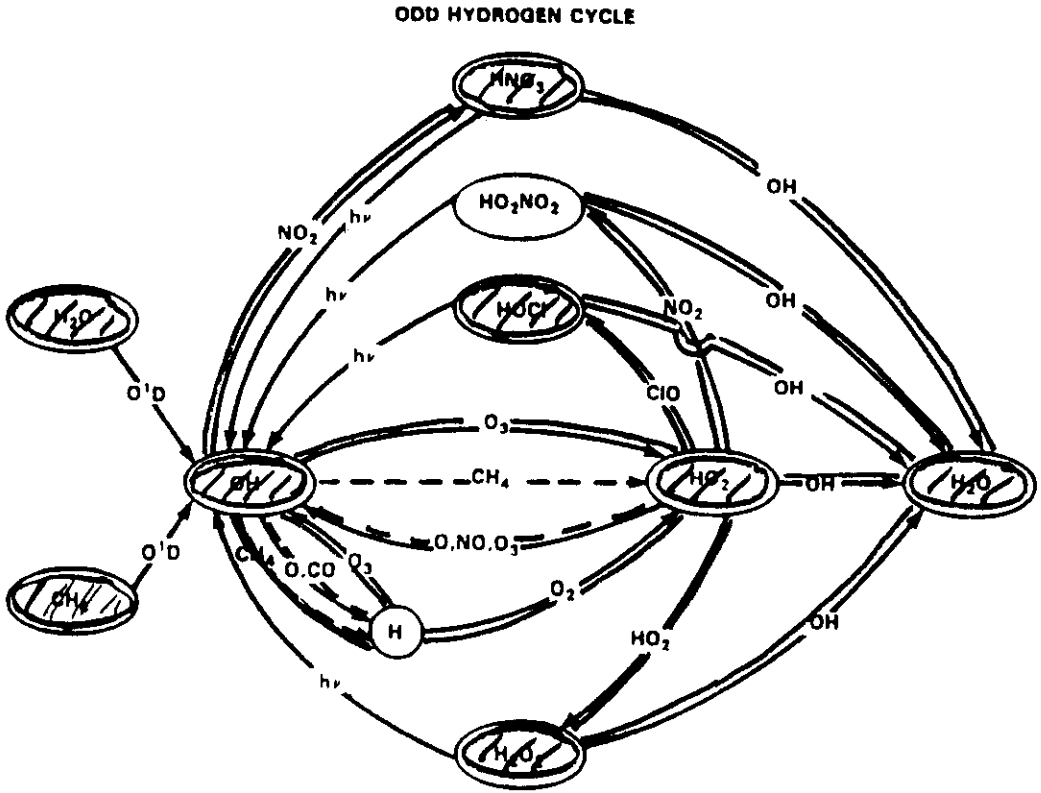

Schematic of the Odd-Hydrogen Cycle.

From *Present State of Knowledge of the Upper Atmosphere: An Assessment Report*, NASA Reference Publication 1162, 1986.

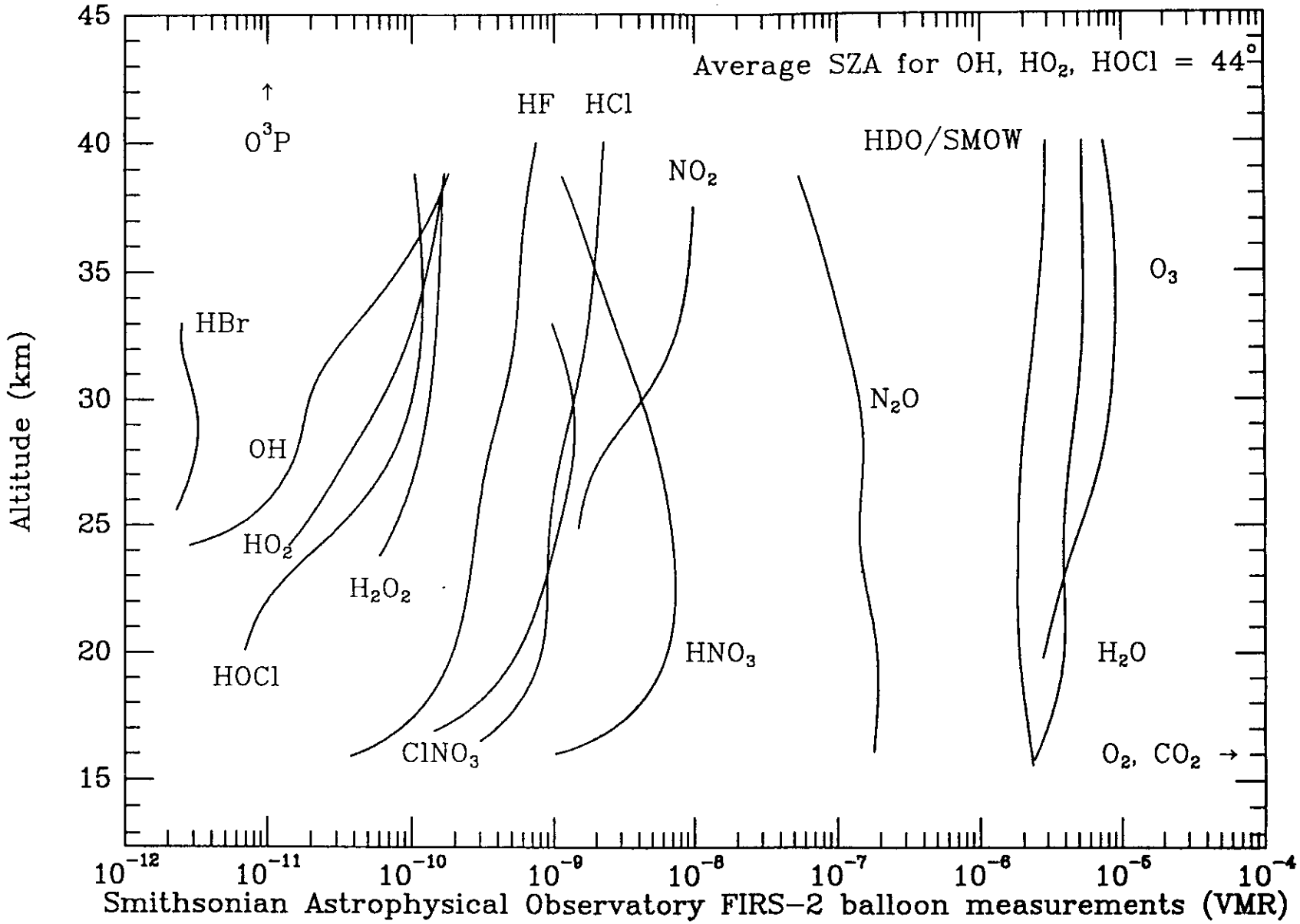
Average SZA for OH, HO_2, HOCl = 44°
O^3P
HF
HCl
NO_2
HDO/SMOW
O_3
HBr
N_2O
OH
HO_2
H_2O_2
HOCl
HNO_3
H_2O
$ClNO_3$
O_2, CO_2 →
Altitude (km)
45
40
35
30
25
20
15
10^{-12}
10^{-11}
10^{-10}
10^{-9}
10^{-8}
10^{-7}
10^{-6}
10^{-5}
10^{-4}
Smithsonian Astrophysical Observatory FIRS-2 balloon measurements (VMR)

HOx dominates below ~22 km

Conclusions from FIRS-2 measurements

- We have made the first simultaneous measurement of HO_x, Cl_x, and NO_x species throughout the middle atmosphere. The relative contributions to ozone destruction from the HO_x, NO_x, and Cl_x catalytic cycles are determined from 20-40 km.
- Comprehensive budgets of NO_y, and Cl_y are measured.
- Chlorine budget studies suggest that a small channel exists for production of HCl from ClO + OH and/or ClO + HO_2, diminishing the effectiveness of the Cl_x catalytic cycle in the upper stratosphere.
- O_3 formation and loss rates in the upper stratosphere are now shown to be in balance; under-prediction of stratospheric O_3 above 35 km was a long-standing problem.
- OH near 40 km has been under-predicted.
- HBr measurements provide constraint on bromine budget, Br_x chemistry (in particular, it provides limits to the effectiveness of BrO + HO_2).
- Closely-coupled chemical relationships in the upper stratosphere have been tested, e.g.

$$[HOCl] = k_1[HO_2][ClO]/(j_{HOCl} + k_2[OH])$$

$$[H_2O_2] = k_3[HO_2]^2/(j_{H_2O_2} + k_4[OH])$$

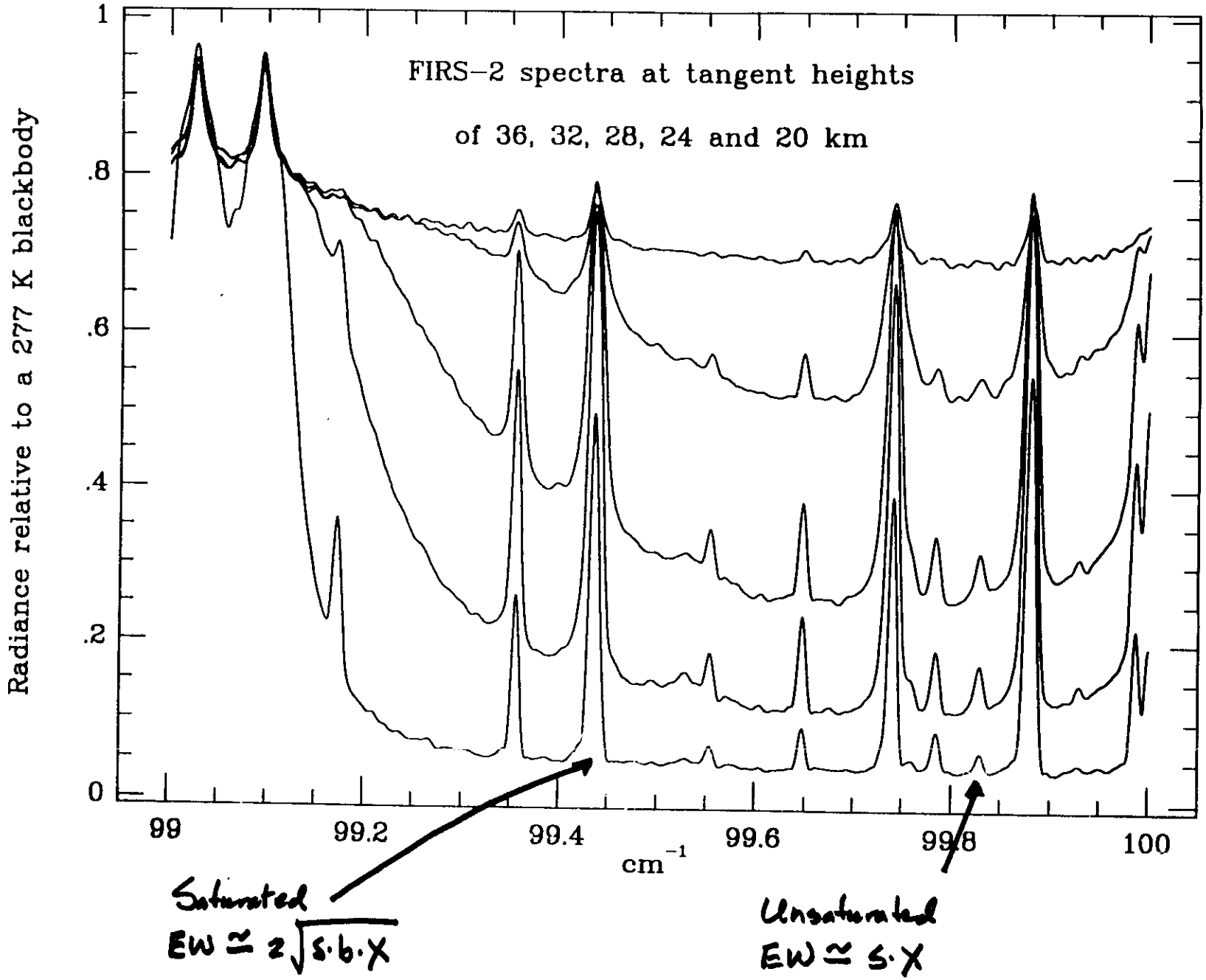
FIRS–2 spectra at tangent heights
of 36, 32, 28, 24 and 20 km
Radiance relative to a 277 K blackbody
1
.8
.6
.4
.2
0
99
99.2
99.4
99.6
99.8
100
cm⁻¹
Saturated
EW ≃ 2√5.6·X
Unsaturated
EW ≃ 5·X

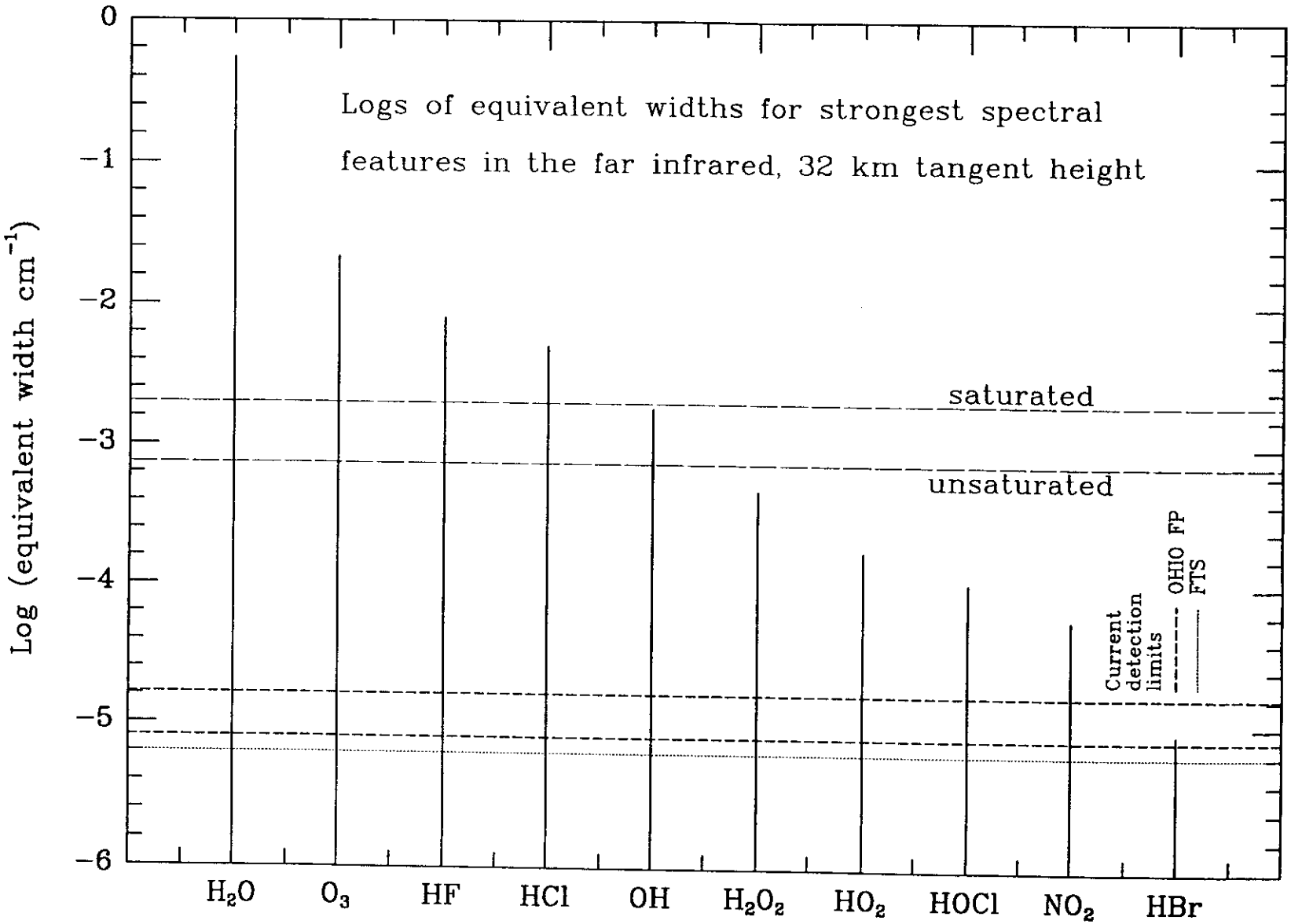
Logs of equivalent widths for strongest spectral features in the far infrared, 32 km tangent height
Log (equivalent width cm^{-1})
0
−1
−2
−3
−4
−5
−6
saturated
unsaturated
Current detection limits
OHIO FP
FTS
H_2O
O_3
HF
HCl
OH
H_2O_2
HO_2
HOCl
NO_2
HBr

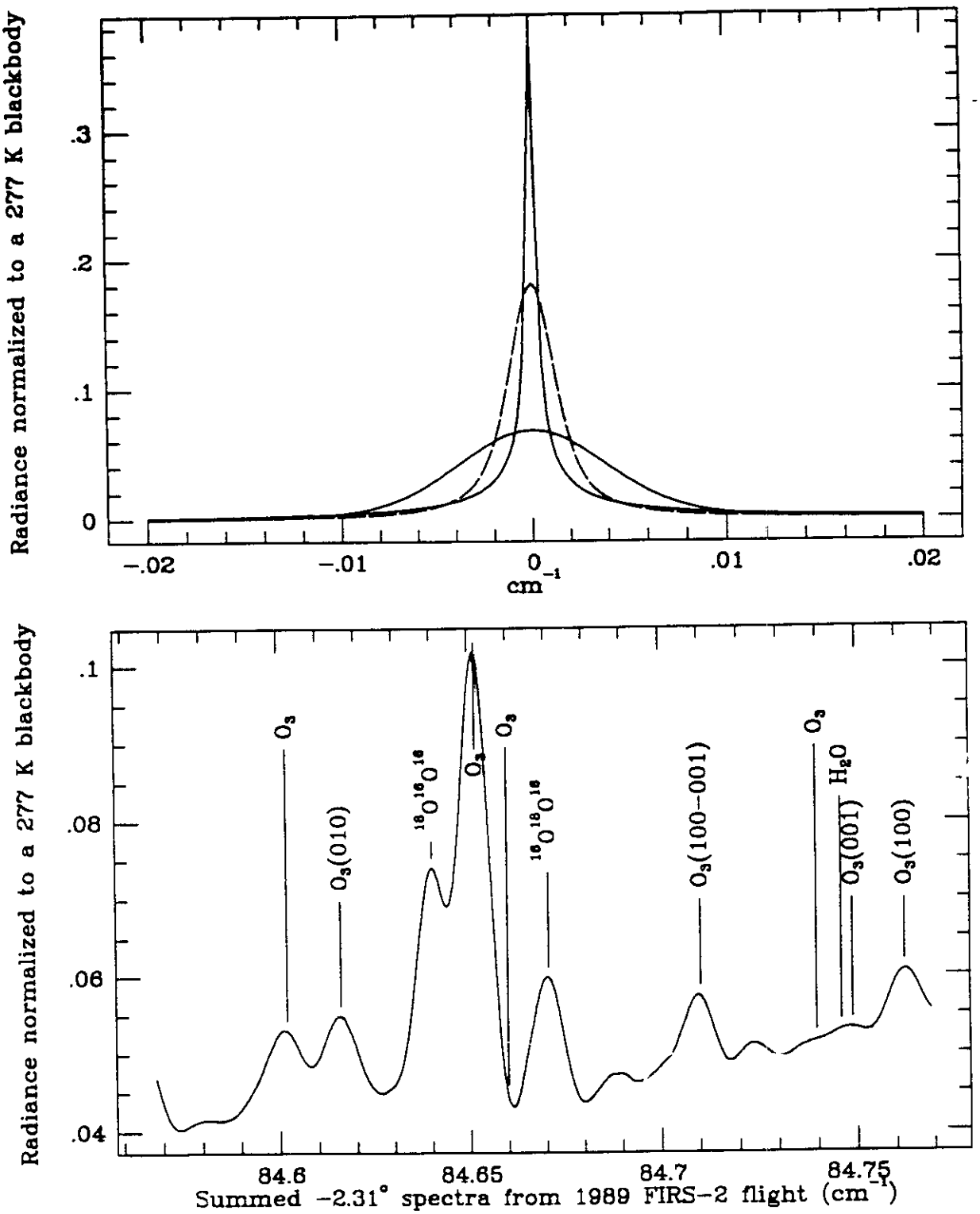
Radiance normalized to a 277 K blackbody
.3
.2
.1
0
−.02
−.01
0
.01
.02
cm⁻¹
Radiance normalized to a 277 K blackbody
.1
.08
.06
.04
O3
O3(010)
18O16O16
O3
O3
16O18O16
O3(100−001)
O3
H2O
O3(001)
O3(100)
84.6
84.65
84.7
84.75
Summed −2.31° spectra from 1989 FIRS−2 flight (cm⁻¹)

Line Locations for THz Measurements of Trace Stratospheric Species

OH		HO_2		H_2O_2		HF		HCl		HOCl		ClO		HBr		NO_2	
THz	cm^{-1}	THz	cm^{-1}	THz	cm^{-1}	THz	cm^{-1}	THz	cm^{-1}	THz	cm^{-1}	THz	cm^{-1}	THz	cm^{-1}	THz	cm^{-1}
2.51433	83.869	0.62566	20.780	2.81734	93.976	4.91468	163.936	3.12199	104.138	2.98378	99.528	0.64945	21.663	1.50055	50.053	2.98374	99.527
3.03627	101.279	4.25849	142.048	3.36279	112.171	6.13197	204.540	3.74222	124.827	4.28628	142.975			1.50102	50.069	3.10196	103.470
3.03664	101.291	4.30681	143.660			244, 893		4.35367	145.223	4.28668	142.988			2.99536	99.914	3.12317	104.178
3.54379	118.208	4.32432	144.244					4.36018	145.440	4.31549	143.949			3.48976	116.406	3.17440	105.886
3.55119	118.455	4.37126	145.810					4.96809	165.718	4.31641	143.980			3.49084	116.442	3.20348	106.856
4.21230	140.507	4.39032	146.445					4.97551	165.965	4.40547	146.951					3.25435	108.554
5.35823	178.731	4.56198	152.171					5.58783	186.390	4.67133	155.819					3.48401	116.214
5.36387	178.920	4.58797	153.038							4.75945	158.758					3.48492	116.244
5.65034	188.475	4.65355	155.226														
5.66351	188.914	4.71896	157.407														

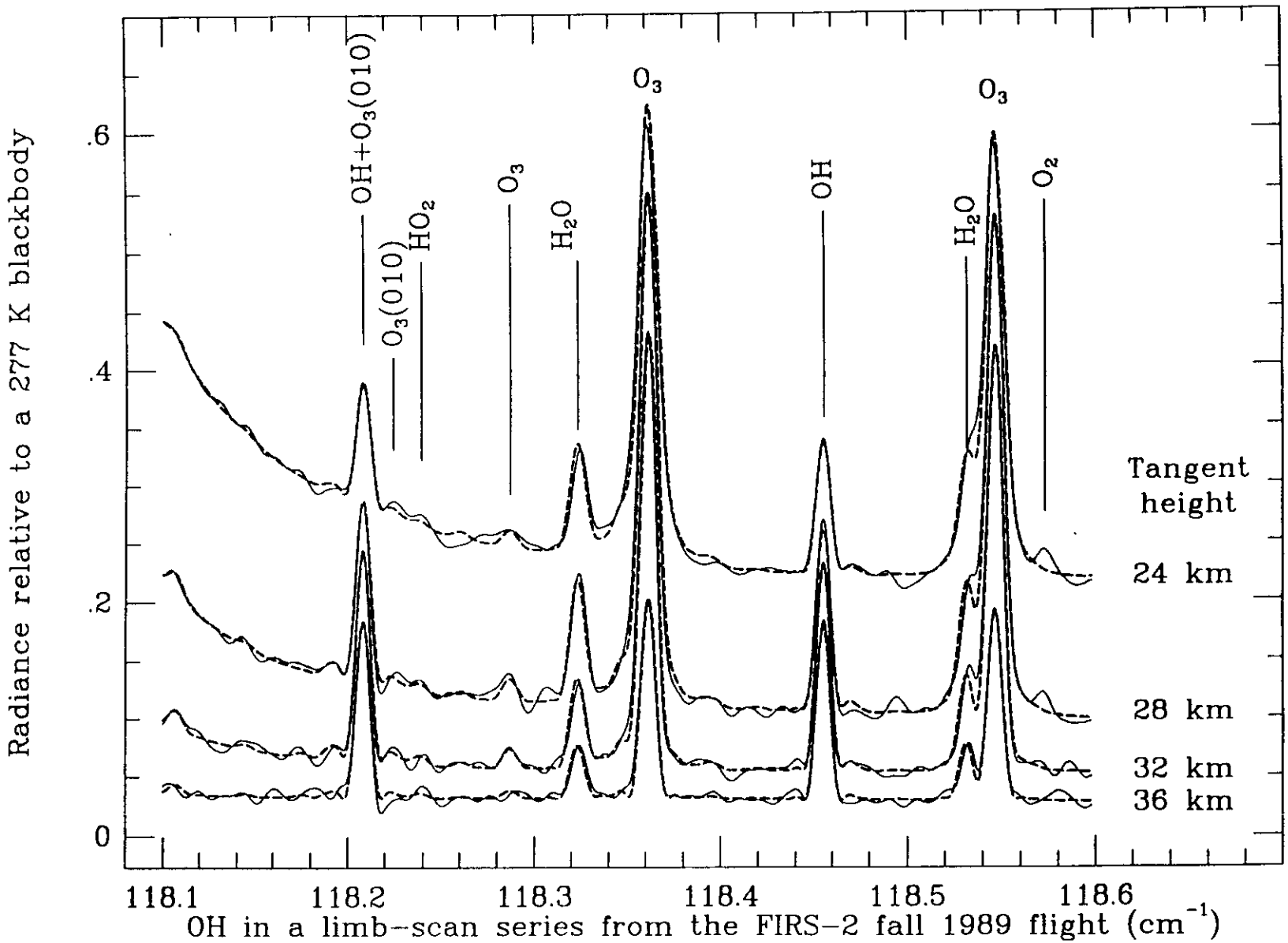
Radiance relative to a 277 K blackbody
0
.2
.4
.6
OH+O3(010)
O3(010)
HO2
O3
H2O
O3
OH
H2O
O3
O2
Tangent height
24 km
28 km
32 km
36 km
118.1
118.2
118.3
118.4
118.5
118.6
OH in a limb-scan series from the FIRS-2 fall 1989 flight (cm-1)

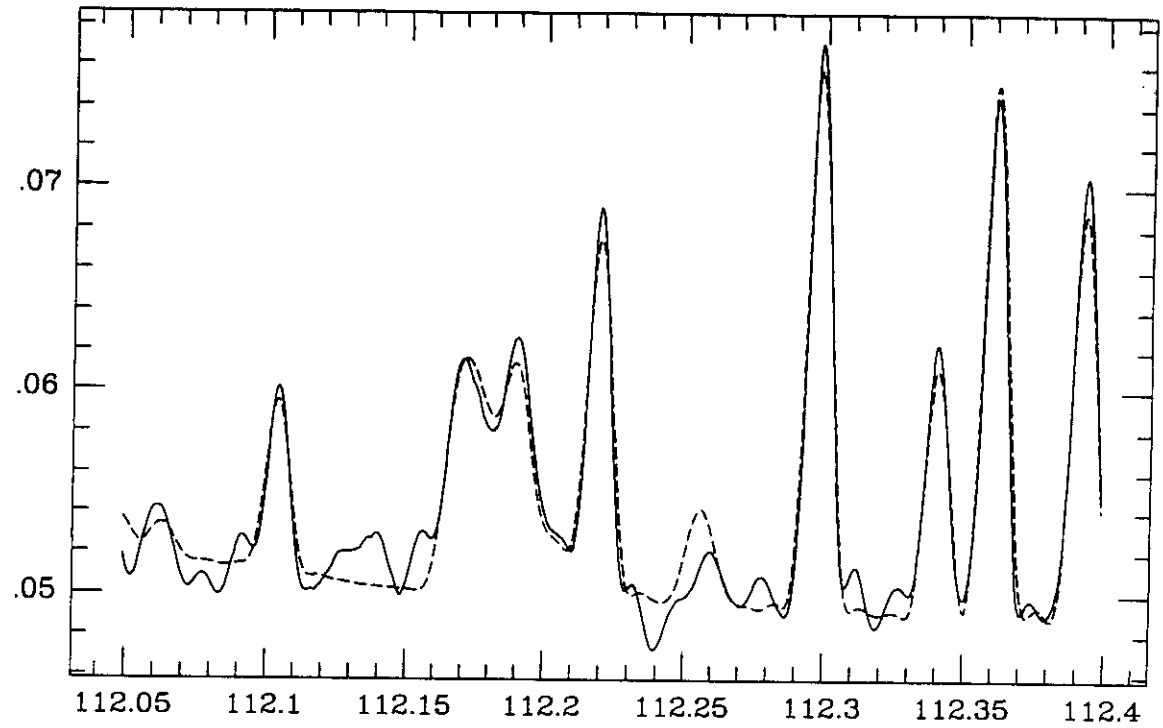

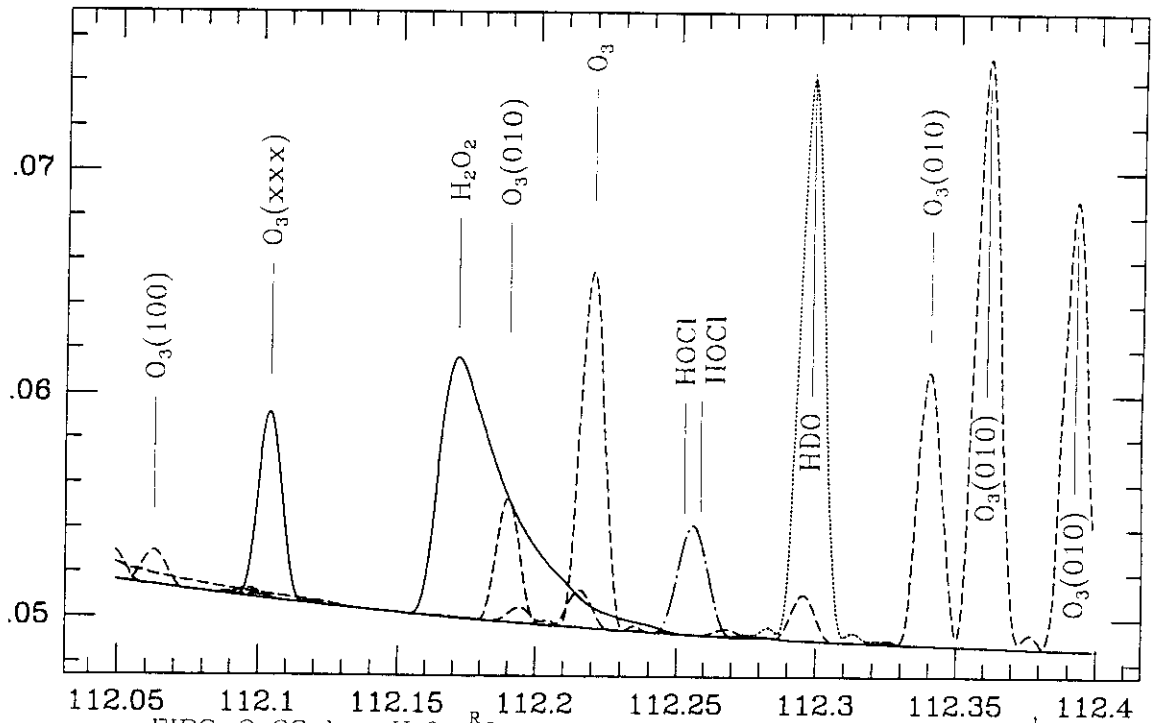

FIRS-2 32 km H_2O_2 $^RQ_5$ measurements and fitting (cm^{-1})

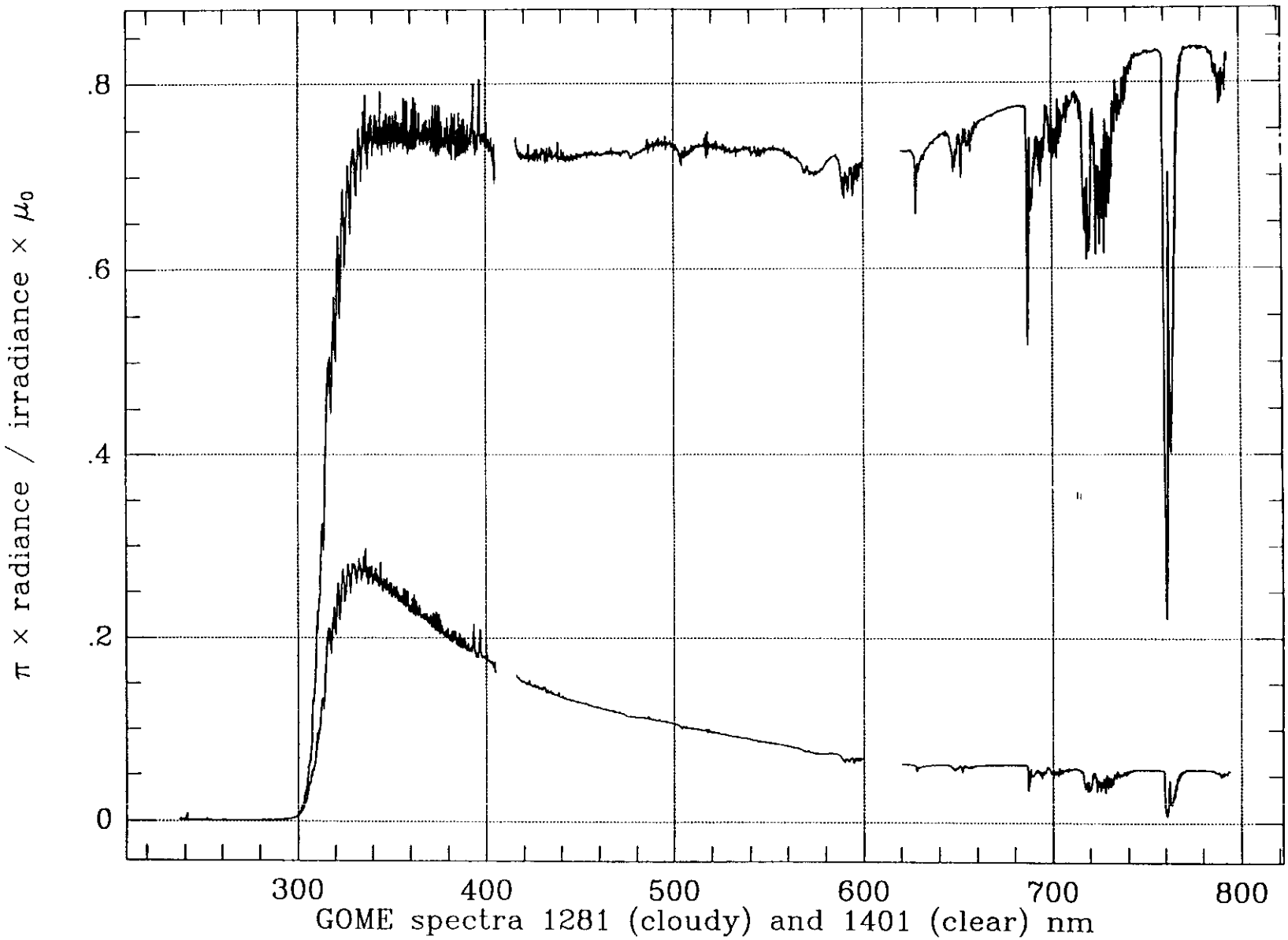
π × radiance / irradiance × μ0
.8
.6
.4
.2
0
300
400
500
600
700
800
GOME spectra 1281 (cloudy) and 1401 (clear) nm

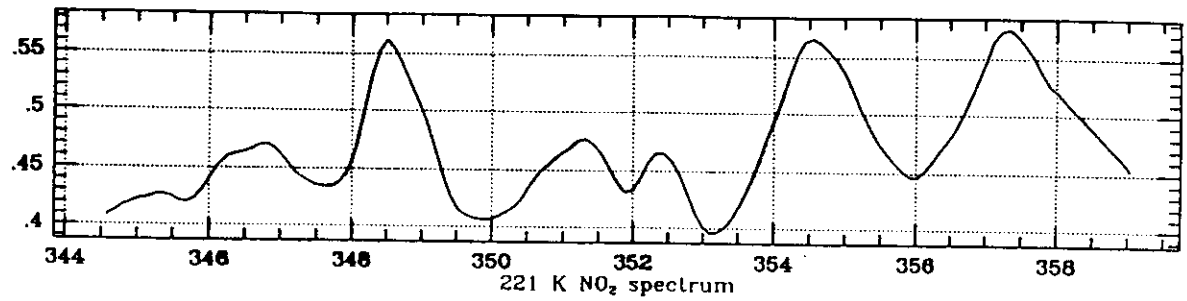

221 K NO_2 spectrum

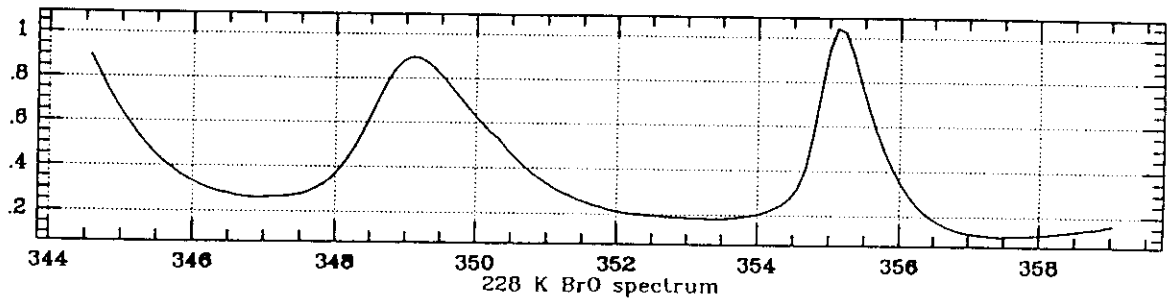

228 K BrO spectrum

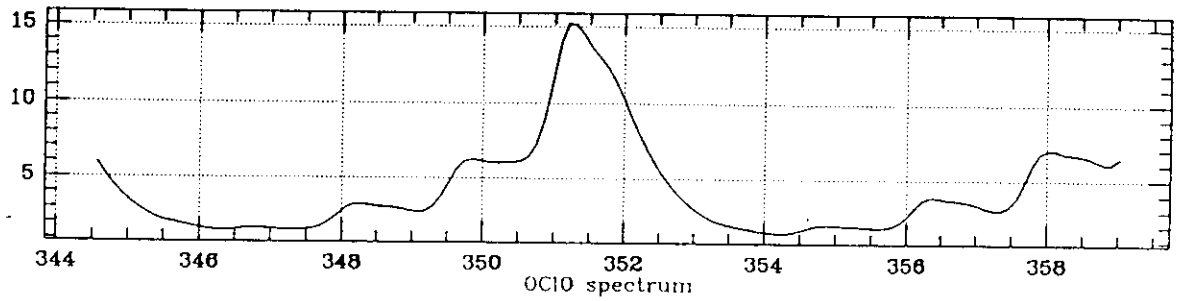

OClO spectrum

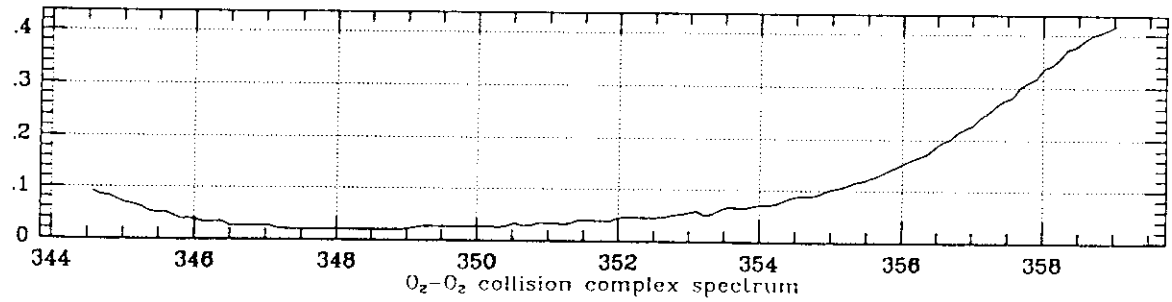

O_2–O_2 collision complex spectrum

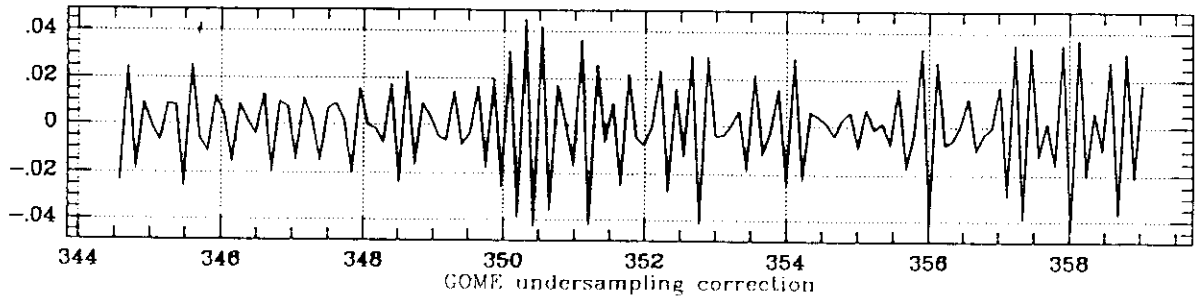

GOME undersampling correction

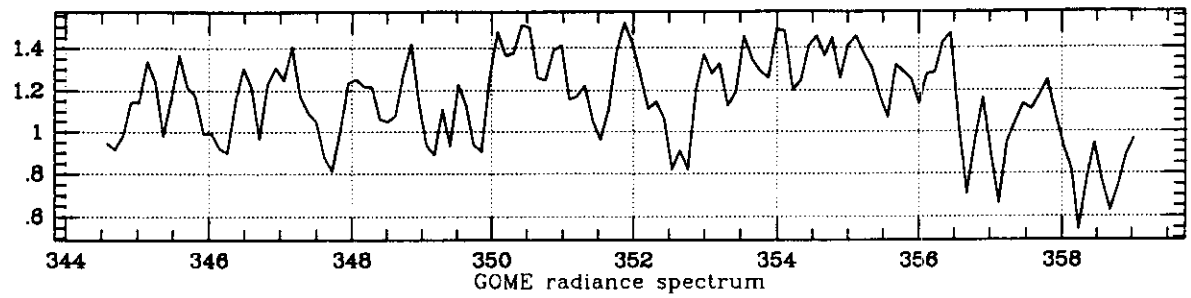

GOME radiance spectrum

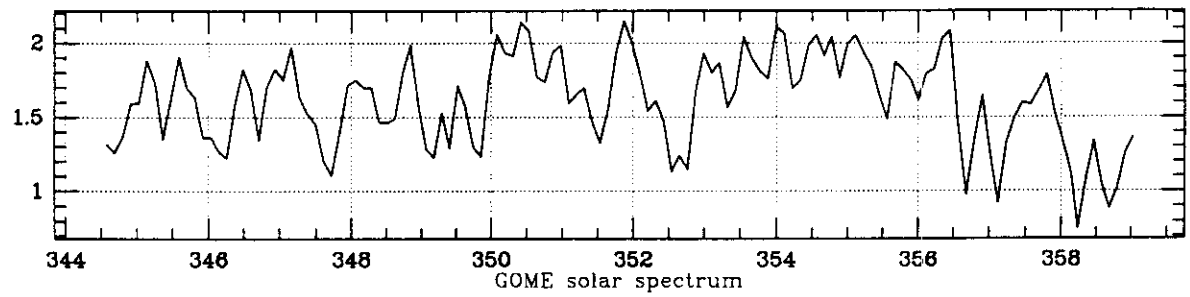

GOME solar spectrum

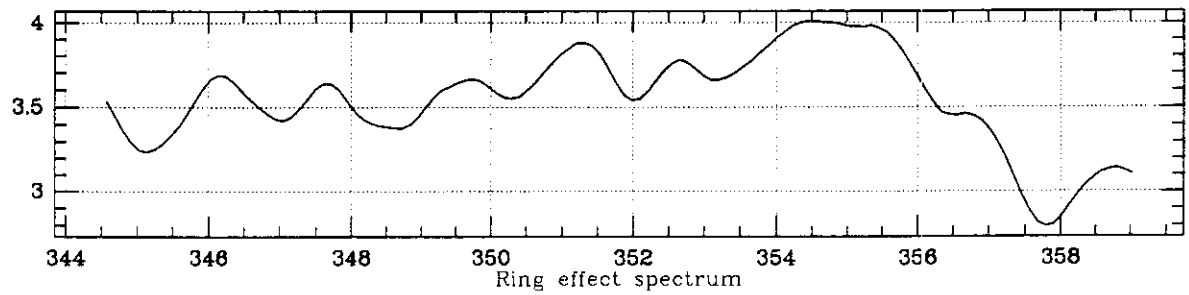

Ring effect spectrum

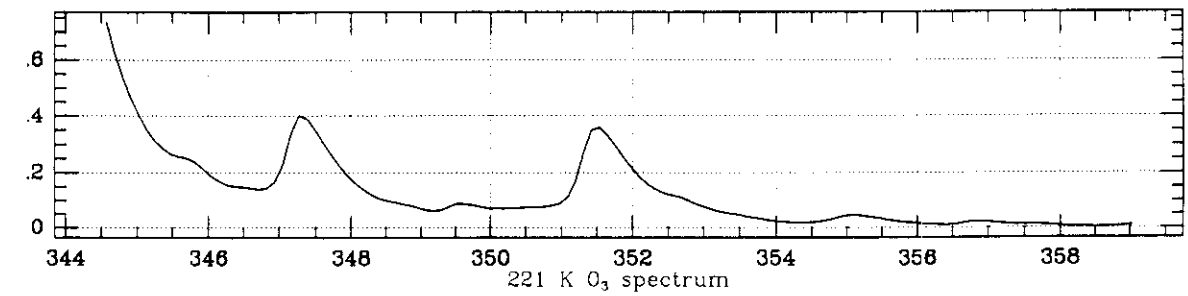

221 K O_3 spectrum

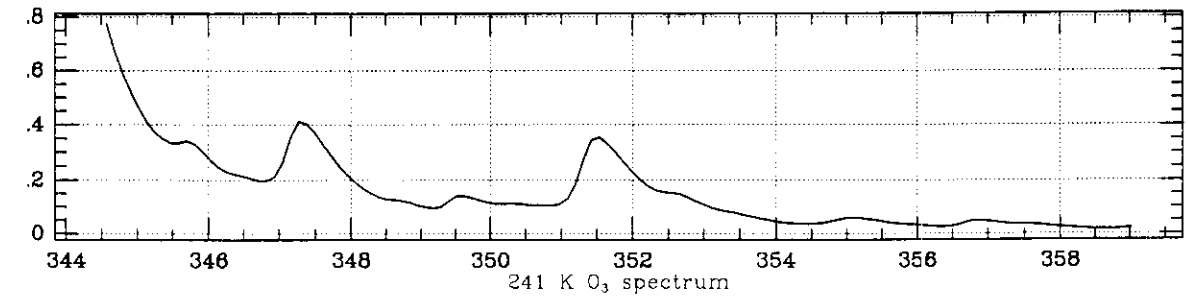

241 K O_3 spectrum

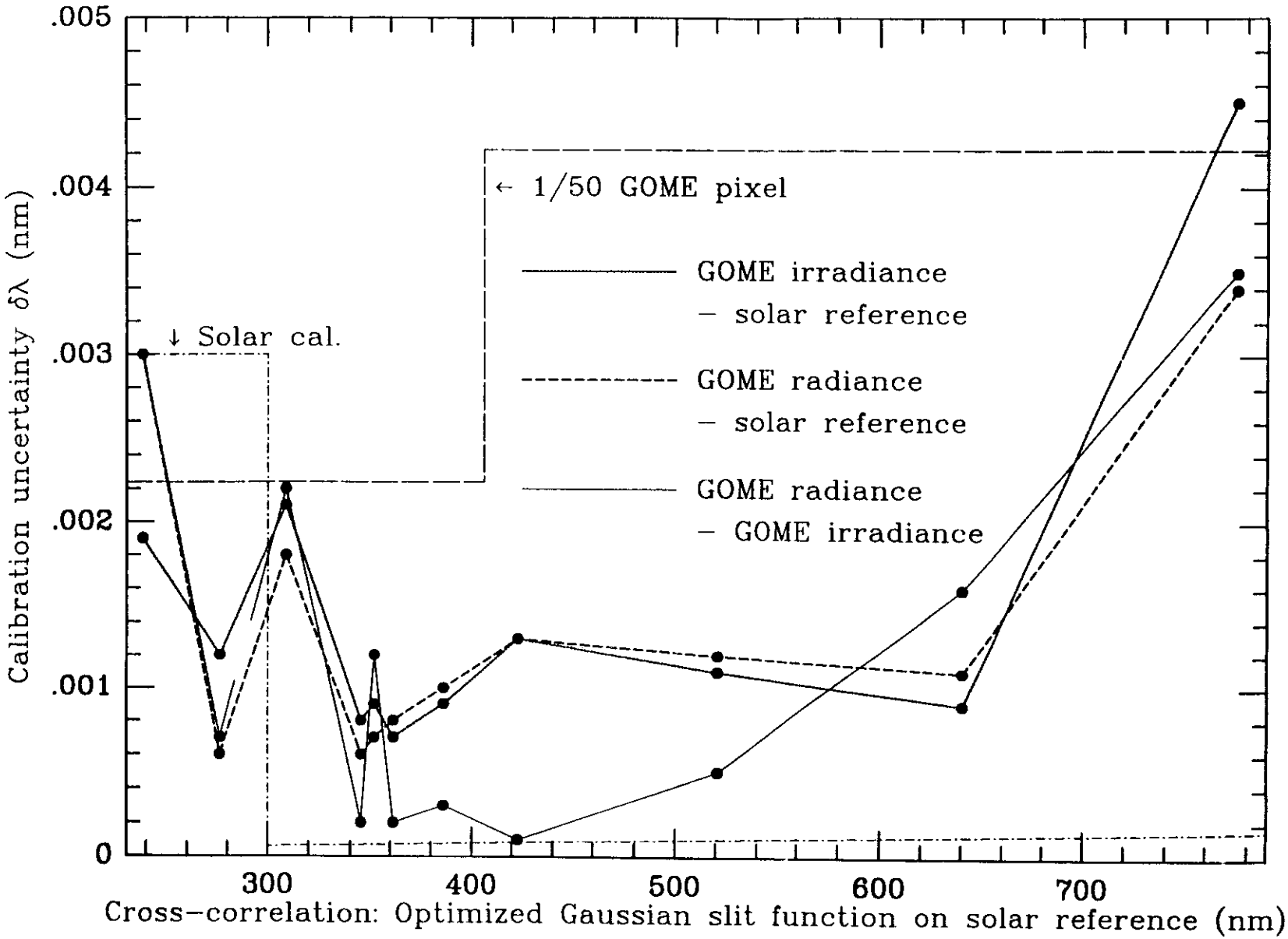
.005
.004
.003
.002
.001
0
Calibration uncertainty δλ (nm)
← 1/50 GOME pixel
↓ Solar cal.
GOME irradiance
– solar reference
GOME radiance
– solar reference
GOME radiance
– GOME irradiance
300
400
500
600
700
Cross–correlation: Optimized Gaussian slit function on solar reference (nm)

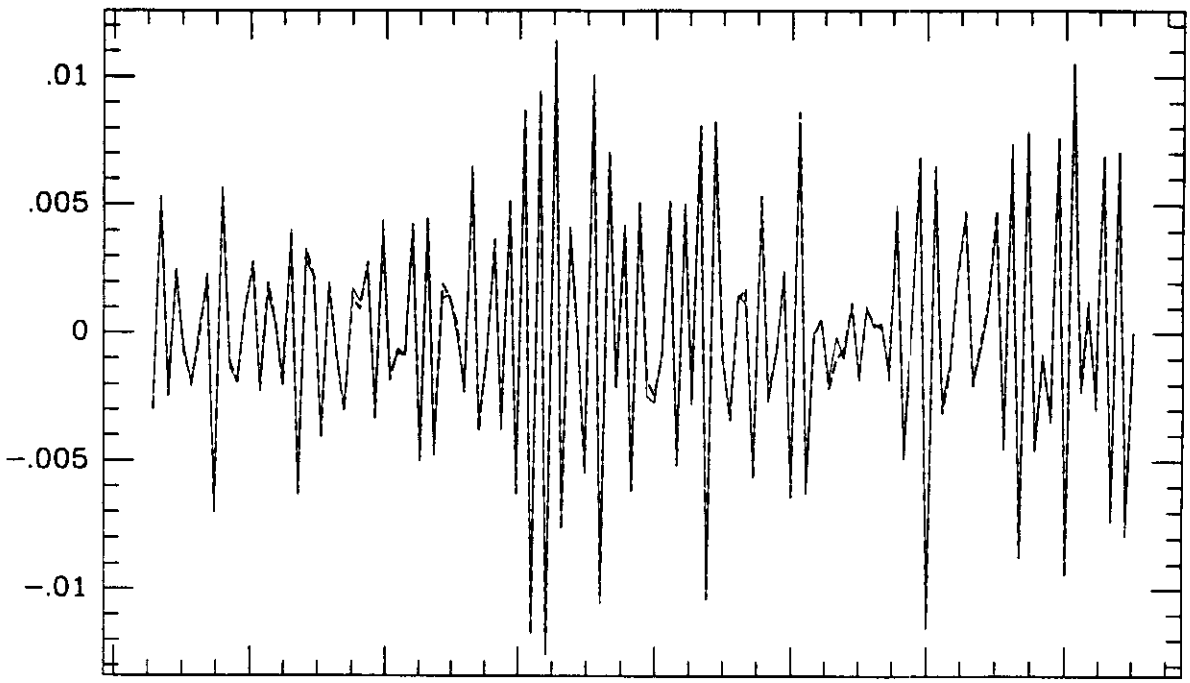

GOME Orbit 70501020, fitting residuals for 1 and 101 spectra (nm)

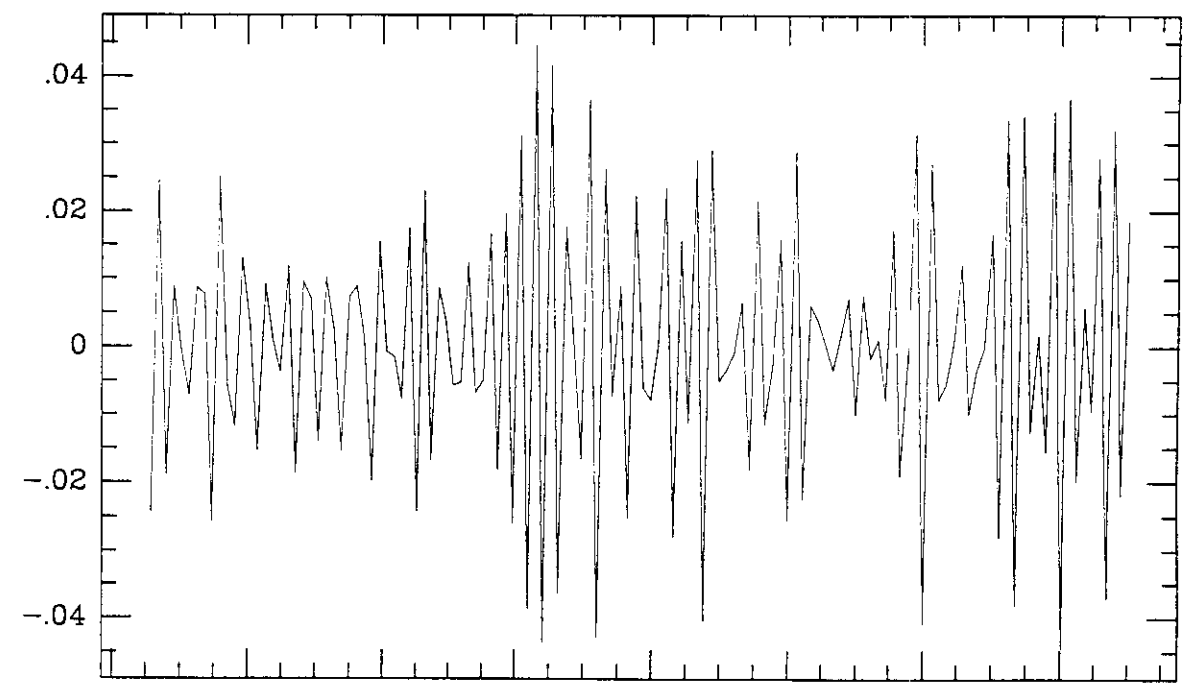

Calculated undersampling correction (no GOME spectra)

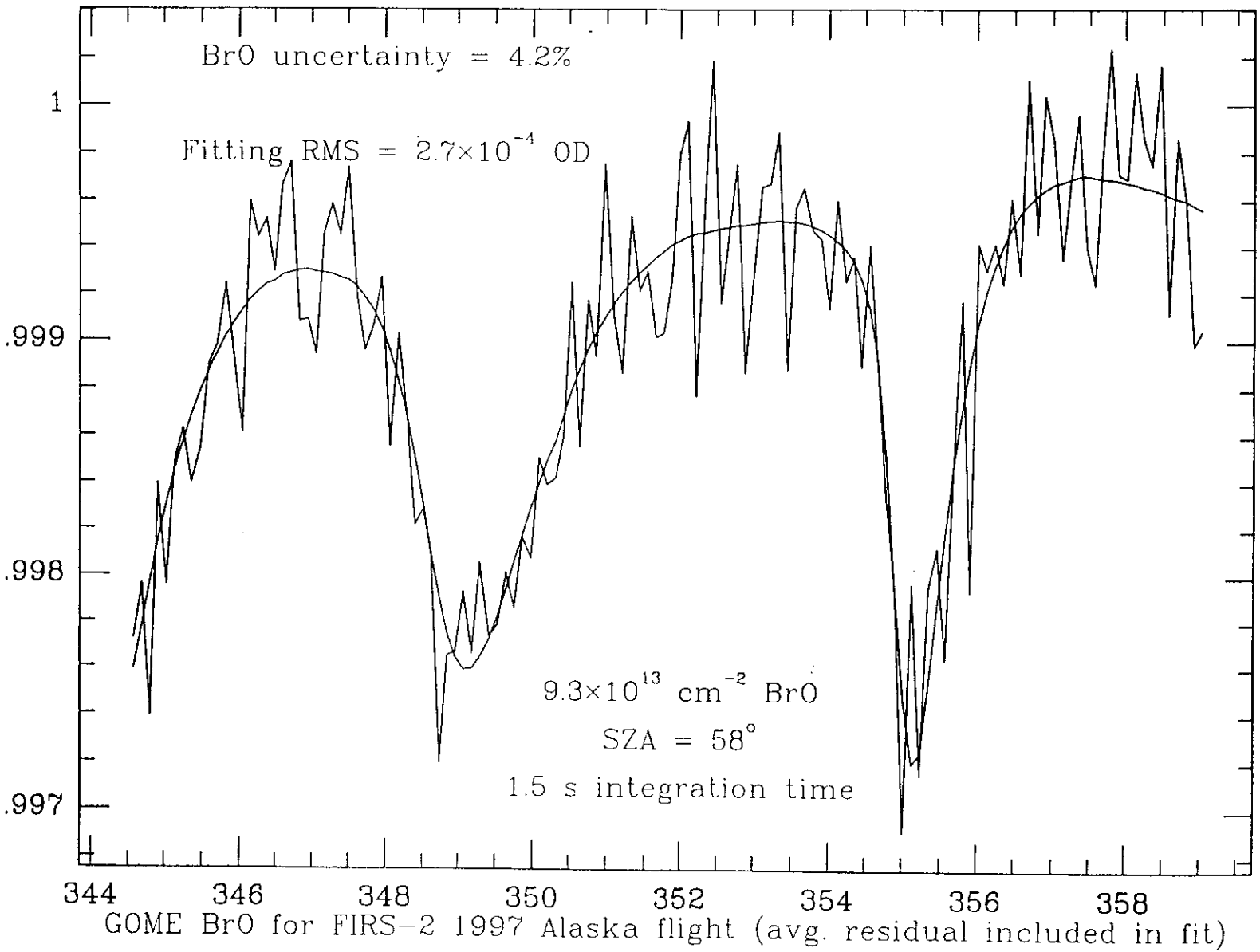

GOME BrO for FIRS-2 1997 Alaska flight (avg. residual included in fit)

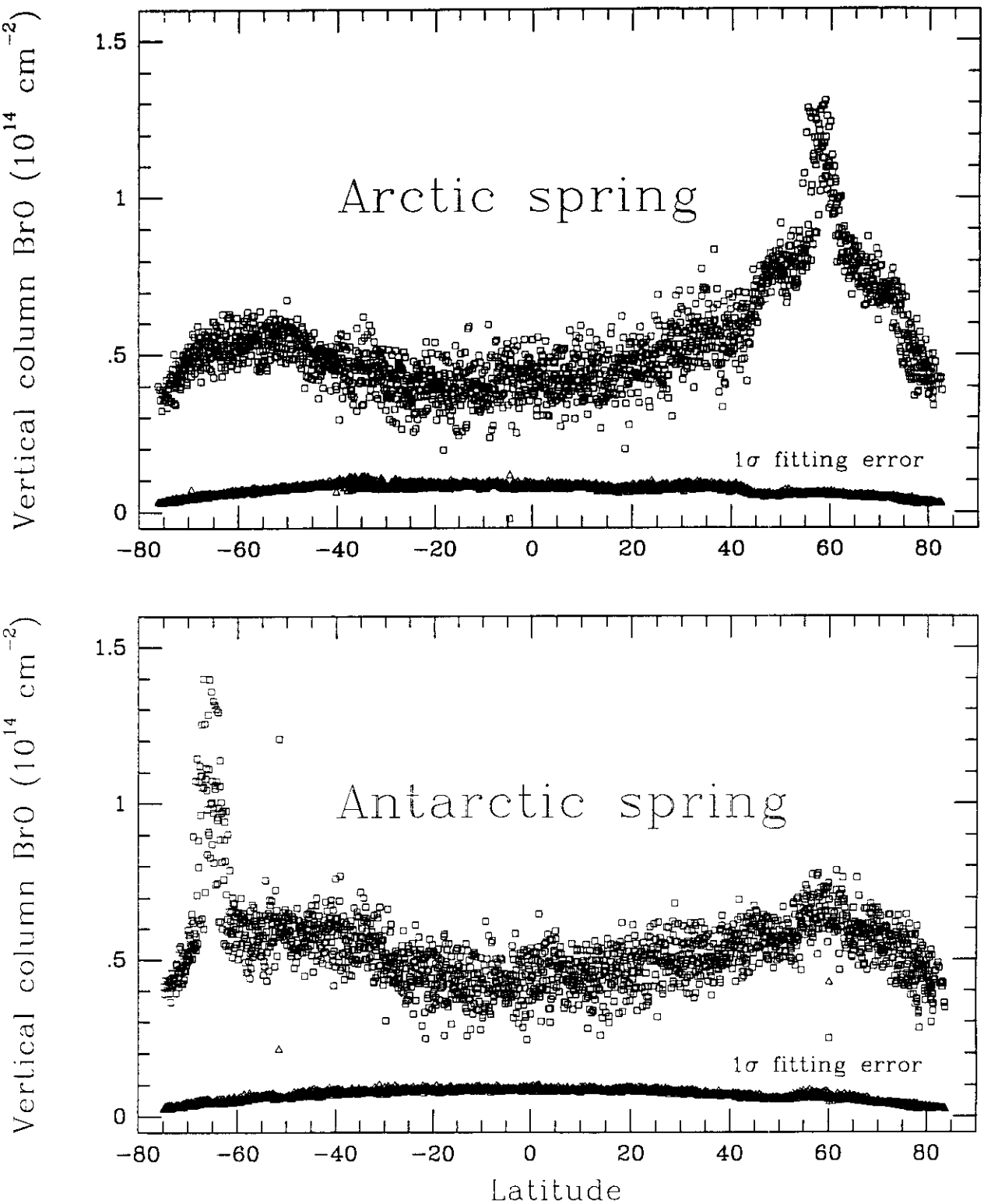
Arctic spring
1σ fitting error
Antarctic spring
1σ fitting error
Vertical column BrO (10^{14} cm^{-2})
Vertical column BrO (10^{14} cm^{-2})
Latitude
1.5
1
.5
0
−80
−60
−40
−20
0
20
40
60
80

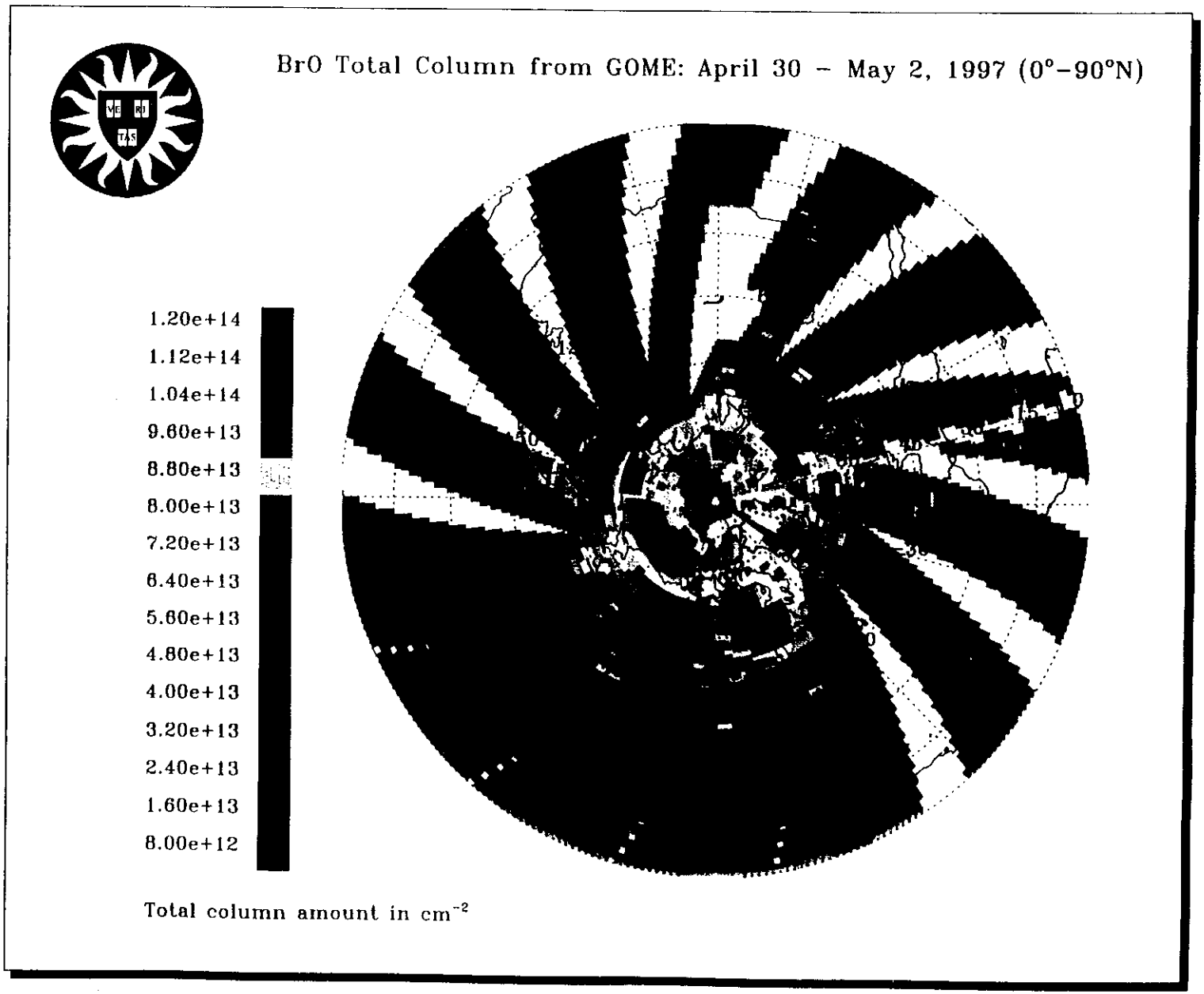
BrO Total Column from GOME: April 30 – May 2, 1997 (0°–90°N)
1.20e+14
1.12e+14
1.04e+14
9.60e+13
8.80e+13
8.00e+13
7.20e+13
6.40e+13
5.60e+13
4.80e+13
4.00e+13
3.20e+13
2.40e+13
1.60e+13
8.00e+12
Total column amount in cm-2

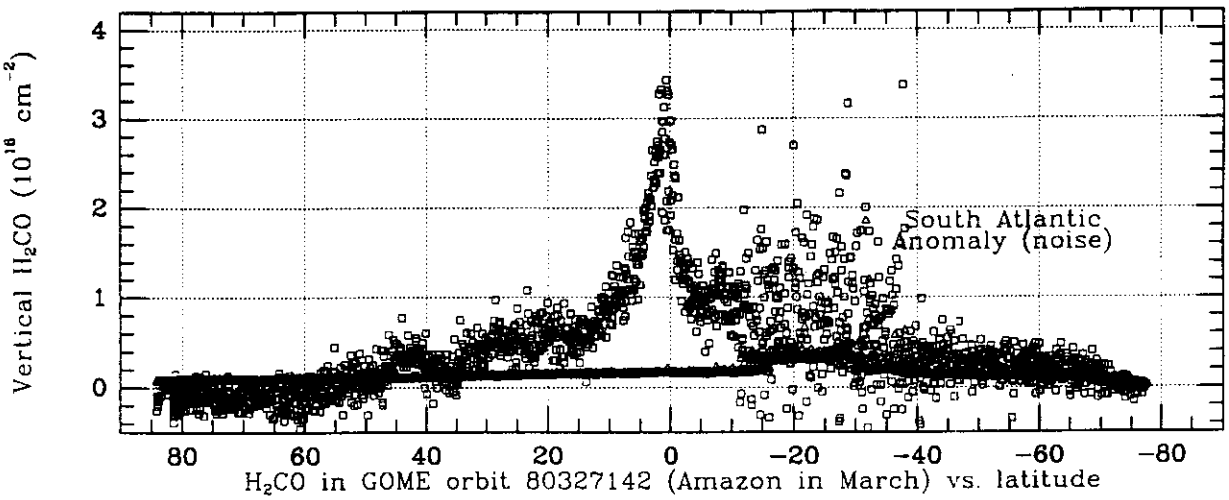
Vertical H_2CO (10^{16} cm^{-2})
South Atlantic Anomaly (noise)
80 60 40 20 0 −20 −40 −60 −80
H_2CO in GOME orbit 80327142 (Amazon in March) vs. latitude

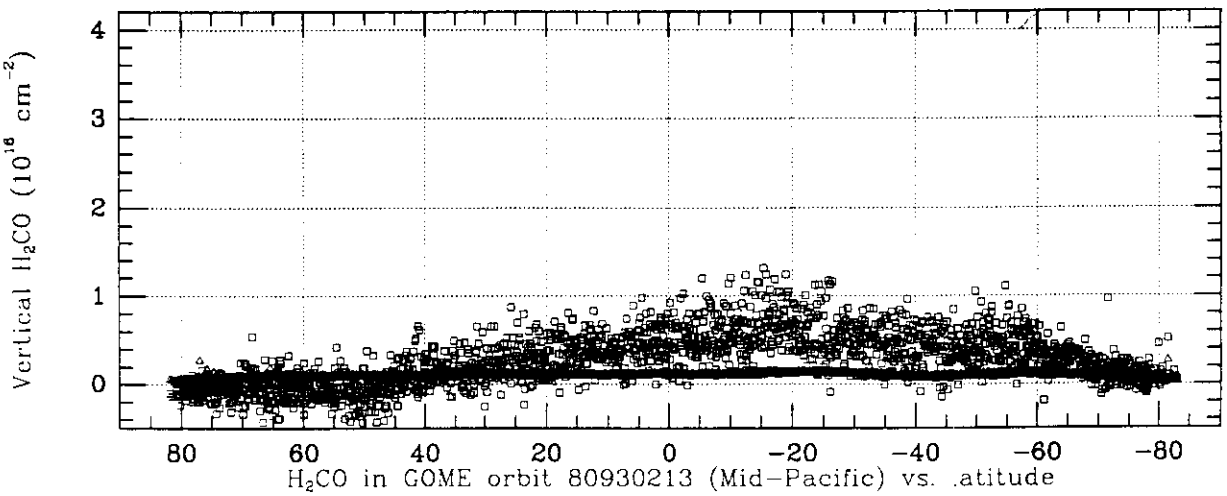
Vertical H_2CO (10^{16} cm^{-2})
80 60 40 20 0 −20 −40 −60 −80
H_2CO in GOME orbit 80930213 (Mid−Pacific) vs. .atitude

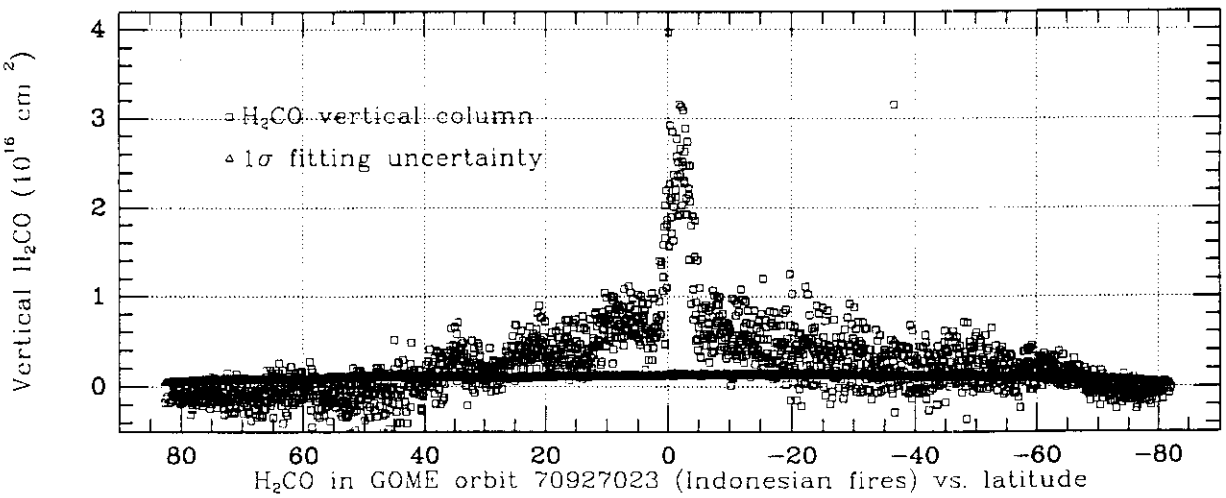
Vertical H_2CO (10^{16} cm^{-2})
H_2CO vertical column
1σ fitting uncertainty
80 60 40 20 0 −20 −40 −60 −80
H_2CO in GOME orbit 70927023 (Indonesian fires) vs. latitude

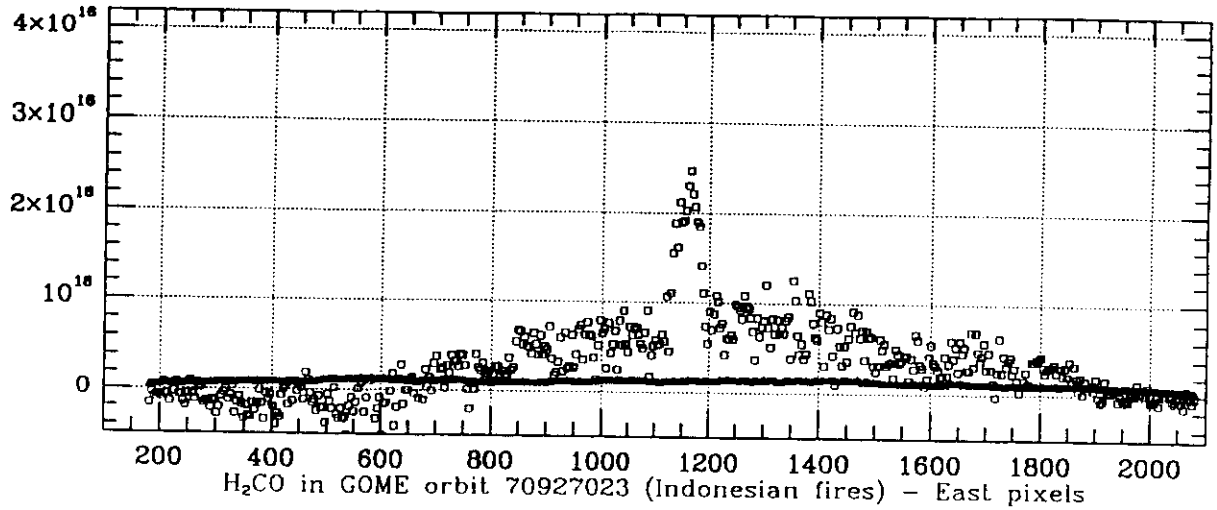
4×10^16
3×10^16
2×10^16
10^16
0
200
400
600
800
1000
1200
1400
1600
1800
2000
H2CO in GOME orbit 70927023 (Indonesian fires) – East pixels

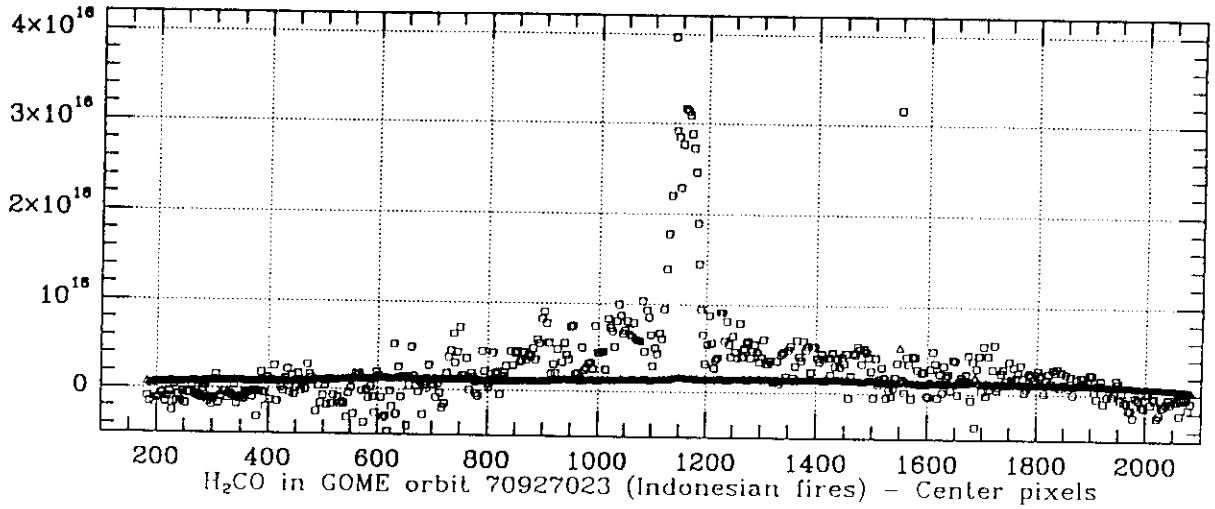
4×10^16
3×10^16
2×10^16
10^16
0
200
400
600
800
1000
1200
1400
1600
1800
2000
H2CO in GOME orbit 70927023 (Indonesian fires) – Center pixels

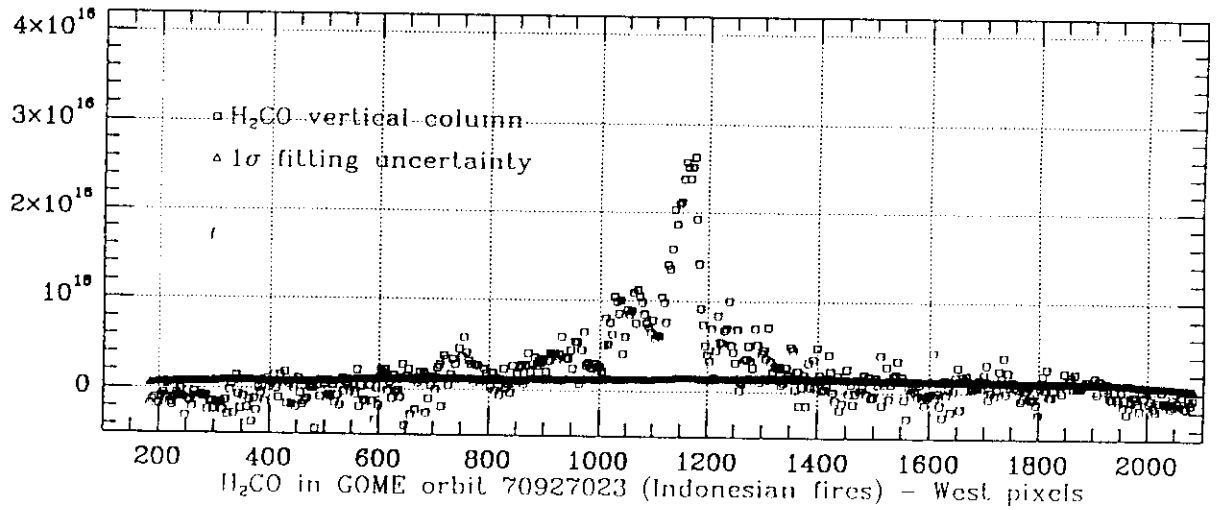
4×10^16
3×10^16
2×10^16
10^16
0
H2CO vertical column
1σ fitting uncertainty
200
400
600
800
1000
1200
1400
1600
1800
2000
H2CO in GOME orbit 70927023 (Indonesian fires) – West pixels

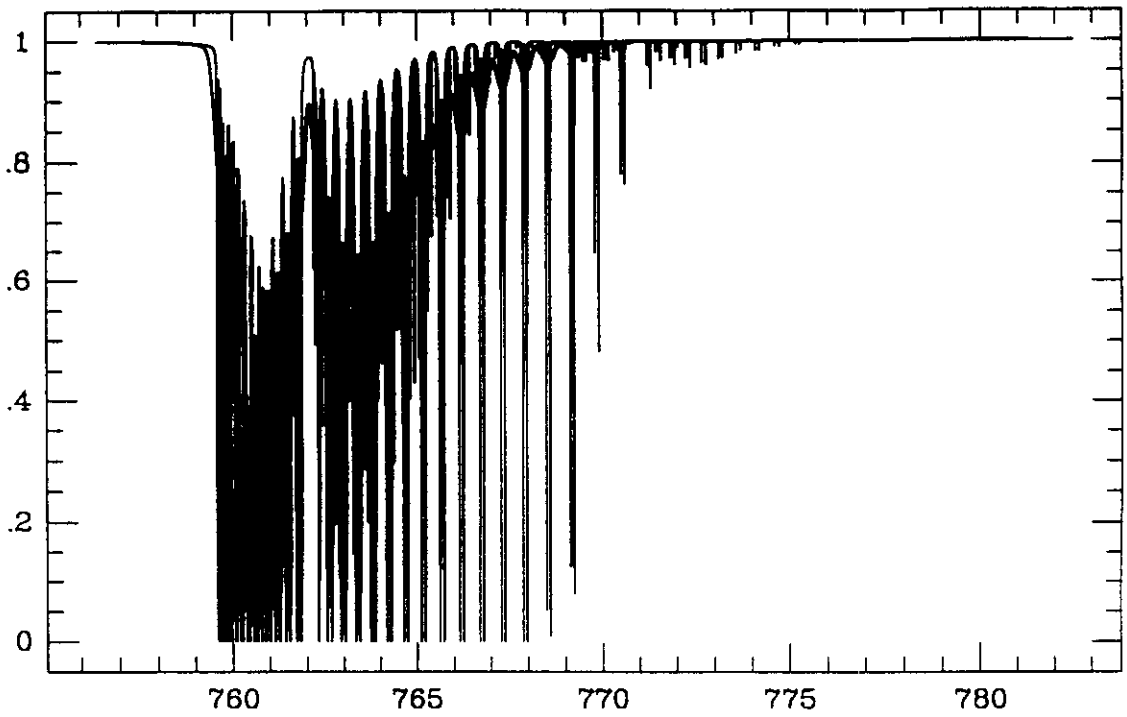

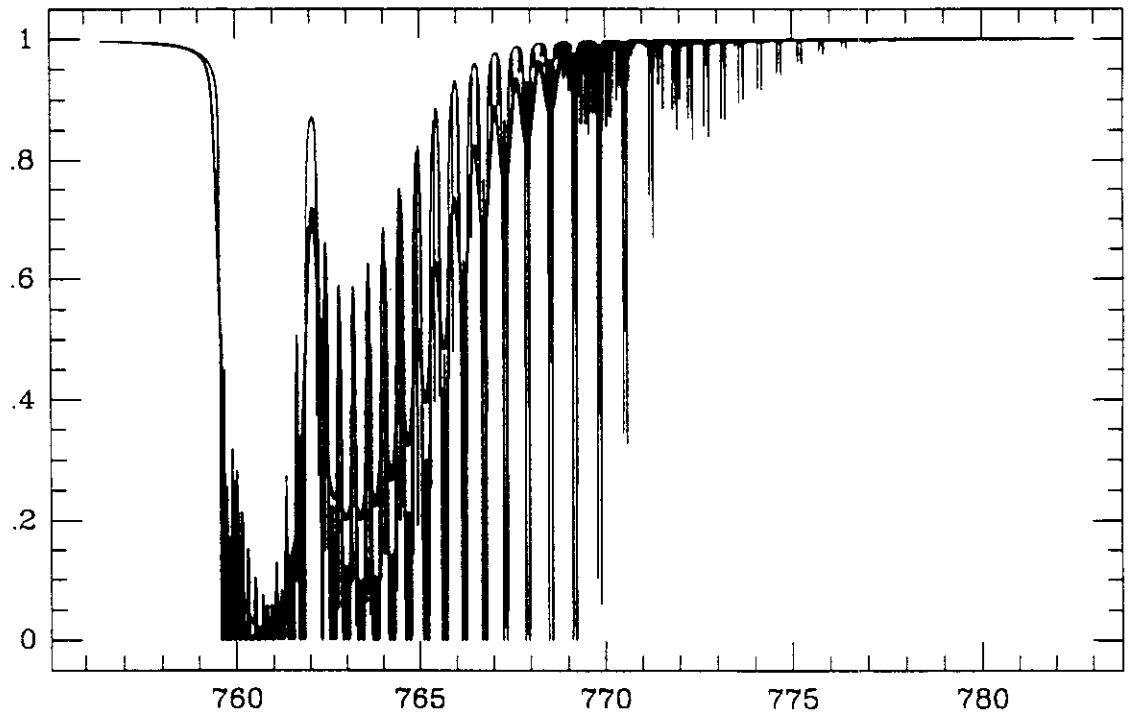

Convolution test – GOME

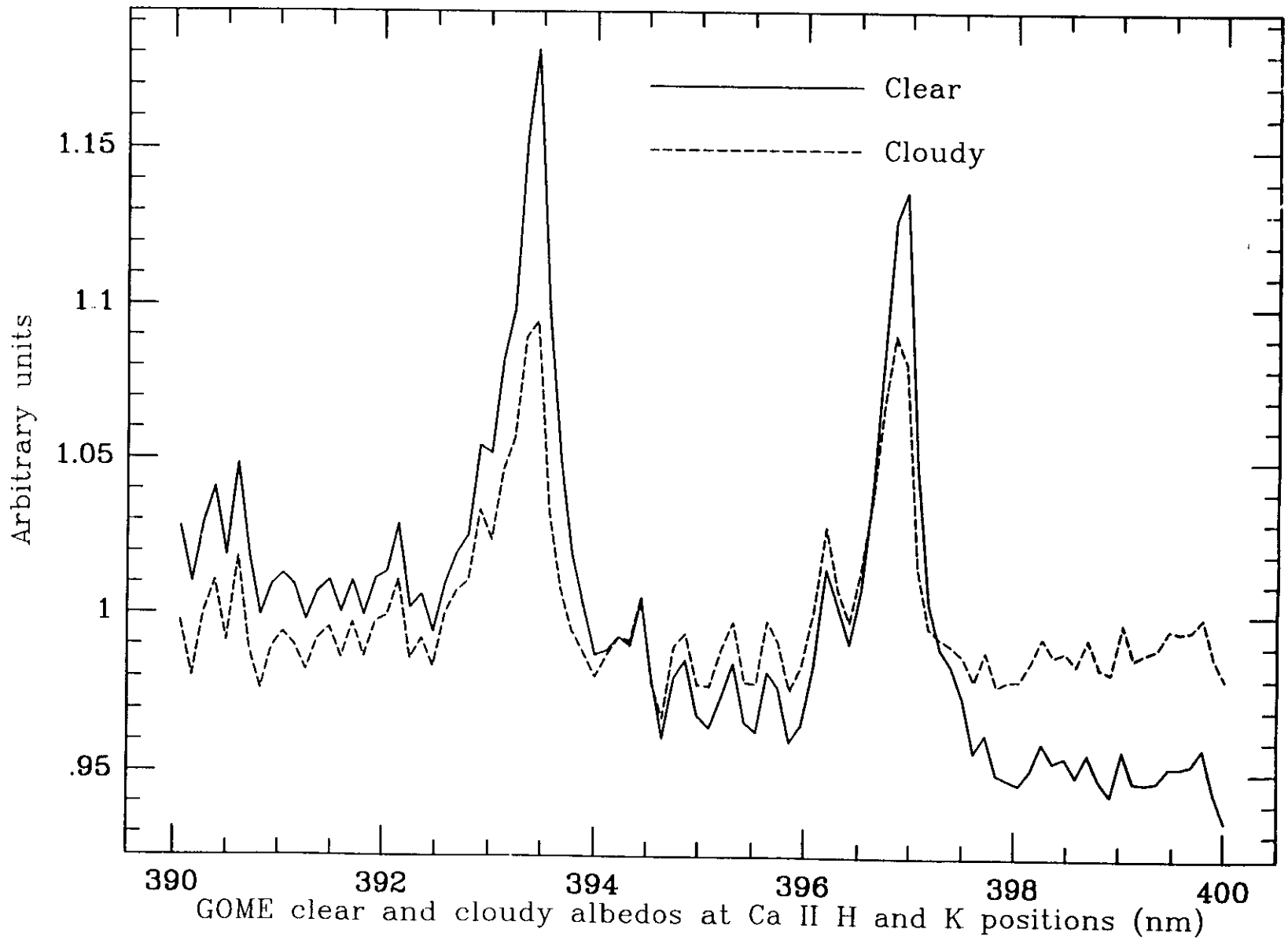
Clear
Cloudy
Arbitrary units
1.15
1.1
1.05
1
.95
390
392
394
396
398
400
GOME clear and cloudy albedos at Ca II H and K positions (nm)

JOURNAL OF GEOPHYSICAL RESEARCH VOLUME 62, NO. 2 JUNE, 1957

A METHOD FOR THE DETERMINATION OF THE VERTICAL OZONE DISTRIBUTION FROM A SATELLITE*

BY S. F. SINGER AND R. C. WENTWORTH

Department of Physics, University of Maryland, College Park, Maryland

(Received October 30, 1956)

The Nimbus-4 Backscatter Ultraviolet (BUV) Atmospheric Ozone Experiment – Two Years' Operation

By DONALD F. HEATH[1]), CARLTON L. MATEER[2]) and ARLIN J. KRUEGER[1])

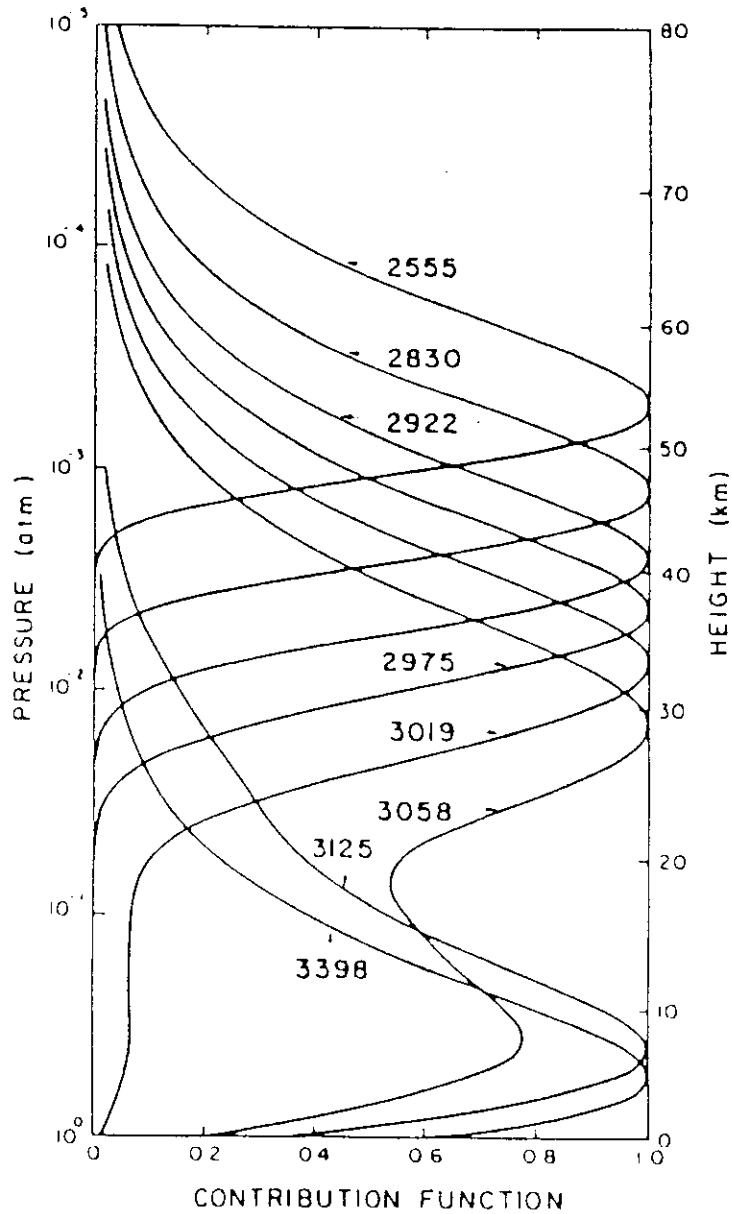

Figure 1

Effective scattering levels for solar radiation scattered in the nadir direction of the satellite for all order of scattering; solar zenith angle = 60° and total ozone = 336 m atm-cm

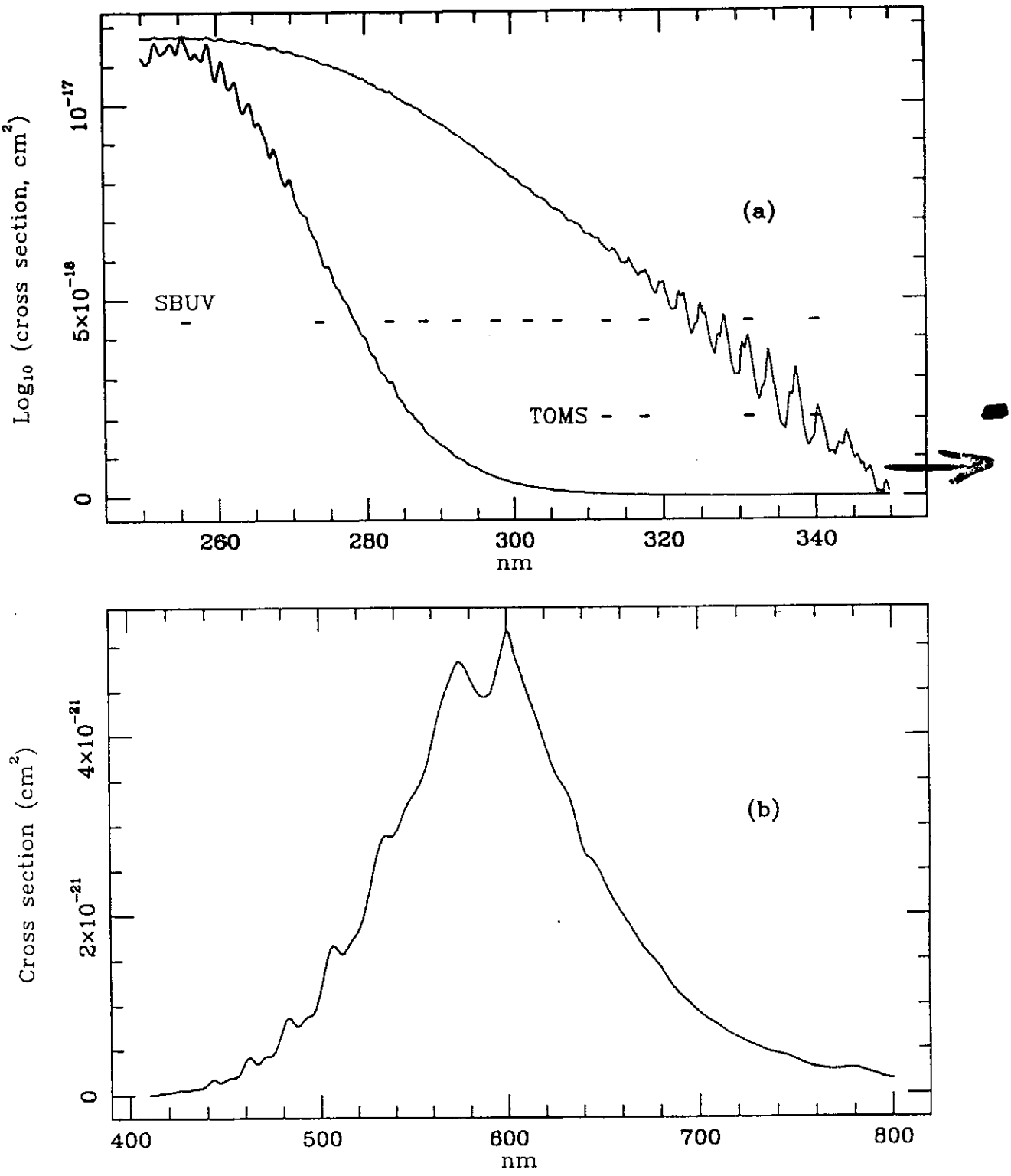
Log10 (cross section, cm2)
10-17
5x10-18
0
(a)
SBUV
TOMS
260
280
300
320
340
nm
Cross section (cm2)
4x10-21
2x10-21
0
(b)
400
500
600
700
800
nm

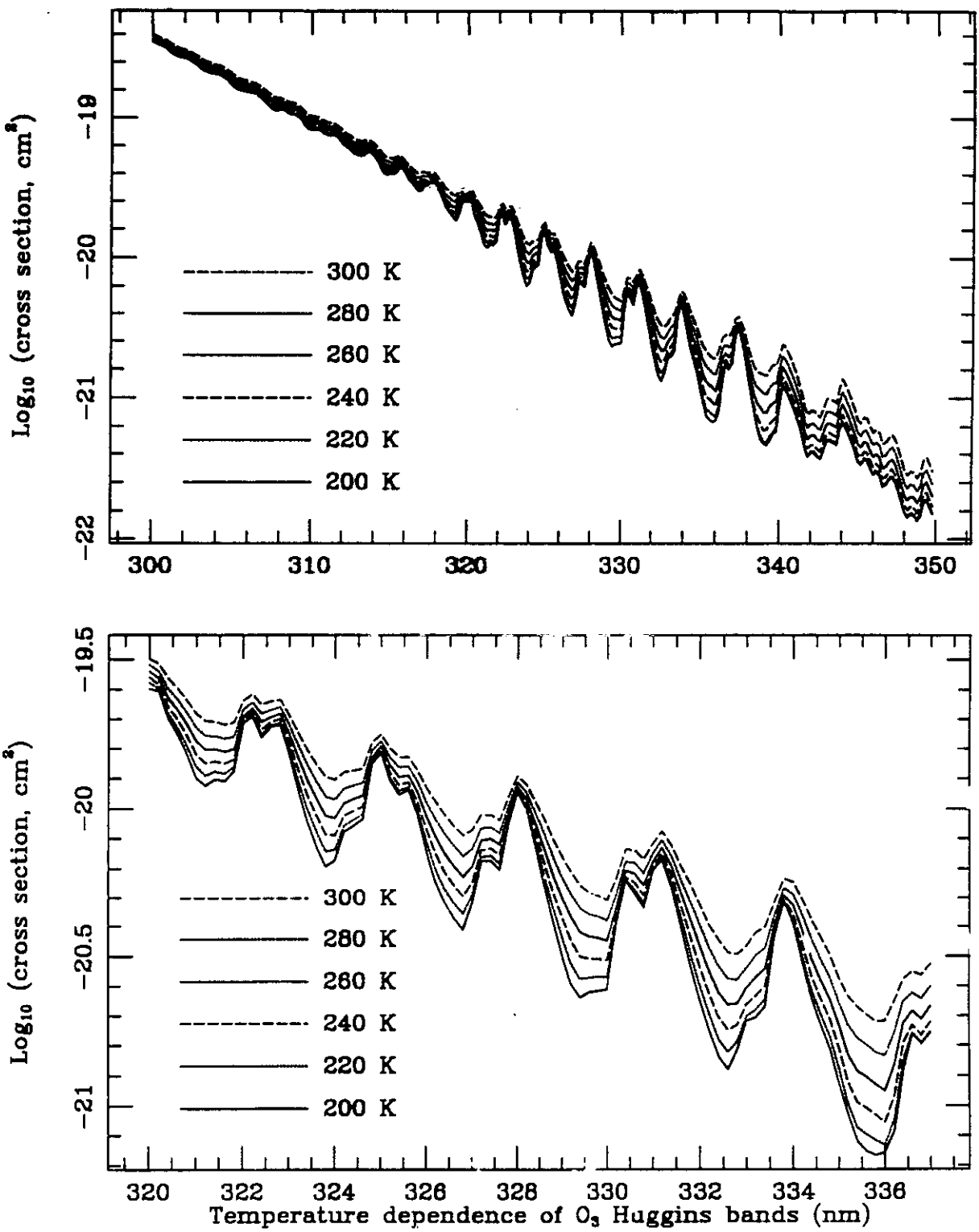
Log10 (cross section, cm2)
-19
-20
-21
-22
300 K
280 K
260 K
240 K
220 K
200 K
300
310
320
330
340
350
Log10 (cross section, cm2)
-19.5
-20
-20.5
-21
300 K
280 K
260 K
240 K
220 K
200 K
320
322
324
326
328
330
332
334
336
Temperature dependence of O3 Huggins bands (nm)

Ozone Profiles / Tropospheric Ozone from GOME

Chance et al., Satellite measurements of Atmospheric ozone profiles, including tropospheric ozone, from ultraviolet/visible measurements in the nadir geometry: A potential method to retrieve tropospheric ozone, J. Quant. Spectrosc. Rad. Trf. 57, 467-476, 1997.

Munro et al., Direct measurement of tropospheric ozone distributions from space, ~~Geoscience~~ Nature 392, 168-171, 1998.